

# **Generation of metal nanoparticles in spherical polyelectrolyte brushes and their application in heterogeneous catalysis**

DISSERTATION

zur Erlangung des akademischen Grades eines

Doktors der Naturwissenschaften (Dr. rer. nat.)

in Fach Chemie der Fakultät für Biologie, Chemie und Geowissenschaften

der Universität Bayreuth

vorgelegt von

**Geeta Sharma**

Aus Nasik, Indien

Bayreuth, 2005

Die vorliegende Arbeit wurde in der Zeit von Januar 2001 bis November 2003 am Polymer-Institut der Universität Karlsruhe(TH) durchgeführt und von Dezember 2003 bis Dezember 2004 am Lehrstuhl für Physikalische Chemie I der Universität Bayreuth fortgesetzt.

Vollständiger Abdruck der von der Fakultät Biologie, Chemie, und Geowissenschaften der Universität Bayreuth genehmigten Dissertation zur Erlangung des akademischen Grades Doktor der Naturwissenschaften (Dr. rer. nat.)

Dissertation eingereicht am: 07.04. 2005

Wissenschaftliches Kolloquium am: 05. 07. 2005

Prüfungsausschuß

Prof. Dr. M. Ballauff (Erstgutachter)

Prof. Dr. R. Kempe (Zweitgutachter)

Dekan: Prof. Dr. O. Meyer

## Acknowledgements

I am grateful to Prof. Dr. Matthias Ballauff, my thesis advisor for providing me an interesting theme for my work and for his constant encouragement, guidance and advice throughout my work.

I would like to express my gratitude to Prof. Dr. Rhett Kempe for his direction and numerous fruitful scientific discussions on the catalysis studies. I would like to specially thank Dr. Torsten Irrgang and Christian Karl for carrying out the laborious catalysis experiments and Sebastian Proch, Martin Hoffmann for the mechanistic studies and theoretical studies.

I appreciate Mr. Futoi, Mr. Send, Björn Haupt and Dr. Markus Drechsler for the TEM and cryo-TEM measurements and useful discussions in their interpretation.

I would like to thank our institute secretaries Ms. Manuela Winkler, Ms. Ilona Deger, Ms. Ute Meyer and Ms. Christine Thunig for dealing with the paperwork necessary for my stay in Germany.

I would also like to thank Mr. Wolfgang Abogast, Mr. Karlheinz Lauterbach, Ms. Helena Hörig, Mr. Hans Kühn and Ms. Christa Bächer for their technical support in the laboratory work.

I would like to acknowledge my co-workers Dr. Alexander Wittemann, Jérôme Crassous, Li Li, Yu Mei and the entire group for their cooperation and support in my work.

Finally, I would like to express my appreciation to Prof. Matthias Ballauff and Mushtaq Patel for a detailed reading and correction of this manuscript, for without their help writing this work would have been much more difficult.



## Table of contents

|   |           |
|---|-----------|
| <b>I Introduction.....</b>  | <b>1</b>  |
| <b>Theory</b>   |           |
| <b>II Definition of brushes.....</b>  | <b>4</b>  |
| II.1 Classification of brushes.....   | 5         |
| II.2 Methods of Synthesis.....  | 8         |
| II.3 Spherical polyelectrolyte brushes and their behaviour.....                       | 9         |
| <b>Results and discussion</b>   |           |
| <b>III Synthesis of spherical cationic brushes .....</b>                              | <b>12</b> |
| III.1 Synthesis and characterization of cationic core particles (PS-Co-HMEM).....     | 13        |
| III.2 Synthesis of cationic brushes by photoemulsion polymerisation.....              | 16        |
| III.3 Synthesis poly-aminoethylmethacrylate hydrochloride(AEMH) brushes.....          | 19        |
| III.4 Determination of Brush parameters - Contour length, Grafting density.....       | 22        |
| III.5 Synthesis of Poly-vinylbenzylamine hydrochloride (VBAH) brushes.....            | 25        |
| III.6 Synthesis of polyvinylpyridine(PVP) brushes.....                                | 26        |
| <b>IV Behaviour of cationic brushes</b>   |           |
| IV.1 Effect of salt concentration .....   | <b>29</b> |
| IV.2 Effect of pH.....  | 31        |
| IV.3 Brushes as nanoreactor to generate nanoparticles.....                            | 34        |
| <b>V Generation of metal nanoparticles</b>  |           |
| V.1 Metal nanoparticles: General synthetic methods and applications.....              | 37        |
| V.2 Introduction of Gold ions in the brushes and synthesis of Gold nanoparticles..... | 42        |
| V.3 Cryogenic temperature TEM of polyelectrolyte brushes with gold ions.....          | 44        |
| V.4 HRTEM images of the gold nanoparticles.....                                       | 49        |
| V.5 UV/VIS spectra of gold nanoparticles.....   | 57        |
| V.6 Synthesis of platinum nanoparticles.....  | 59        |
| V.7 Cryo TEM images of Pt nanoparticles.....  | 60        |
| V.8 Generation of silver nanoparticles and TEM Images.....                            | 64        |
| <b>VI Catalysis by metal nanoparticles</b>  |           |
| VI.1 Catalytic activity of bulk metals.....   | 66        |
| VI.2 Origin of catalytic activity in metal nanoparticles.....                         | 67        |
| VI.3 Metal catalyst nanoparticles on oxide support .....                              | 68        |

|   |           |
|---|-----------|
| VI.4 Chemical reactions catalysed by metal nanoparticles..... | 70        |
| VI.5 Catalysis by platinum nanoparticles.....                 | 71        |
| VI.6 Catalysis by Gold nanoparticles.....                     | 77        |
| <b>Summary (English).....</b>                                 | <b>79</b> |
| <b>Summary (Deutsch).....</b>                                 | <b>81</b> |
| <b>VII Appendix</b>   |           |
| VII.1 Tables.....   | 83        |
| VII.2 Experimental techniques and characterization.....       | 83        |
| VII.3 Analytical methods and instrumentation.....             | 92        |
| VII.4 References.....   | 97        |
| VII.5 Glossary.....   | 113       |

## I Introduction

Nanoparticles exhibit different properties as compared to their bulk materials due to quantum size effects (Lewis 1993, Alivisatos 1996, Henglein 1993, Ball *et al.* 1992, 1993). The quantum size effects are related to alterations in the electronic band structure of the metal particle due to its small size and the presence of a high fraction of a co-ordinately and electronically unsaturated atoms at the surface of the metal nanoparticles (Shipway *et al.* 2001). These peculiar properties of nanoparticles have important implications in material science such as surface enhanced spectroscopy (Svoboda *et al.* 1994, Feldstien *et al.* 1997, Fukumi *et al.* 1994, Hagland *et al.* 1993), catalysis (Toshima *et al.* 1997, Schmidt *et al.* 1998, Thomas *et al.* 1988, Schmid *et al.* 1990, 1992, Watze *et al.* 1987, Boudart *et al.* 1994, Xu *et al.* 1994), optics (Colvin *et al.* 1994, Weller *et al.* 1995), magnetics, microelectronics (Hermanson *et al.* 2001, Asakawa *et al.* 2000), information storage (Sun *et al.* 1994), sensors, photoelectrochemically active electrodes (Maye 2003), magnetic fluids (Li *et al.* 2001, Sun *et al.* 2000), photonic crystals (Ozin *et al.* 2001, Romanov *et al.* 1999, Fink *et al.* 1998, Urbas *et al.* 1999, Norris *et al.* 2001, Netti *et al.* 2001), biological sensors (Emory *et al.* 1998, Bruchez *et al.* 1998, Chan *et al.* 1998), medical diagnostics, ceramics, pigments in paints and cosmetics etc.

Numerous investigations are being carried out today is aimed at the synthesis of metal nanoparticles in the size range 1-10 nm (Roucoux *et al.* 2002, Bönnemann *et al.* 2001, Aiken III *et al.* 1999) The stabilization of metal nanoparticles is a challenging issue as their high surface energy of the metal nanoparticles tends to aggregate them to form bigger clusters. Hence, most of the synthetic techniques are targeted to produce monodisperse nanoparticles, which are stable over a long period. Generally, metal atom precursors are used to grow nanoclusters in the presence of stabilizers. The stabilizers interact with the surface of the nanoclusters to overcome agglomeration and at the same time controls their growth, very often to a predetermined size. Some of the stabilizers include solvent molecules, ion pairs, surfactants (Fendler *et al.* 1995, Duff *et al.* 1993, Ahmadi *et al.* 1996, Collier *et al.* 1997), micelles (Spatz *et al.* 2000, 1996, Djalali *et al.* 2002, Clay *et al.* 1995), ligand molecules (Kumar *et al.* 2003, Brust *et al.* 1994, 1995, Porter *et al.* 1998, Weisbacker *et al.* 1996, Templeton *et al.* 1998, Johnson *et al.* 1997, Mayya *et al.* 1997, Leff *et al.* 1996, Bharathi *et al.* 1997), polymers (Antonietti *et al.* 1997, Teranishi *et al.* 1998, Mayer *et al.* 2000), dendrimers (Crooks *et al.* 2001) and gels (Biffis *et al.* 2003, Svergun *et al.* 1998).

Besides this, the deposition of preformed metal nanoparticles on substrates to produce various interesting nanocomposite particles have been developed. The substrates vary

from spherical colloids (Caruso *et al.* 2001, Gittins *et al.* 2002, Dokoutchaev *et al.* 1999, Shchukin *et al.* 2003, Pol *et al.* 2003, Lindlar *et al.* 2002, Ji *et al.* 2001, Khan *et al.* 2001, Siiman *et al.* 2000), porous materials (Bronstein *et al.* 1996) to biological templates such as DNA (Harnack *et al.* 2002, Cobbe *et al.* 2003, Kumar *et al.* 2001), plants and micro organisms (Gardea-Torresdey *et al.* 2002, Ahmad *et al.* 2003).

The usage of spherical colloids as the substrate to load metallic nanoparticles is being researched recently for its direct application in photonic crystals (Lim *et al.* 2003, Oldenburg *et al.* 1998, 1999, Graf *et al.* 2002). The metals used are gold, silver, palladium, and platinum. However, the routes described involve the deposition of preformed particles on a suitably modified surface. The alternative way to produce metal nanoparticles directly on the substrates have not been studied so widely (Djalali *et al.* 2002, Liu *et al.* 2002, Youk 2003, Ghosh *et al.* 2003).

The major theme of this thesis is to generate metal nanoparticles on the surface of the polystyrene spheres bearing cationic polyelectrolyte brushes. Polymer brushes refer to an assembly of polymer chains tethered to a surface or an interface. Above a critical grafting density, in order to avoid overlapping, chains stretch away from the surface. The synthesis of brushes have been carried out by mainly two routes physisorption and covalent attachment. The covalent attachment is preferred over physisorption due to desorption of polymeric chains in non favourable conditions.

In the present work, chains of poly(aminoethylmethacrylate hydrochloride) (PAEMH) are covalently attached to the surface of polystyrene core by photo-emulsion polymerisation. By this “grafting-from technique” a cationic spherical polyelectrolyte brush is generated (Guo *et al.* 1999). The grafting of the PAEMH chains achieved by photo-emulsion polymerisation is so dense that the brush limit is reached in these systems, i.e., the average distance of the chains on the surface is much smaller than their average dimensions. The chloride counterions are subsequently exchanged by  $\text{AuCl}_4^- / \text{PtCl}_6^{2-}$  ions. As an alternative route, the hydrochloride can be converted into the free base first and then reacted with metal ions. Moreover, it can be demonstrated that ca. 95 % of the counterions are confined in the brush layer (Das *et al.* 2002). This confinement predicted some time ago by Pincus “closes” the nano-reactor and prevents the formation of metal-particles in the aqueous phase (Pincus 1991). The metal ions thus immobilized can be reduced in the final step to yield metallic metal particles on the surface. In this way, the well-established physics of the polyelectrolyte brush layer can be used for chemical reactions on the surface of colloidal particles. The surface of the latex sphere hence becomes a “nano-reactor” in which the reduction is done.

The mentioned way of generating metal nanoparticles is comparable to the use of micelles (Spatz *et al.* 1998, Selvan *et al.* 1999, Lindlar *et al.* 2002, Djalali *et al.* 1999, 2002) or dendrimers (Esumi *et al.* 2000, 1998, Manna *et al.* 2001, Garcia *et al.* 1999) as “nano-reactors”. Evidently, the metal ions must be firmly immobilized in this nano-reactor to prevent the exchange of the metal ions into the continuous phase. It is hence important to elucidate the interactions of suitable metal ions with model colloids having a well-defined surface structure. As the particles are formed without any stabilizing reagents, the metal nanoparticles are freely accessible to chemical and physical interaction with other molecules.

Catalytic properties in nanoparticles are generated or enhanced due to high surface area-to-volume ratio, high edge concentration and quantum size effects as compared to the bulk metals (Lewis 1993, Haruta 1997, Chen 1997, Chen *et al.* 1998). For example, gold, the metal in bulk is catalytically active when sized at nanoscale (Sault *et al.* 1986, Saliba *et al.* 1998, Hammer *et al.* 1995, Sanchez *et al.* 1999). The other widely used metals for catalysis are platinum (Alvarez *et al.* 2000), palladium (Crooks *et al.* 2001) and silver (Joly *et al.* 2000). Usually, the catalyst systems are composed of metal nanoparticles on a metal oxide support. The role of support material in origin of catalytic activity in the metal nanoparticles has been a topic for theoretical and experimental studies. On one hand, the theoretical studies prove that the nanosized nanoparticles are catalytically active without any support, on the other, experiments prove that the activity due to the junction effect, because of the interaction of the support and the metal nanoparticles (Frost 1988, Weng *et al.* 1992).

The current study of synthesis of metal nanoparticles is further extended to study their catalytic activity in heterogeneous hydrogenation reactions. Due to the inert polystyrene used as support particles in the synthesis of the metal nanoparticles, the participation of the support particle in the electronic interactions with the metal nanoparticles can be ruled out. The effect of reaction conditions on the stability of metal nanoparticles is an important issue in the field of catalysis. A decrease in the efficiency is observed after a number of runs. Hence, the further investigations are carried out by recycling the catalyst and observing the efficiency of the catalyst in the subsequent runs.

## II Brushes - Definition

The polymer brushes can be defined as the linear polymeric chains attached to a surface or an interface, where the distance between the grafting points of the polymer chains on the surface is less than the radius of gyration of the polymeric chains (Milner 1991, Halpern *et al.* 1992). Such a condition stretches the polymeric chains to their maximum to avoid the repulsions (Fig. 1).

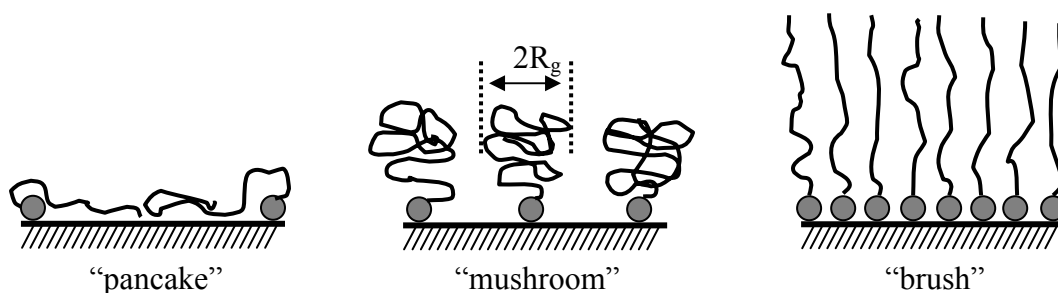


**Fig. 1** Possible conformations of polymers attached to a planar solid surface with different grafting densities. The distance between the grafting points, when exceeds the hydrodynamic radii of the grafted polymer the “pancake” or “mushroom” conformation results depending on the affinity of the chains to the surface. With the decrease in the distance of the grafting points, the conformation starts showing a transition from pancake or mushroom to brush conformation.

End tethering of the polymer reduces the degree of freedom for different macromolecular conformations ending up in the stretch conformation of the polymer. The free energy of the  $F$  of the chains is obtained from a balance between the interaction energy between the statistical segments  $F_{int}$  and the energy difference between the stretched and the unstretched polymer chains  $F_{el}$  (elastic free energy) caused by the entropy loss of the chains.

$$F = F_{int} + F_{el}$$

The important parameters for the description of brushes are segment density profile  $\Phi(Z)$  of the surface attached chains, the brush height  $h$  as a function of the grafting density  $\sigma$  and the molecular weight of the surface attached chains and the solvent quality of the medium.

The stretched conformation has a direct consequence on the properties like osmotic pressure, interaction parameters and water activity. The conformation of the brushes can be changed by changing the solvent quality. These properties can be studied by conventional experimental methods. With the advanced microscopic and surface sensitive spectroscopic

techniques, it is possible to visualize the brushes directly (Yamamoto *et al.* 2000, Goodman *et al.* 2004, Mei *et al.* 2003).

The formation of a brush modifies the properties of the grafting surface, making the brushes a very interesting subject towards the application in a wide range of fields. For example, ultra low friction surfaces are obtained by coating of two surfaces, which slide against each other with polymer brushes (Klein *et al.* 1993). Autophobic surfaces can be produced by grafting polymer brushes, which are not wetted by free polymer (Reiter *et al.* 1996, 2000). Non-fouling biosurfaces can be synthesized according to the requirements in artificial implants (Ward 1989), cellculture dishes and biosensors (Ito *et al.* 1992). Other types include temperature responsive brushes (Takai *et al.* 1994), electrically switchable brushes and brushes for applications in separation techniques (Hennion *et al.* 1978, Van Zanten 1994).

## II.1 Classification of brushes

The polymer brushes are classified according to their geometry and the charges they bear. The brushes can be planar (Biesalski *et al.* 1999), spherical (Jayachandran *et al.* 2002, Guo *et al.* 1999), cylindrical (Cheng *et al.* 2001, Djalali *et al.* 2002)) or comb like (Börner *et al.* 2002, Koper *et al.* 2003) depending on the geometry of the surfaces on which they are grafted. According to the charges, brushes can be classified as positively charged, negatively charged or neutral depending on the charges of the monomer units.

### Classification based on geometry

#### Planar brushes:

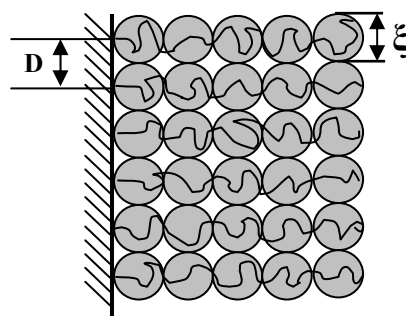


**Fig. 2** Schematic diagram of a planar brush. The polymer chains are grafted on planar surfaces such as silica, glass, gold etc.

Planar brushes result when chains are grafted on a planar surface (Fig. 2). A planar brush is

built up of strings of volume-filling blobs of size  $\xi$  equal to the distance between the attached points  $D$ . A blob contains  $g$  segments of monomers of a single chain. The monomer density and the blob size is same throughout the brush. In planar brushes, electrostatic interactions between the chains and the osmotic pressure are dominant forces. The neutralization length  $\zeta$  where the interaction between a fixed charge and its counter ion decays strongly can be given by Debye length in dense brushes (Pincus 1991). Hence, for the thickness ' $L$ ' of the brush greater than that of the  $\zeta$ , electrostatic interactions are balanced within the brushes confining all the counter ions within the brush. Experimentally, these theoretical predictions were confirmed by Ahrens *et al.* and Tran *et al.* who showed that the distribution of counterions in planar polyelectrolyte brush follows closely the monomer profile of the monomeric units.

### Spherical brushes

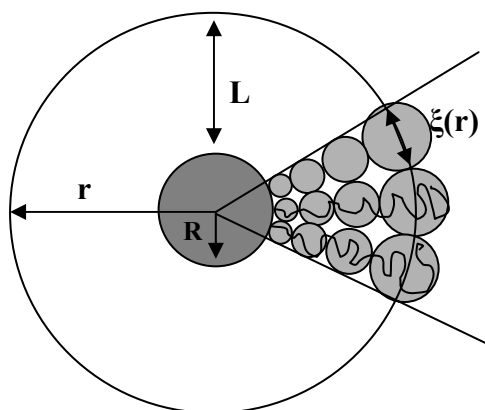


**Fig. 3** Schematic diagram of a spherical brush (Daoud *et al.* 1982). The spherical brushes can be formed by micelles of a block copolymer, or grafting polymer on preformed spheres of a polymer or an inorganic material.

Linear polymer chains densely grafted onto the spherical surfaces forms spherical brushes (Fig. 3). Hydrophobic spherical particles such as polystyrene latex can be made highly stable in hydrophilic solvents by grafting of charged polymers i.e., polyelectrolyte. Spherical brushes are characterised by the core radius  $R$ , the contour length  $L_c$  of the grafted polymeric chains and the grafting density  $\sigma$ , the number of chains per unit area. The brushes are modelled in terms of volume-filling blobs where the size of the blob  $\xi(r)$  varies linearly with the radial distance  $r$  from the grafting surface. The monomer density decreases with the increase in the distance from the grafting surface. For polyelectrolytes, the Daoud and Cotton model (Daoud *et al.* 1982) was analytically extended by Hariharan *et al.* (Hariharan *et al.*

1998) to give the number of segments  $N_\xi$  and segment density inside a blob  $\rho(r)$  in good solvents as

$$\frac{\xi}{l_k} \approx N_\xi^{3/5} \left( \frac{\nu}{l_k^3} \right)^{1/5}, \quad \rho(r) = \frac{k_0 R^{4/3} \sigma^{2/3}}{l^3 \nu^{1/3} r^{3/3}},$$

where  $l_k$  is the Kuhn length and  $\nu$  is the excluded volume parameter that characterizes the polymer-solvent interaction. The thickness 'L' of the spherical polymer brush in a good solvent extending from the surface is given by (Hariharan *et al.* 1998):

$$\left( \frac{L}{R} + 1 \right)^{5/3} = 1 + k \frac{L_c}{R} \left( \frac{\sigma \nu}{l_k^3} \right)^{1/3},$$

where k is a constant.

The electrostatic interactions between the polyelectrolyte and the counterions are of long range, larger than that of monomer length.

### **Classification of brushes according to charges:**

The brushes can be classified as positively charged, negatively charged or neutral according to the charges of the constituting polymers. The charged brushes are anionic [(Polystyrene sulfonates, Polyacrylic acid), Guo *et al.* 2000, Biesalski *et al.* 2003] and cationic [(poly(ar-vinylbenzyl)trimethyl ammonium chloride, Sumerlin *et al.* 2003), Vinylbenzylamine hydrochloride (current work), Poly((2acryloyl)ethyl)trimethyl ammonium chloride (Mei *et al.* 2003), Poly(-trimethylbenzylammoniumchloride), Polyaminoethylmethacrylate hydrochloride (Sharma *et al.* 2004), quaternized polyvinyl pyridine (Biesalski *et al.* 1999, 2000)]. The uncharged or neutral polymers include hydrophobic polystyrene and hydrophilic polyacrylamide (Jones *et al.* 2002, Balamurugan *et al.* 2003). Another class of polymers is of zwitterionic polymers similar to amino acids having both the charges at different *pH* values ( {poly(3-[2-(N-methylacrylamido)-ethyl]dimethylammonio] propane sulfonate)-b-poly(N,N-dimethylacrylamide), Sumerlin *et al.* 2003}. The feasibility of generating different functionalities in brushes make their usage possible in a wide range of applications. The functionalities can be generated by using the monomer bearing the required moiety or by treating the polymer chemically after its formation accordingly. The former method gives homogeneous distribution of functionalities over the polymer whereas the latter procedure produces inhomogeneous charge distribution. The charged brushes are further classified into quenched and annealed brushes. The quenched polyelectrolytes have charges fixed along the chain, independently of the external conditions (polystyrene sulfonate and quaternized

polyvinylpyridine). For annealed polyelectrolytes, the distribution and overall fraction of charges vary according to the pH of the solution and the polymer concentration (Pincus 1991, Guo *et al.* 2001, Guenoun *et al.* 1995, 1998, Prinz *et al.* 2000).

## II.2) Synthetic techniques

Brushes are synthesized by a number of techniques such as physical adsorption, Langmuir-Blodgett technique and covalent attachment. The important brush parameters such as grafting density, stability of the brushes, thickness of the brushes and polydispersity depend on the preparatory methods. Every technique has its own advantages and disadvantages. While some techniques are better suited for synthesis at small scale, the others at industrial scale. Depending upon the application, the synthetic techniques are chosen.

**Physical adsorption** of the polymeric chains onto suitably modified surfaces produce brushes. The polymers are usually block polymers with one of the polymer having affinity to adsorb on the surface and the other to form brushes which are preferably soluble in the solvent. The structure of the resulting brushes depend on the lyophobic/lyophilic ratio of the block copolymer (Hariharan *et al.* 1998, Singh *et al.* 1994, An *et al.* 1999, Walter *et al.* 1999, Kelley *et al.* 1998). Langmuir-Blodgett technique can also be used to yield polymeric brushes from a dilute phase where the grafting density can be adjusted (Kent *et al.* 1992, 1995, de Hann *et al.* 1995). The choice of the solvent poses difficulty in this technique, as the solvent has to be non-selective for the block copolymer to be adsorbed. Otherwise micelles of block copolymers are formed which result in inhomogeneous brushes. The physically adsorbed brushes also face the problems of desorption by reversal of the charges of the adsorbing surfaces or in an environment of molecules with preferred adsorption as compared to the substrate, which causes the chains to desorb. The brushes are also thermally and solvolytically unstable. (Zhao *et al.* 2000, Currie *et al.* 1999, Prinz 2000). These disadvantages can be overcome by covalent attachment.

**Covalent attachment** can be achieved in two ways- “**grafting to**” and “**grafting from**” approaches. In “**grafting to**” approach, the functionalised polymeric chains are reacted with the suitably modified surface. The length of the polymer to be grafted can be controlled as they are synthesized before the formation of the brushes. The method has kinetic limitations as the crowding at the surface inhibits the diffusion of the chains at the surface leading to lower grafting densities (Luzinov *et al.* 2000, Jordan *et al.* 1996, Tran *et al.* 1999, 2001, Sukhishvili *et al.* 1997, Piehler *et al.* 2000).

“Grafting from” technique is described as *in situ* polymerization of the monomer on the surface of the substrate by using the immobilized initiator on the substrate. Various routes include radical (Prucker *et al.* 1998, Deboer *et al.* 2000, Meier *et al.* 1994, Uchida *et al.* 1997, Kawai *et al.* 2000, Sidorenk *et al.* 1999), anionic (Jordan *et al.* 1998, 1999, 2001) cationic (Ingall *et al.* 1999, Zhao *et al.* 1999, Jordan *et al.* 1998), ring-opening (Husseman *et al.* 1999), ring opening metathesis (Buchmeiser *et al.* 2000, Juang *et al.* 2000) and atomic transfer radical polymerization (ATRP) (Börner *et al.* 2002, Ista *et al.* 2001, Cheng *et al.* 2001, Zhao *et al.* 2000, Matyjaszewski *et al.* 1999, Kim *et al.* 2000, Wu *et al.* 2001, Von Wern *et al.* 2001, Ejaz *et al.* 1998, Huang *et al.* 1999, 2002, Husseman *et al.* 1999, Perruchot *et al.* 2001). The “grafting from” technique is better suited for the synthesis of the long and dense brushes as the diffusion of the chains is not a barrier in the synthesis. As the radicals are not able to diffuse away, the propagation step is more effective than the termination steps. Though very dense brushes are formed, the precise control over the grafting density beforehand is not possible and also the brushes formed are of high polydispersity. Living radical polymerization can be used to graft monodisperse chains where the polymerization can also be reinitiated to accommodate different monomers. So far, Habicht *et al.* have synthesized the longest brushes of polystyrene on gold by living radical polymerization where in dry brush thickness is 135 nm (Habicht *et al.* 1999).

### II.3 Spherical Polyelectrolyte Brushes

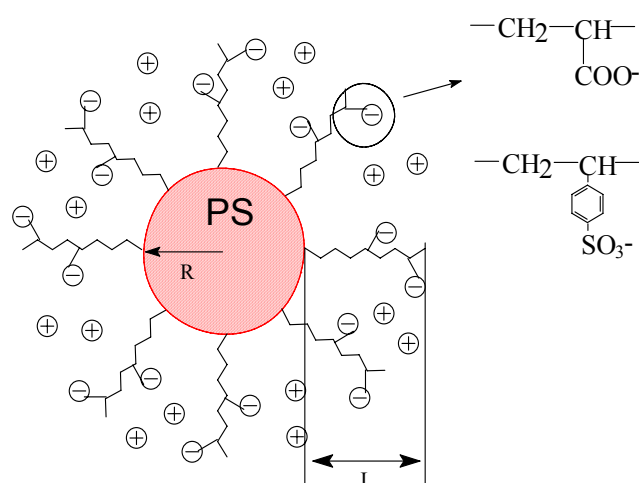


**Fig. 4** Schematic representation of spherical anionic polyelectrolyte brushes grafted onto a polystyrene surface. The grafted polymer is of polyacrylic acid or polystyrenesulfonates. The brush parameters  $R$ ,  $L$  and the grafting density depend on the synthesis (Guo *et al.* 1999).

Anionic spherical polyelectrolyte brushes (Fig. 4) have been synthesized by Guo *et al.* by “grafting from” technique. Here, polystyrene spheres provide the grafting surface and polyacrylic acid (annealed brushes) and polystyrene sulphonate (quenched brushes) form the brushes. The brush is grafted by the photoreaction of the vinyl part of the monomer with the thin shell of photoinitiator on the polystyrene surface. The brushes formed were later characterised by determining the grafting density and contour length of the grafted polymers. (Guo *et al.* 1999)

In the further research, the behaviour of the spherical brushes was studied as a function of ionic strength and pH. The brushes can shrink or swell to their maximum thickness according to the concentration of salt. For monovalent salts, there are three regimes - osmotic, for concentrations ( $ca < 10^{-5}$  M) salted, for concentrations ( $ca > 10^{-3}$  M) and beyond these concentrations, neutral regimes (Zhulina 1995, Fler 1996). In osmotic regimes, the brush thickness is independent of salt concentration and is fully swollen (Pincus 1991, Zhulina *et al.* 1994, 1995, Fler *et al.* 1996). This is due to the osmotic pressure exerted by the ions inside the brushes whose ionic strength is less than external environment. In the salted regime, the electrostatic interactions are screened and the screening increases with the increasing ionic strength. As a result, a monotonic decrease in the brush thickness is seen with increasing concentration of salt (Zhulina *et al.* 1995, Fler 1996). For divalent salts, the shrinking is much more pronounced than the monovalent salts, because of the contribution of more ionic strength from the same number of ions.

Annealed brushes e.g., polyacrylic acids have functional groups  $-COOH$ , where the degree of dissociation varies with the pH. Hence, at higher degree of dissociation, electrostatic repulsion in the chains causes them to stretch. So at high pH values the brush starts swelling. The swelling is seen between pH 3-7, as the dissociation constant  $pK$  of acrylic acid is 4.6. At low pH values, the brush is in shrunken state as the electrostatic repulsion is reduced. A plot of brush thickness vs. pH appears as “S” shaped with an elongated head, as after pH 7 the brush comes in fully swollen state (Fig. 5). The quenched brushes do not show any sensitivity towards pH as the functional groups (e.g.  $-SO_3Na$ ) have a permanent charge and hence the degree of dissociation is not dependent on the pH (Guo *et al.* 2000).

A study of the osmotic coefficient (ratio of real to ideal osmotic pressure), which is a direct measure of osmotically active counter ions, of the quenched polyelectrolyte brushes in aqueous solution is also reported (Das *et al.* 2002, Hansen *et al.* 2003). The study

demonstrates that nearly all the counterions are confined within the charged spherical polyelectrolyte brushes. The osmotic coefficient for free polyelectrolyte chains is much lower in the case of the polyelectrolyte brushes suggesting directly the trapping of counter ions in an osmotic brush predicted by theory.

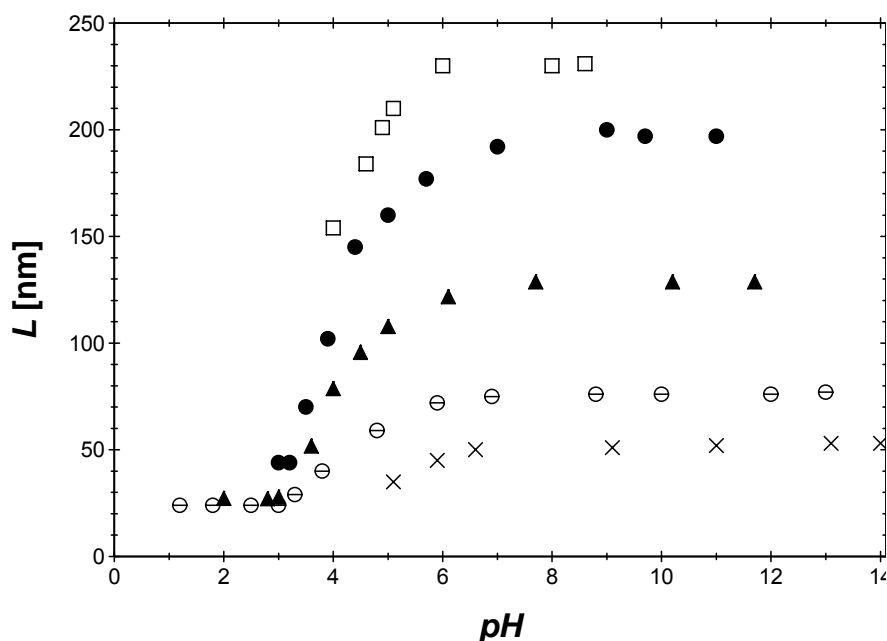


**Fig. 5** Hydrodynamic radii( $L$ ) of the annealed anionic polyelectrolyte brushes as a function of  $pH$  at constant ionic strength.  $\square$  0.0001M ,  $\bullet$  0.001M,  $\blacktriangle$  0.01M,  $\ominus$  0.01M,  $\times$  1M (Guo et al. 2001)

The present work aims at the synthesis of annealed cationic spherical polyelectrolyte brushes by photoemulsion polymerisation of cationic monomers on the spherical polystyrene latex. The annealed cationic brushes bear protonated amines as functionality. The interaction between the positive charges along the backbone of the polymers and the negatively charged metal complex ions is used to complex the metal ions in the brushes. The metal ions are confined within the brush due to the “osmotic effect” as will be discussed later. Hence, the brushes act as “nanoreactors” for the synthesis of the metal nanoparticles. The localised ions are reduced chemically to generate metal nanoparticles. The mechanism of the brushes to form the metal nanoparticles can be compared with that of the micelles, dendrimers and other nanostructured assemblies, which localise the metal ions in a similar way to generate metal nanoparticles.

The synthesis of metal nanoparticles often requires stabilizing agents like thiols and phosphorus derivatives, which passivates the surface, making them catalytically inactive. As

the particles formed by this way do not use any of these stabilizing agents, the particles are used for the heterogeneous catalysis.

## Results and Discussion

### III Synthesis of Cationic Brushes

Cationic or polybasic brushes have been formed in past by several researchers. Wesley *et al.* synthesized spherical polybasic brushes by selective adsorption of poly(methyl methacrylate) from the block copolymer Poly(methylmethacrylate)[PMMA]-poly(2-dimethylamino)ethylmethacrylate) [PDMAEMA] onto the surface of PMMA beads. As the PDMAEMA is not compatible with PMMA, only PMMA part gets adsorbed, leaving brushes of PDMAEMA, 8nm in thickness on the surface of PMMA (Wesley *et al.* 2000). Other cationic brushes include planar brushes of quaternized polyvinylpyridine (Murata *et al.* 2003, Bielski *et al.* 1999, Minko *et al.* 2002, Prinz 2000), polyethyleneimine (PEI), (Koper 2003) polypyrrole (Huijs *et al.* 2000), poly (L-glutamic acid) or poly-(L-lysine) (Hayashi *et al.* 2002), hydrophilic polymer shells containing amino groups on latexes with poly(methyl methacrylate) core (Li *et al.* 2003), electroactive brushes of polyaniline for metallization with gold and copper (Kang *et al.* 2000),  $\omega$ -primary amino functionalised polystyrenes (Kukula *et al.* 2002), poly (N, N, -dimethylacrylamide) (Jayachandran *et al.* 2002) and Poly(vinylamine) (Hughes *et al.* 1977, Lewis *et al.* 1984). Synthesis of quenched cationic brushes by photoemulsion polymerisation is achieved by Mei (Mei *et al.* 2003). The cationic brushes were further studied by AFM for their interaction with the charges of the surface.

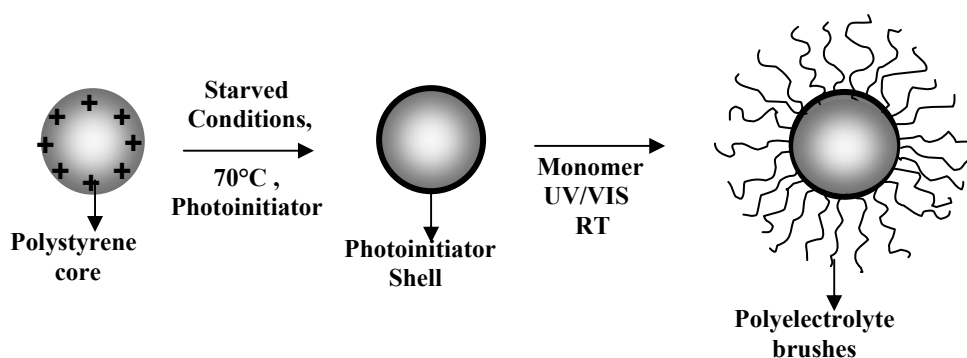


**Fig. 8** Schematic diagram showing the formation of polyelectrolyte brushes. In the 1<sup>st</sup> step polystyrene core is synthesised by emulsion polymerisation, in 2<sup>nd</sup> step photoinitiator layer is generated under starved conditions in the last stages of formation of the latex in and in the 3<sup>rd</sup> step the polyelectrolyte brushes are generated by polymerising water soluble monomer using photoemulsion polymerisation technique (Guo *et al.* 1999).

The present work focuses at the synthesis of annealed polybasic brushes by photoemulsion polymerisation. Polyvinyl amine brushes are difficult to synthesize by deprotection of the thalimide groups as discussed before, considering the mechanism of the reaction and harsh conditions of deprotection or hydrolysis for the colloid stability. A three-stage process achieves the synthesis. A thermal initiator initiates first polymerisation of styrene in presence of a surfactant by the conventional emulsion polymerisation technique. In the second stage, just before the completion for polymerisation, the photoinitiator is added under starved conditions, where the rate of addition is less than the consumption of the photoinitiator. The photoinitiator, which is also a monomer, copolymerises with the styrene to generate a closed layer of photoinitiator around the particles. In the last stage, a mixture of the latex particles and monomer to be grafted is irradiated with UV-VIS rays to cleave the photoinitiator to generate the radicals. The radicals polymerise the monomer to form the brushes on the surface of the latex particles.

### **III.1 Synthesis of cationic core particles**

In case of anionic brushes, core particles were made by emulsion polymerisation of styrene using KPS as initiator and SDS as surfactant. The initiation of polymerisation in emulsions by potassium persulfate produces a surface of negative charge with the chemical groupings, sulphate, hydroxyl and under some conditions carboxyl (Van der Hulst 1970). The polymerisation of acrylic acid and sodium styrene sulphonate on these surface produced stable latexes, but polymerisation of cationic monomers failed due to the aggregation of the latex. The aggregation started with the addition of the monomer or during the polymerisation. The phenomena can be due to the dissimilarity in the charges of core and the monomers. The synthesis of cationic brushes requires the surface of the core to be positively charged (Madaeni 2000). In earlier studies, the use of oppositely charged surfactant and initiator leads to a decrease in the rate of polymerisation and higher polydispersity (Alexander 1967).

Cationic latex can be synthesized using a cationic initiator either with or without the use of the emulsifier (Goodwin 1978). Cationic monomers such as trimethyl-ethylmethacrylate ammonium salts, dialkyl amino ethyl methacrylates, aminoalkylmethacrylate hydrochloride vinyl benzyl trimethylammonium chloride, vinyl benzyl triphenylphosphonium chloride, vinylbenzylamine hydrochloride and polymerisable soaps have been used to impart the cationic character to the latex (Delair 1994, Brouwer 1990, Sakota 1976, Cochin 1997). The water soluble initiators such as Azo bis isobutyramidine hydrochloride ABA.2HCl (Maroto 1998), azo N, N'-dimethyleneisobutyramidine

hydrochloride ADMBA.2HCl (Goodwin 1979), and oil soluble initiator 2, 2'-azobis(2-methylpropionitrile) AIBN (Ferrick 1989) have been used to synthesize cationic latexes. The use of cationic initiator generates amidine or amine groups as the chemical end groups, whereas quaternary ammonium groups can be generated by the copolymerisation with cationic monomers. The cationic emulsifiers used in the synthesis of the latexes are alkylpyridinium salts, quaternary ammonium emulsifiers, dodecyltrimethylammonium bromide, hymin and tetradecyldimethylbenzylammonium chloride (Gomez – Cisneros *et al.* 2002, Ottewill 1966). The emulsifier free polymerisation of styrene can also be carried out using a cationic initiator which results in a cationic latex stabilised by the hydrophilic part of the initiator bound to the polymer ends residing on the surface of the particles (Kazukuki 1976, Wiebolt 1998).

Hexadecyltrimethylammonium bromide/dodecyltrimethylammonium bromide and V-50 were used for the first time by Miraballes-Martinez for the emulsion polymerisation of styrene (Miraballes-Martinez 2001). The studies included the different reaction conditions for the synthesis. The variables entailed the reaction temperature, amount of initiator and the emulsifier and the chain length of the quaternary ammonium emulsifier. The increase of CTAB concentrations increased the yields and the particle sizes. The latexes produced were polydisperse because CTAB forms very stable micelles in the reaction medium. Using a concentration of CTAB below cmc  $9.5 \times 10^{-4}$ , monodisperse particles are produced but the particles are very large. The increase in the amounts of the V-50 increased the particle sizes due to the increase in the ionic strength, which induces the coagulation of the particles by compression of the electrical double layer and by changing the solubility of the emulsifier. An increase in temperature upto 90°C gave higher yields and smaller particle sizes. The increase in the temperature favours a rapid decomposition of the initiator, which increases the rate of the reaction and the yields as well. The cationic surfactants produce more stable latexes than corresponding anionic surfactants at the same concentrations (Antonietti 1991, Capek 2001, Ya Jiang Yang *et al.* 1992, Atik 1982).

In the present study, CTAB is chosen as surfactant and V-50 as thermal initiator. The concentration of CTAB used is above CMC. As discussed above, the size of the particles can be varied according the amounts of initiator and surfactant. A study is conducted to see its effect. Table 1 (See Appendix) shows the various compositions. It is evident from the table that decreasing amounts of both surfactant and the thermal initiator increases the particle size. The first composition is used for further synthesis. The decomposition temperature of V-50 is 54°C, hence the styrene polymerised at faster rate as compared to the KPS initiated

polymerisations at lower temperatures. The rate of polymerisation was determined gravimetrically. It was found the conversion is nearly complete between first 15-20 minutes after introducing the thermal initiator into the reactor. The Fig. 6 shows the rate of conversion as compared to time of the reaction.

The composition used is shown in Table 1 (See Appendix). The photoinitiator is added after 20 mins of the reaction, when the polymerization is ~95% complete. The photoinitiator is in monomeric form and insoluble in water. It reaches the oil phase, i.e., styrene on the particles and copolymerises with it. The addition is done in “starved conditions” where the rate is adjusted such that the rate of consumption is higher than the rate of addition. This ensures the formation of a complete shell. The shell thickness is typically 2nm. The particles were studied by Disc centrifuge, DLS and TEM. The Fig. 7 shows the TEM images of the particles after the emulsion polymerization.

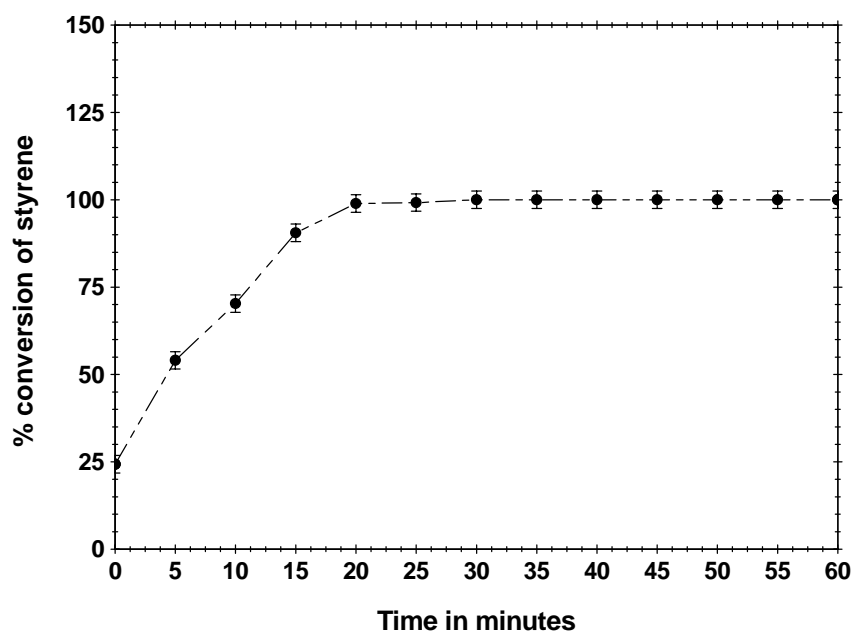


**Fig. 6** Synthesis of latex particles. Conversion of styrene is plotted as a function of Time/min after the addition of thermal initiator. Conversion is complete after 20-25mins after which it remains constant. Conversion is calculated by measuring the solid content after every 5 minutes. Zero time is taken just after the addition of the thermal initiator. (Composition: 2 mol styrene, 14.58 mmol CTAB, 3.234 mmol, and 47 mol water). The particle size of the core obtained is 40 nm in radius.

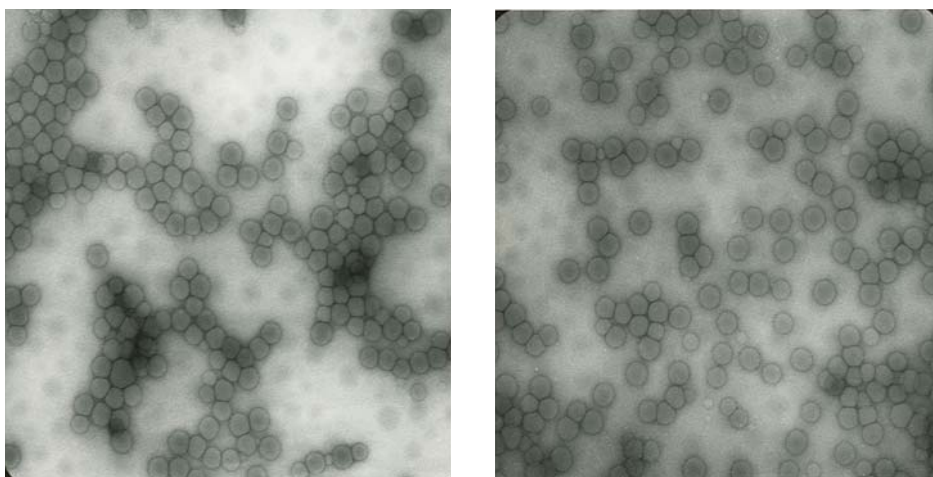


*Fig. 7 Transmission electron microscope images of core particles*

### **III.2 Synthesis of cationic brushes by photoemulsion polymerisation**

The core particles formed as discussed in last section were cleaned before photoemulsion polymerisation. The surfactant added during the polymerisation resides on the polystyrene particles and has to be removed. The cleaning is done by ultra filtration or dialysis. The cleaned core is diluted as to give 2.5% of solid content and then charged into the reactor with the monomer. The brush is grafted by the photoreaction of the vinyl part of the monomer with the thin shell of photoinitiator on the polystyrene surface (Fig. 8). The layer of photoinitiator was generated during the last stages of polymerisation under “starved” conditions. The photoinitiator 2-[p-(2-hydroxy-2-methylpropiophenone)]-ethyleneglycol-methacrylate (HMEM) copolymerises with the styrene, as the photoinitiator is added in last stages, the photoinitiator shell is formed on the surface of the spheres.

The core particles with photoinitiator on the surface were charged in the photoreactor with the monomer to be polymerized on the surface. Water is used as solvent. The photoemulsion polymerisation is carried out in suspension, which scatters radiation elastically. The UV light, which is not directly absorbed by the particles, undergoes multiple scattering and is absorbed later by other particles. As the scattering is elastic, the scattered radiation is also capable of triggering the photoreaction (Fig. 9).

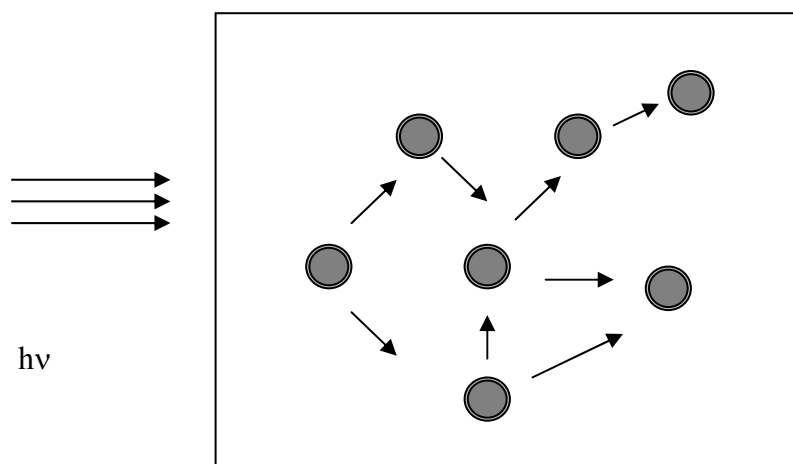


**Fig. 9** Schematic representation of Photo emulsion polymerisation in latex medium. The UV/VIS light is strongly scattered in the turbid medium. As the scattering is elastic in nature, the radiation, which is not absorbed directly, is able to start photo initiation after scattering (Guo et al. 2000).

The photoinitiator decomposes into the fragments, one held on the core particle and the other escapes into the solvent. These radicals combine with the radicals generated by the monomers (Fig 10). The monomer also polymerises with the radical formed in the solvent, so half of the monomer is polymerised in the solvent.

At higher concentrations, there exists a finite probability of the two latex particles combining and forming aggregates. Hence, the effective volume fraction was kept low at about 2.5%. Dynamic light scattering monitored the progress of the reaction. The size of the particles grows with time with becoming constant after the completion of the reaction.

The polydispersity of the core particles was determined by disc centrifuge. Narrowly dispersed particles were chosen for further synthesis. The brushes formed were later characterised by finding the grafting density and contour length of the grafted polymers. The grafted polymer was cleaved at the ester bond by alkaline hydrolysis. The cleaved polymer was characterised by GPC and viscosimetry. The molecular weight determined was used to determine grafting density and contour length (Table 2, See appendix). The brush thickness was found to be dependent on the amount of initiator used and the amount of monomer used. The increasing amounts of photoinitiator also increase the brush thickness because of the stretching of the chains due to the steric effects.

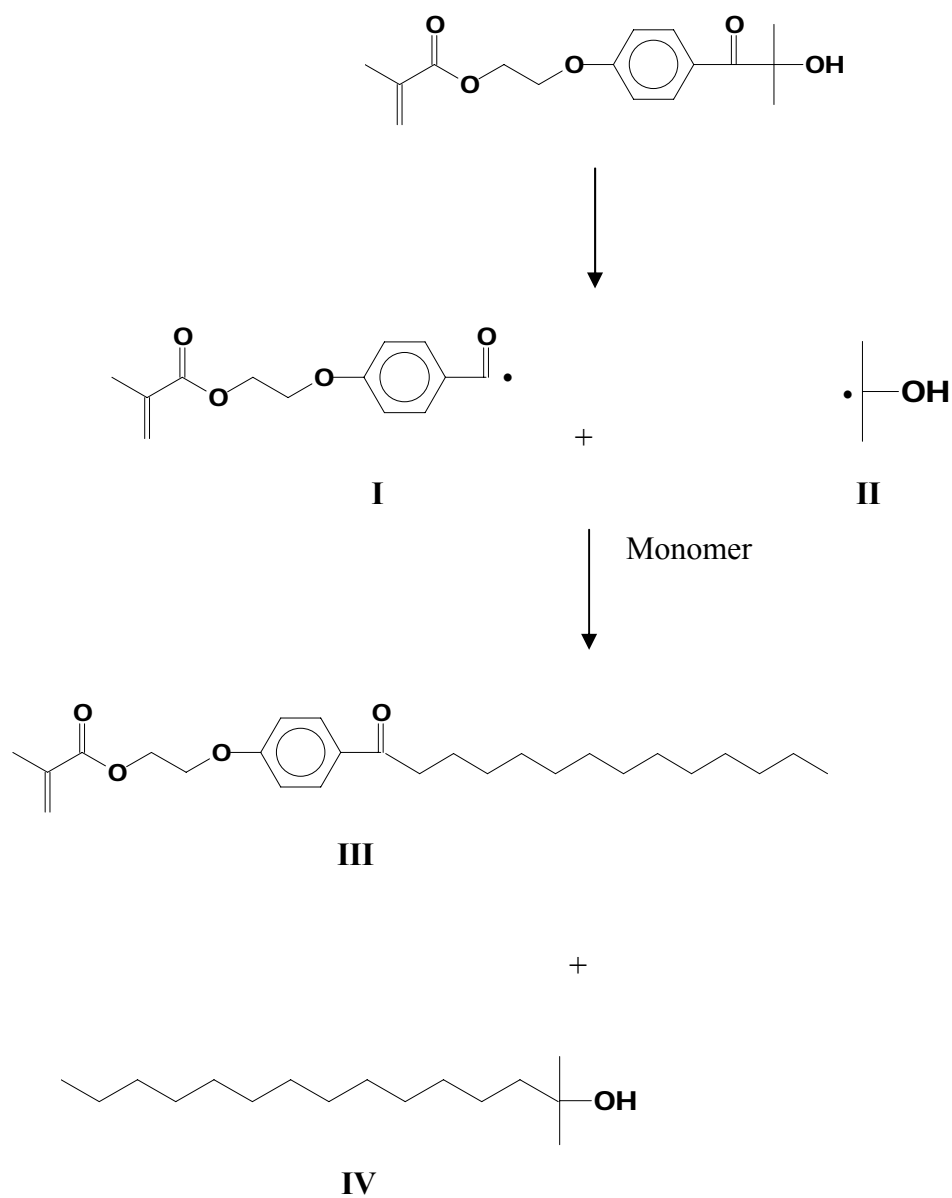


**Fig. 10** Decomposition of photoinitiator HMEM into radicals during photoinitiation by UV/VIS radiation. The polymerisation starts at both the radicals I and II. One half of the monomer polymerising with each radical resulting in the structures III and IV, III is bound to the polystyrene core and structure IV ends up in the solvent.

### III.3 Synthesis and characterization of AEMH brushes:

The monomer is a protonated form of amine as the functional group (Fig. 11). It is freely soluble in water. It is synthesized by the reaction of ethanolaminehydrochloride and methacryloylchloride in ethanol (See experimental section).

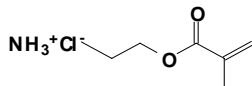


**Fig. 11** Chemical structure of aminoethylmethacrylatehydrochloride (AEMH)

Brushes are grafted on the polystyrene surfaces by photoemulsion polymerisation as described in the last section. The reaction is triggered by UV irradiation (wavelength 200-600 nm), which generates radicals of HMEM by photoemulsion polymerisation. These radicals start radical polymerisation of the monomer. The mixture of diluted core particles and monomer is charged into the photoreactor. The solid content is adjusted at 2.5% as discussed above. The radical polymerisation follows, which can be followed by measuring the hydrodynamic radii of the particles by DLS at regular intervals. The monomer concentration is used from 10 mol% to 100 mol% depending on the desired brush length. Reaction is carried out in an inert environment to rule out the possibility of radical recombination with oxygen molecules.

The rate of polymerisation of AEMH monomer was very fast as compared to anionic brushes (acrylic acid, sodium styrenesulfonates) and quenched cationic brushes poly (2-acryloyl)ethyl)trimethylammonium chloride. The brushes grew to their maximum after only 60 minutes, after which no substantial increase was observed. The brush thickness depends on the amount of photoinitiator used, the amount of monomer and the cleaning of polystyrene core. The dependence on the photoinitiator concentration and amount of monomer has been studied for anionic brushes by X. Guo (Guo *et al.* 2000). The increasing amounts of monomer increased the length of brushes as a result of more number of units available for the polymerisation. The usage of monomer concentration more than 60mol % shows a drastic decrease in the brush thickness possibly due to recombination of radicals. The increase in the photoinitiator concentration increased the number of radicals formed per unit area. Hence the number of chains per unit area increased with the same monomer concentration, which caused more stretching of the chains by virtue of increased mutual repulsion. The studies conducted by Guo *et al.* also emphasised the importance of presence of photoinitiator. Reactions done in the absence of photoinitiator do not give any increase in the hydrodynamic radii even when the amount of monomer was high.

### Effect of Photoinitiator (HMEM) concentration on AEMH brushes:

The photoinitiator are of many types and the yield of the polymerisation depends on the mechanism of the radical generation. Photoinitiators can be categorised by the mechanism they produce radicals. The radicals can be produced via dissociative mechanism, hydrogen abstraction or ARTP mechanism to give living polymerisation. X. Guo has studied three types of photoinitiators- 2-[p- (2-hydroxy-2-methylpropiophenone)]-ethyleneglycol-methacrylate (HMEM), benzoin acrylate and 4-acryloxybenzophenone (ABP). HMEM and BA split upon irradiation of UV-VIS irradiation into two radicals initiating the polymerisation reaction (Salamon 1996, Foussier *et al.* 1995, 1986, Carlini *et al.* 1986, 1983, 1995). HMEM have been found to be the most suitable photoinitiator because of its good solubility in acetone, which gives a control to adjust its concentration for the synthesis. As observed before in case of anionic brushes, increasing the photoinitiator quantity also increases the thickness of the grafted brush.

The usage of more photoinitiator starts growth of more number of chains in the same area, which in turn increases the stretching of the brushes (Fig. 12). The maximum concentration of the photoinitiator used was 4 mol %, above which no further increase was observed as only the upper layer of photoinitiator was available for the reaction. As expected, there were no results by carrying out the reaction without the photoinitiator.

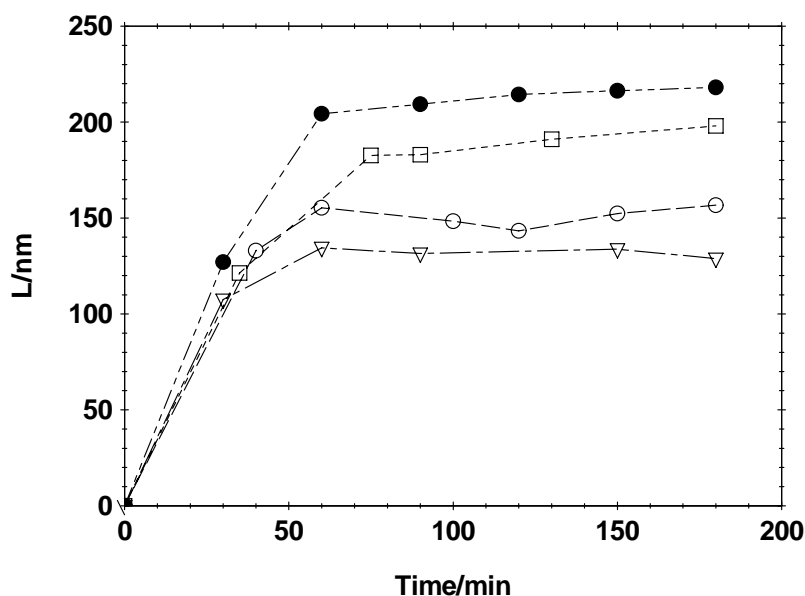


**Fig. 12** Brush Thickness  $L/nm$  (hydrodynamic radii) as a function of  $t$  time/min. Different curves show the effect of changing the amount of photoinitiator at constant monomer concentration. The brush thickness increases with increase in photoinitiator concentration due to more stretching of the chains as the crowding increases. Photoinitiator concentration: (●) 4%, (□) 1%, (○) 1.5%, (▽) 0.5%.

**Effect of Monomer concentration and gel formation:** Increasing amounts of monomer increased the brush thickness, as expected due to more number of monomer units available. Usage of more than 30 mol % of monomer increased the viscosity of the latex, which may be due to the formation of gel structure in the latex (Fig. 13). The latex shows very high viscosity. The phenomenon can be attributed to the structural effects due to the presence of quaternary charged ammonium group and the carbonyl group. The interaction of carbonyl oxygen s and the hydrogen bound to the nitrogen can give rise to the H-bonding which may be responsible for the gelation of brushes (Fig. 14). Similar gelling is reported for the microgel of poly (N-isopropylacrylamide) and polyacrylic acid (Xia *et al.* 2004).

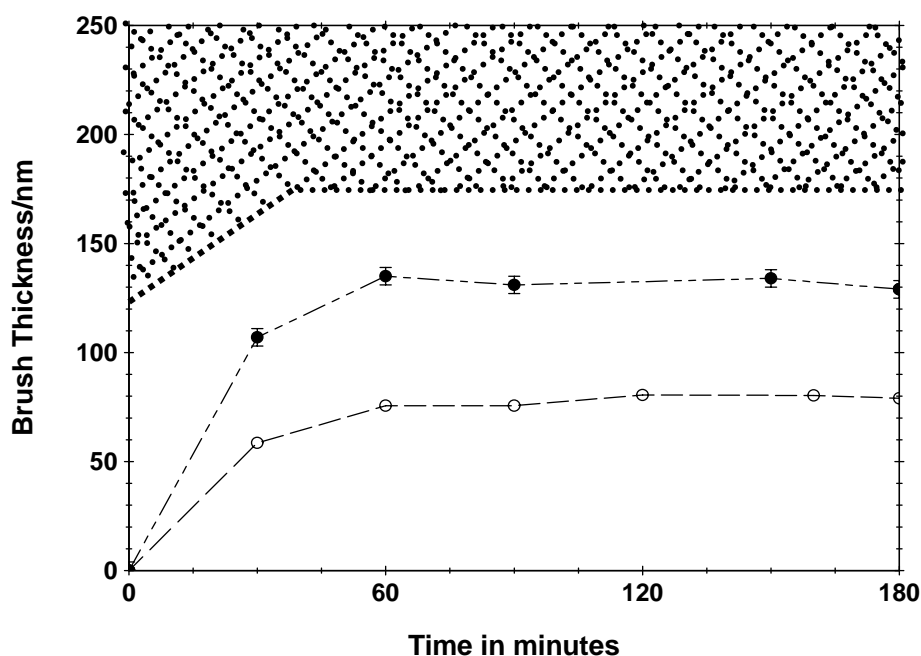


**Fig. 13** Brush Thickness  $L$  (hydrodynamic radii) as a function of time  $t$ /min as determined by dynamic light scattering. The different curves show the effect of monomer concentrations on the final thickness of the brushes. The network of dotted line shows gelation effect at higher monomer concentrations. Monomer (AEMH) concentration (in mol%) is different the curves. Core radii- 40 nm (●) - 20%, (○) – 10%.

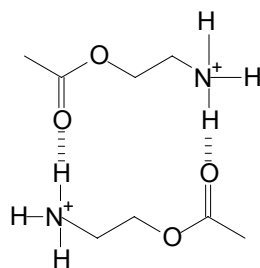


**Fig. 14** Predicted hydrogen bondings in the brushes of polyAEMH resulting in the gelation effect at higher monomer concentrations

This phenomenon is not observed in case of anionic brushes or other cationic quenched brushes like poly ((2-acryloyl) ethyl) trimethylammonium chloride and Poly (trimethylbenzyl ammonium chloride), which were synthesized by same techniques.

In case of anionic brushes, up to 60 mol% of acrylic acid and sodium styrene sulphonates were used without any gelation being observed. Using monomer concentration above this level decreases the brush length drastically due to radical recombination contrary to the results obtained in the current studies. In case of quenched brushes, synthesized by Mei *et al.* the monomer concentration was used more than 100 mol %. The formation of gel is reported in past but at higher concentrations of monomers (Pawlowski *et al.* 2003).

At higher pH, the structure of the gel is destroyed and the latex is coagulated as the charges of the gel are destroyed. Cleaning of latexes played a vital role in the brush thickness. The presence of surfactant reduced the grafting density and increased the brush thickness. Uncleaned latex gave a gel even with small quantities of monomer used at low effective volume fractions, whereas the cleaning of the same core to different extent gave different brush lengths.

### III.4 Characterization:

Important parameters to be determined in the core-shell system are the core radius, contour length ( $L_c$ ), and the grafting density of the brushes. The size of the core particles and the thickness of brush are determined by Dynamic Light Scattering.

#### Contour length:

In “grafting to” process, in contrast to “grafting from“ process, the polymers to be grafted are already characterized. To determine the contour length of the polymer grafted in the “grafting from” technique, the polymer has to be cleaved from the surface. It is done by hydrolysis of

the ester bond, which is formed during the initiation of polymerisation by the radicals of the photoinitiator on the surface (Fig 15).

The hydrolysis of the ester bond is achieved with 2M NaOH at 120°C for 20 days. The system contains two types the ester bonds, one in the photoinitiator and another in the polymer. During the hydrolysis, both of these ester bonds are hydrolysed, resulting in coagulated latex particles with residual photoinitiator, polymeric chains of polymethacrylic acid and molecules of protonated ethanolamines. The mixture is centrifuged at 20000 rev/min for 3 hours. The latex is separated from the polyelectrolytes and small molecules. The polyelectrolyte is then ultrafiltrated through regenerated cellulose of 5000 dalton cut off to obtain polymethacrylic acid. The amount is determined gravimetrically after drying. The polymer was analysed by MALDI (Matrix assisted laser desorption Ionisation) to confirm the complete hydrolysis of the ester bonds.

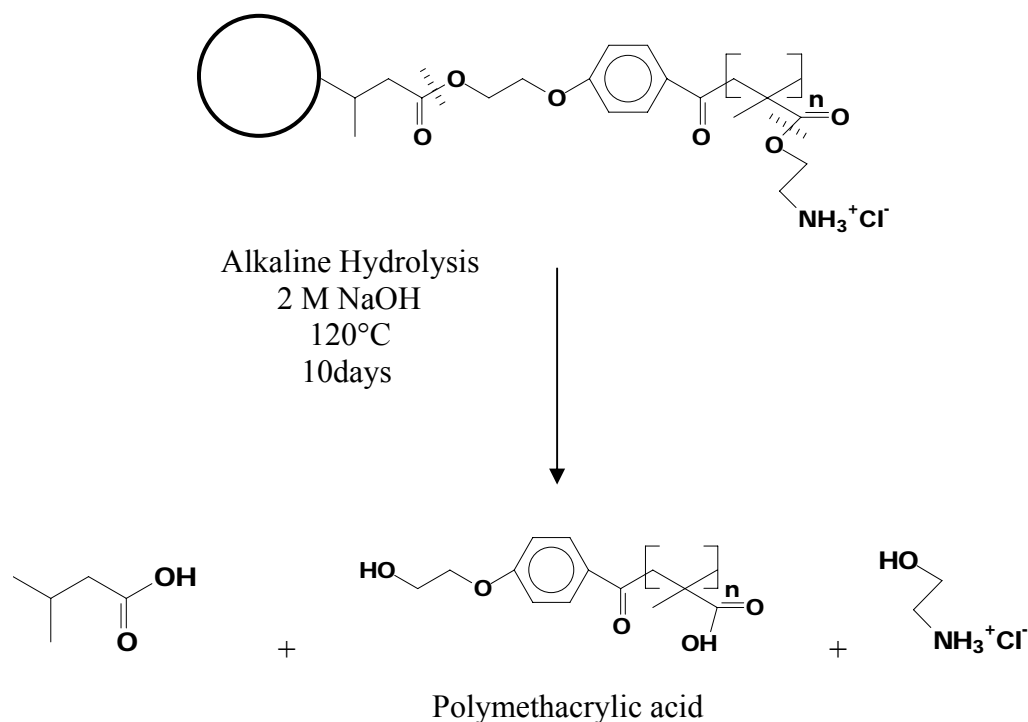


**Fig. 15** Cleavage of brushes from the grafting surface by alkaline hydrolysis. The strong basic environment hydrolyses the ester bond at the grafting point and of the monomer unit to result in the formation of polymethacrylic acid. The contour length of the polymethacrylic acid corresponds to the grafted polymer.

The molecular weights are determined by viscometric methods (Ubbelohde viscometer). The viscosity average molecular weight is determined by the intrinsic viscosity of the polymers with the Mark-Houwink relation:

$$[\eta] = KM_{\eta}^a$$

Where  $M_{\eta}$  represents the viscosity average molecular weight of polymethacrylic acid in 2M  $\text{NaNO}_3$ . At  $25^{\circ}\text{C}$ ,  $K = 4.49 \times 10^{-4}$  ml/g and  $a = 0.65$  (Arnold *et al.* 1955). The viscosity can also be determined in 0.002N HCl at  $30^{\circ}\text{C}$ . The Mark-Houwink constants are  $K = 6.6 \times 10^{-4}$  ml/g and  $a = 0.5$  (Brandup *et al.* 1989). It has been shown by the previous studies that the standard polymers on being given the same treatment of hydrolysis do not degrade. The contour length  $L_c$  can be obtained by dividing the molecular weight by the effective bond length 0.252 nm (C-C bond length) per repeat unit of the monomer.

### **Grafting density:**

The amount of the monomer grafted on the core latex particles can be determined by direct titration on the core shell particles with a standard solution of  $\text{AgNO}_3$ . The  $\text{Ag}^+$  forms insoluble salt  $\text{AgCl}$  with the chlorides of the monomers. The titration is followed by conductivity methods. The latex should be completely cleaned by serum replacement to remove the polyelectrolytes formed in the serum. Table – 2 summarises the characteristics of the systems synthesized. The distance between the two grafted points is smaller than the hydrodynamic radii of the polymeric chains, hence the chains are stretched to their maximum to avoid the overlap.

Grafting density increases with the increased amounts of photoinitiator as more grafting points are generated. The contour length increases with increasing amounts of monomer. The grafting density is reduced drastically in presence of the surfactants as the photoinitiator layer is covered with the surfactant. The contour length decreases and the grafting density increases with cleaning of the core. As discussed earlier, the concentration of monomers more than 30% to that of the polystyrene amount leads to formation of the gel.

| Latex | R(nm) | HMEM(%) | AEMH(%) | M $\eta$ (g/ml) | $\sigma$ (nm <sup>2</sup> ) | Lc(nm) | D(nm) |
|-------|-------|---------|---------|-----------------|-----------------------------|--------|-------|
| S1    | 42    | 0.5     | 30      | 50,000          | 0.037                       | 75     | 5.8   |
| S2    | 40    | 0.5     | 10      | 62,000          | 0.014                       | 93     | 9.5   |
| S3    | 47    | 1.5     | 20      | 1,00,000        | 0.017                       | 149    | 8.6   |
| S4    | 42    | 0.5     | 20      | 95,000          | 0.016                       | 142    | 8.9   |
| S5    | 55    | 4       | 20      | 1,15,000        | 0.018                       | 171    | 8.4   |
| S6    | 40    | 1       | 20      | 1,00,000        | 0.017                       | 147    | 8.6   |
| S7    | 42    | 2       | 20      | 1,00,000        | 0.018                       | 152    | 8.4   |

**Table 2:** Characteristics of the AEMH brushes synthesized

*R = radius of core*

*M $\eta$  = Viscosity average molecular weight of methacrylic acid*

*HMEM(%) = Amount of photoinitiator (HMEM) used in molar percent of styrene used for the synthesis of cores latexes.*

*AEMH(%) = The amount of added AEMH (monomer) in molar percent of styrene used for synthesis of core latexes.*

*$\sigma$  = Grafting density of the chains on the surface*

*D = The average distance between two neighbouring grafted points*

*Lc = Contour length of the methacrylic acid*

### III.5 Brushes of Vinylbenzylamine hydrochloride (VBAH)

The rate of polymerisation of VABH was not so high. As seen from the Fig. 16, the reaction was not complete even after 210 minutes. As the synthesis of this monomer is tedious, most studies were conducted by the brushes of AEMH.

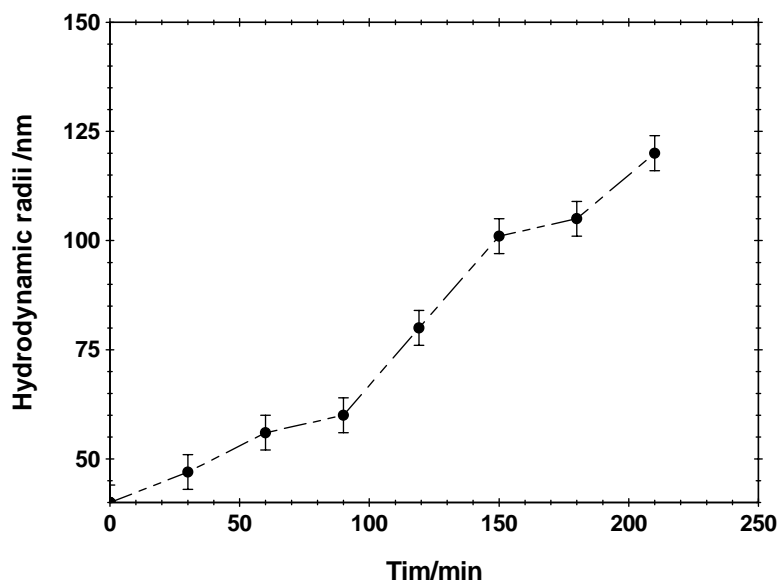


**Fig. 16** Brush Thickness  $L/nm$  (as measured by hydrodynamic radii) as a function of time  $t/min$  for the monomer Vinylbenzylamine hydrochloride (VBAH). The reaction not complete even after 210 minutes as the brush thickness goes on increasing showing any constant value. The core radius used is 40 nm. Monomer concentration used is 30 mol% of the polystyrene. Photoinitiator concentration is 2 mol%.

### III.6 Synthesis of polyvinylpyridine brushes:

Vinyl pyridine is a weak base with negligible solubility in water. The polymer is soluble only in very polar solvents like alcohol, DMF, benzene or in acidic water. The alkyl halide quaternized polyvinylpyridine is soluble in aqueous solutions. There are reports of polymerisation of vinyl pyridine in ethanol (Akin *et al.* 1992). Planar polyvinylpyridine brushes has been synthesized by Rhe *et al.* in benzene using self assembled monolayers of an azo initiator on the surface of the substrate (Kawaguchi *et al.* 1999, Kawaguchi *et al.* 1998, Bielaski *et al.* 2002). The polyvinylpyridine can be quaternized or can be made to complex with cupric ions in ethanol–water mixtures (Acar *et al.* 2001).

The photoemulsion polymerisation technique uses water soluble monomers for the synthesis of brushes. The resulting latexes are highly stable due to charged surface of the latexes, which are hydrophilic. But for the water insoluble polymers like polyvinylpyridine the photoemulsion polymerisation gives a hydrophobic surface to the latexes which results in the aggregation of latex due to phase separation of polyvinylpyridine and water phases. The protonation of the monomer first and then polymerisation does not work due to the self-polymerisation mechanism of the protonated monomers. Charge transfer complexes of pyridinium ions act as charged photoinitiator for the polymerisation (Hizal *et al.* 1994). It is an acid catalysed polymerisation.

The above problem can be solved by using a mixture of alcohol: water mixture in the ratio of 92.8 % alcohol: 7.2 % water. Polyvinylpyridine is soluble in the mentioned mixture at 25°C. The latex before photoemulsion polymerization was diluted to 2.5 wt% by absolute alcohol to adjust the ratio as discussed. The polystyrene latexes showed swelling in ethanol. This has been reported in past (Rubio-Hernandez 1994). Vinyl pyridine was dissolved in the diluted latex and the mixture was charged in the photoreactor to give the polyvinylpyridine brushes (Fig. 17). The brushes formed are sensitive to temperature.

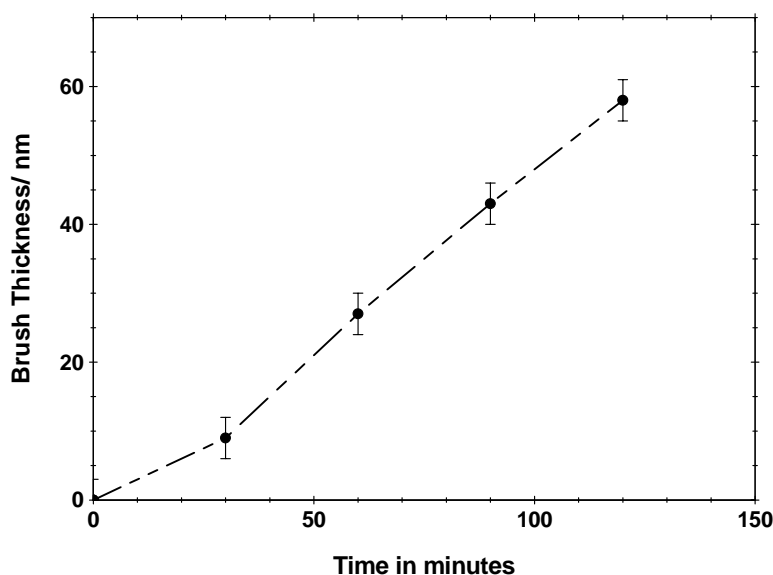


**Fig. 17** Brush thickness/nm as a function of time/min: Hydrodynamic Radius of core: 58 nm, Hydrodynamic radius of brush: 72 nm (In ethanol). Photoinitiator-Benzoin acrylate (1mol%), Solvent-92.8: 7.2 Ethanol: water, Vinyl pyridine concentration in mol% of core amount-30%. The reaction is not complete as a constant value of brush thickness is not reached. The rate of polymerization is slow as compared to other anionically or cationically charged monomers.

### **Effect of photoinitiator concentration and solvent strength**

As observed previously (See page 19), the brush thickness varies with the amounts of photoinitiator and monomer concentration used. Fig. 18 shows the effect of photoinitiator concentration. Increase in the photoinitiator concentration increases the brush thickness considerably, though the reaction is not complete in either of the curve. The increase can be attributed to the effects of stretching of the chains on increasing the photoinitiator concentration as discussed in previously. In addition to these factors, the brush thickness also depends on the ratio of ethanol to water in the solvent. As the ethanol content of the solvent goes down, the brush thickness also reduces as shown in Fig 19.

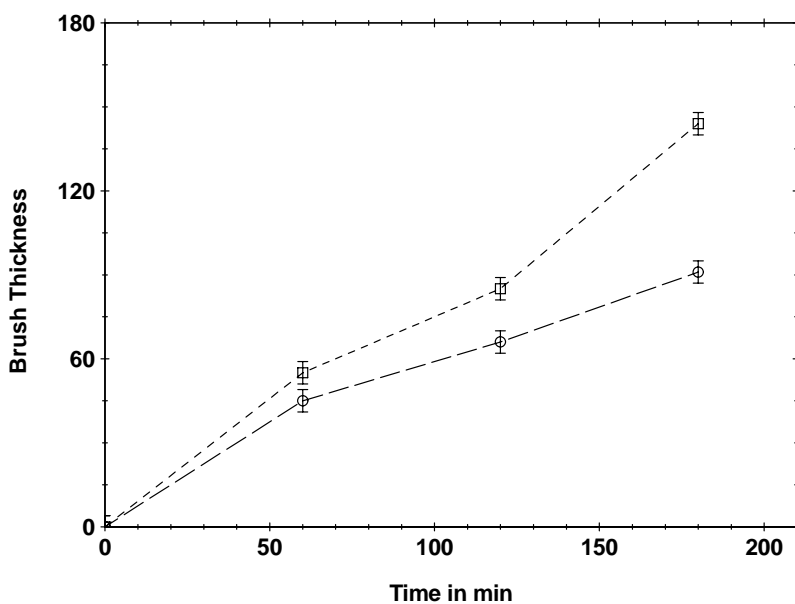


**Fig. 18** Brush thickness/nm as a function time. The variable parameter in the two curves is the photoinitiator concentration.

Solvent: 85% ethanol /H<sub>2</sub>O, Monomer: 60% VP, Hydr. Rad.: 45nm (In H<sub>2</sub>O), Hydr. Rad.: 80nm (In Ethanol) (○)- 0.5% HMEM, (□)- 1% HMEM

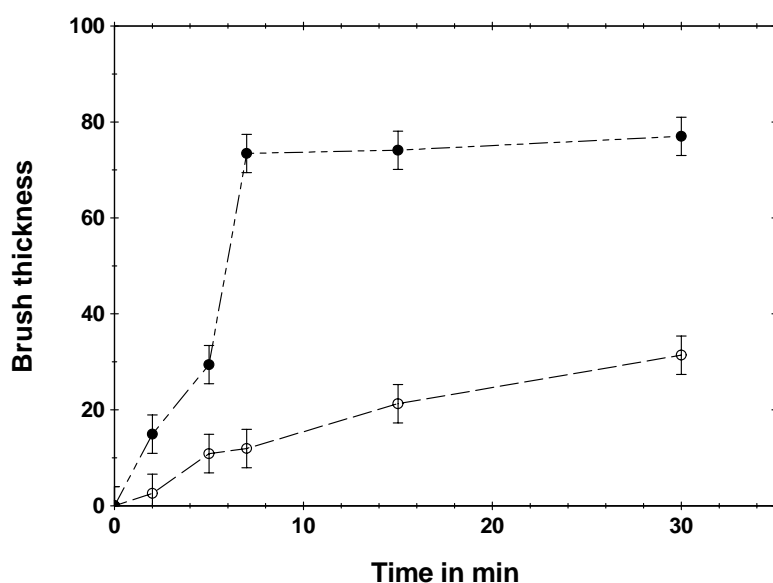


**Fig. 19** Brush thickness/nm as a function of Ethanol/water ratio. As seen from the curves, the polymerisation rate and the brush thickness depends on the solvent strength. Decreasing the strength of the solvent decreases the final brush thickness keeping the other experimental conditions same. The phenomenon can be due to the different conformations of the polymer in  $\theta$  solvent conditions.

(○)- 80:20, (●) 92.8:7.2, Monomer: 60% VP, Hydr. Rad.: 40 nm (In H<sub>2</sub>O), Hydr. Rad.: 78 nm (In ethanol) Photoinitiator: 0.5% HMEM

#### IV Behaviour of spherical cationic brushes

Besides grafting density  $\sigma$  and the contour length  $L_c$ , the geometry of the grafting surface becomes an important parameter for the spherical brushes as the  $R$ , radius of the grafting surface also becomes important parameter to define brush characteristics.

As discussed earlier (See Section II.3), the theoretical studies of the spherical polyelectrolyte brushes are modelled by Hariharan *et al.*, by extending the model of Daoud and Cotton model for neutral brushes. The model is validated by the experimental data by Guo *et al.* for anionic brushes the brush thickness  $L$  of the spherical brush in a good solvent extending from the surface is given by:

$$\left(\frac{L}{R} + 1\right)^{5/3} = 1 + k \frac{L_c}{R} \left(\frac{\sigma \nu}{l_k^3}\right)^{1/3}$$

(Biver *et al.* 1997, Hariharan *et al.* 1998), where  $k$  is a constant.  $l_k$  is the Kuhn length and  $\nu$  is the excluded volume parameter that characterizes the polymer-solvent interaction. The brush thickness is dependent on ionic strength, pH and solvent strength.

##### IV.1 Effect of ionic strength

Planar as well as spherical brushes are investigated theoretically and experimentally as a function of salt concentration (monovalent and multivalent) and solvent quality. The systematic experimental studies on the spherical anionic brushes have been done by Guo *et al.* to see the effect of monovalent and divalent ions (Guo *et al.* 2000, 2001). Fig. 20 shows the behaviour of poly (AEMH) brushes in presence of a monovalent salt NaCl. Poly (AEMH) brushes are annealed brushes, which can deprotonate at high pHs. The hydrodynamic radius of the brushes is plotted as a function of added salt concentration  $C_a$  (Fig. 20). The ionic strength of the purified water assumed to be  $10^{-7}$  M. As can be seen from the curve, the brush thickness decreases with increasing salt concentration. The curve can be divided into three parts the osmotic regime, the salted regime and the neutral regime. As seen from the curve, in osmotic regime the brush is fully swollen, in salted brush regime the brush thickness starts to decrease with increasing salt concentrations. In neutral regime, the brush behaves like a neutral brush. Pincus and Zhulina have theoretically studied the discussed behaviour of the polyelectrolyte brushes in terms of electrostatic interactions (Pincus 1991, Zhulina *et al.* 1994, 1995, Fler 1996).

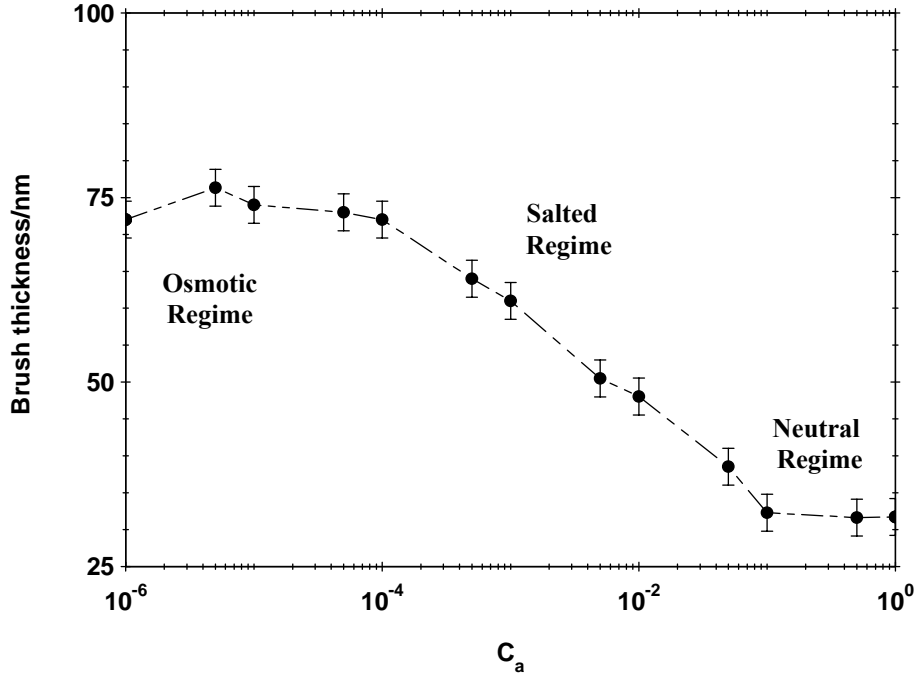


**Fig. 20** Brush thickness  $L$  (Hydrodynamic radii) of poly (AEMH) brush as a function of NaCl concentration  $C_a$  in aqueous solution. The three brush regimes- Osmotic, Salted and neutral are depicted in the Fig..

At very high salt concentration, the electrostatic interactions are totally screened, the ionic strength outside and inside of the brush are the same. The brush behaves like a **neutral brush** (Zhulina *et al.* 1995, Fler 1996).

$$L \propto N(v\sigma)^{1/3}$$

Where  $L$  denotes the thickness of brush,  $N$  the number of statistical segments of a polyelectrolyte chain and  $v$  the excluded volume parameter. At  $C_a > 10^{-3}$  M and higher, the thickness decreases monotonically with the addition of the salt due to the screening of electrostatic interactions by salt. This is **salted brush regime** (Zhulina *et al.* 1995, Fler 1996). Although the electrostatic interactions are still screened, they become comparable to the excluded volume interactions. Resulting from electrostatic interactions, the excluded volume parameter  $v$  for a neutral polymer in equation is replaced by the volume parameter

$$v_e = 4\pi l_p \kappa^{-2}$$

Or

$$v_e \propto c_a^{-1}$$

The thickness of the brush is given by

$$L \propto N(v_e \sigma)^{1/3} \propto N \sigma^{1/3} c_a^{-1/3}$$

In this region, the brush thickness will increase monotonically with decreasing of external salt concentration. Below  $C_a < 10^{-5}$  M, the brush length shows no dependence on the salt concentration showing the *Osmotic brush regime* (Pincus *et al.* 1991, Zhulina *et al.* 1994, 1995, Fler 1996). If the salt concentration is further decreased, such that the local ionic strength inside the brush becomes noticeably different from their bulk values, it leads to the transition from salt brush to osmotic brush. Here, due to the Donnan effect the mobile co-ions are expelled from the brush and the counterions are mainly confined inside the brush, and the electrostatic interactions are effectively described in terms of the osmotic pressure of the trapped counterions. The concentration of the counterions inside the brush is equal to that of the immobilized charge of the grafted chains, and thus the brush becomes electroneutral as a whole. The brush thickness is determined from the balance between the osmotic pressure of the mobile ions inside the brush  $\Pi$  and the elastic force arising in the stretched chains  $F_{el}$ . The osmotic pressure can be expressed as

$$\Pi \propto \frac{\alpha \sigma N}{L}$$

Where  $\alpha$  is the average charged degree of the polyelectrolyte chains and the elastic force per unit chain.

$$F_{el} \propto \sigma L / N$$

The force balance is given by

$$\Pi = F_{el}$$

Thus, the thickness of brush  $L$  scales as

$$L \propto N \alpha^{1/2}$$

The thickness of the brush is independent of the added salt concentration  $C_s$  and the grafting density  $\sigma$ .

## IV.2 Effect of pH:

In annealed brushes, the functional groups are as such which can be ionised or deionised with pH change. Examples include brushes of polyacrylic acid, polyamine brushes. The brushes in charged state stretches completely because of the electrostatic repulsion. In uncharged brushes electrostatic repulsion is reduced which causes brush to shrink as shown in Fig. 21. On the other hand the “quenched brushes” have fixed charges, these are not affected by the pH change, hence in full range of pH the brushes is fully stretched. Guo *et al.* conducted pH studies on polyacrylic acid brushes. The brushes swelled at high pHs due to ionisation of the

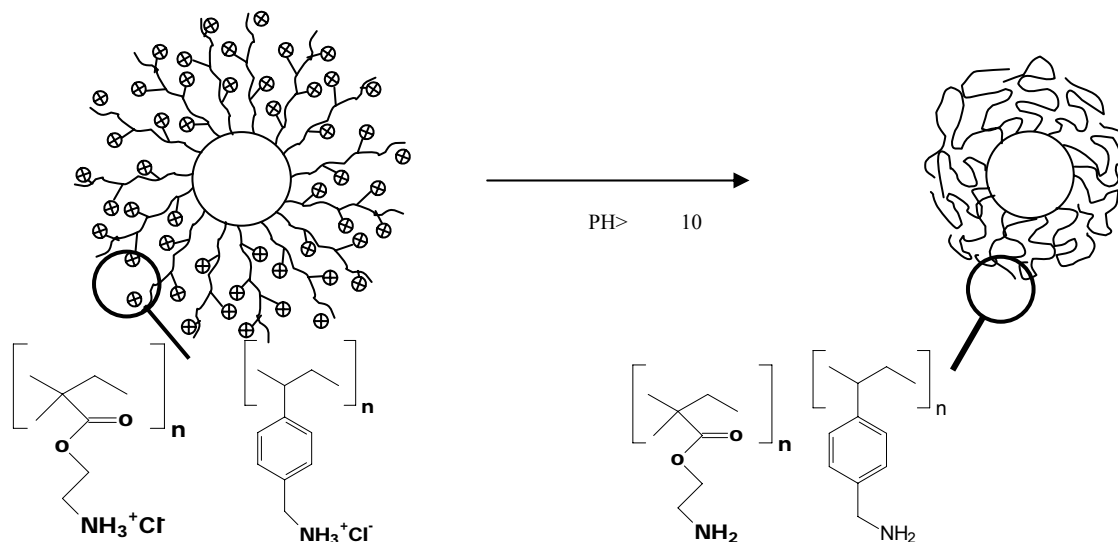


**Fig. 21** Deprotonation of polyAEMH and polyVBAH brushes at higher pHs. The charged brushes lose protons to result in shrunken uncharged brushes due to the loss of electrostatic repulsions of the charges.

carboxylic groups, which led to increased electrostatic repulsions. The swelling was reported between 3 to 7 pH. The protonation of primary groups is determined by potentiometric titration by G. Koper for the comb like brushes of polyethyleneimines (Koper et al 2003). The pKa's of primary amine were observed to be around 10.3 but the primary amine groups were protonated at pH around 9.5, secondary and tertiary group protonate at around 4.5 and less than 1 respectively. The pK of the amines groups in the discussion are shown to be dependent on the ionic strength. The pK increase with ionic strength with for the primary and secondary groups. The protonation of tertiary groups could not be detected so accurately.

Fig 22 shows brush thickness  $L$  as a function of pH. The latex was titrated at constant ionic strength. To maintain constant ionic strength was necessary to eliminate the effect of screening of electrostatic interactions. The titration was done by standard solution of NaOH against standard solution of HCl. The ionic strength was adjusted by adding precalculated amount of NaCl. The brush thickness was determined by observing the hydrodynamic radii by DLS. The Fig. 22 and shows effect of pH on poly (AEMH) and Fig. 23 on the poly (VABH) brushes. The amine groups are both primary but the pKa of poly-(AEMH) is higher than that of poly-(VBAH). This can be due to the ester functionality present in the poly-(AEMH) groups. The ester functionality may form H bonds with the protons of other chains and hence may require higher pH than poly-(VBAH) to deprotonate. The pK is approximately 10 and 8.5 for poly (AEMH) and poly (VBAH) respectively as detected by the mentioned titration.

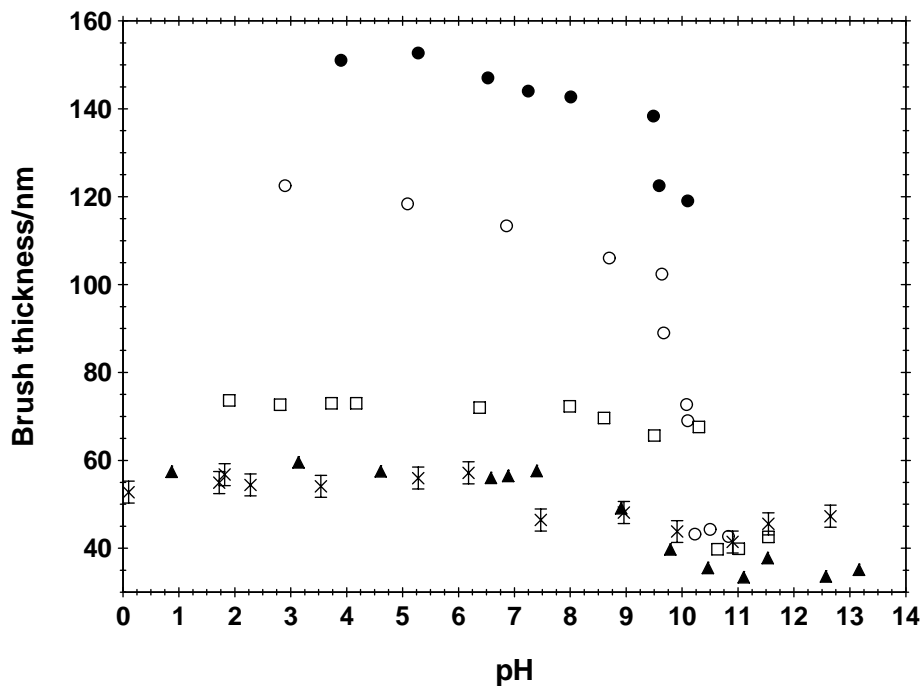


**Fig 22** Thickness of poly (AEMH) brushes as a function of pH at different ionic strengths. Each curve is at a constant ionic strength. A sharp decrease in brush thickness is observed at pH around 10. (x) 1M; (▲) 0.1; (□) 0.01; (o) 0.001; (Δ) 0.0001

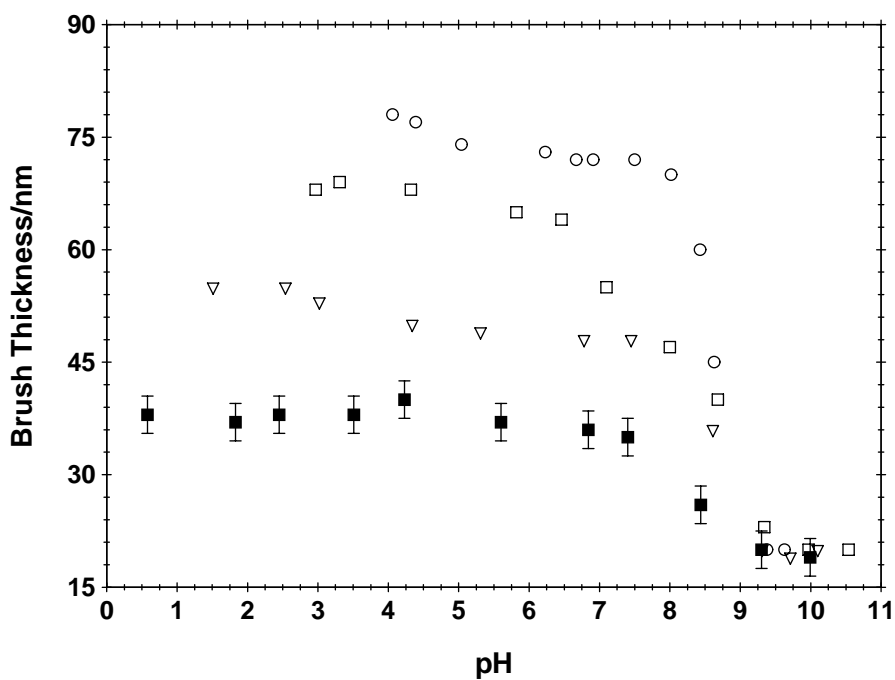


**Fig 23** Thickness of poly (VBAH) brushes as a function of pH at different ionic strengths. Each curve is at constant ionic strength. The sharp decrease in the brush thickness is observed at pH between 8-9. (x) 1M; (▲) 0.1; (□) 0.01; (o) 0.001; (Δ) 0.0001

### IV. 3 Polyelectrolytes Brushes as nanoreactor to generate metal nanoparticles

HAuCl<sub>4</sub> is widely used for making the gold nanoparticles (Youk 2003, Lim *et al.* 2003, Ghosh *et al.* 2003, Pol *et al.* 2003). HAuCl<sub>4</sub> can interact with a variety of organic and inorganic compounds to form complexes such as with the unsaturated hydrocarbons, aromatic and aliphatic compounds containing nitrogens. The nitrogen replaces the chlorides in HAuCl<sub>4</sub> in different stoichiometries to form complexes. The heterocyclic amines and related compounds are well known to form complexes in neutral pHs and ionic compounds in acidic pHs (Adams *et al.* 1982, Cattalini *et al.* 1966, Kukushkin *et al.* 1981, Ahrens *et al.* 1999). Interaction of polymeric amines with the metal complexes yield a ionic pairs [R<sub>3</sub>NH]<sup>+</sup>[AuCl<sub>4</sub>]<sup>-</sup> (Alguacil *et al.* 2001) by the electrostatic interactions and complexes are AuCl(NH<sub>2</sub>R) (Kumar *et al.* 2003). The protonated polyamine groups serve as first as well as second sphere coordinating ligands. The optimum pH regime for complexation is 3-9. (Schlaepfer *et al.* 1990, Myasoedova *et al.* 1997, Zelewsky *et al.* 1993) M<sup>n+</sup> ions (transition metals) bind via complexation releasing protons of the polymer, whereas negatively charged complexes such as PtCl<sub>4</sub><sup>2-</sup> are ion exchanged easily with the anions of the polymer. The interaction of AuCl<sub>4</sub><sup>-</sup> and PtCl<sub>4</sub><sup>2-</sup> in the brush system follows the same mechanism.

The brush thickness at high ionic strength shrinks due to the screening of charges as described before (See page 29). From 10<sup>-4</sup> M concentration of NaCl, which is a monovalent salt, the brush starts decreasing. In presence of divalent ions the onset of the salted regime is much before than for the monovalent like NaCl. Guo *et al.* (2001) has studied the effect of divalent ions such as MgSO<sub>4</sub> on the anionic brushes. The shrinking of the brushes is much more pronounced. Similar studies with HAuCl<sub>4</sub> shows the decrease of brush thickness starts from 10<sup>-5</sup> M. The low concentration of HAuCl<sub>4</sub> is required to produce the shrinking (Fig 24). The gold salt was added exactly in 1:1 stoichiometry of the nitrogens present in the brush, which was calculated by titration with AgNO<sub>3</sub> as described before. The addition of excess salt at the same concentration aggregated the system. The sharp decrease in the brush thickness may be due to complexation of two or more amine functionalities with the AuCl<sub>4</sub><sup>-</sup> ions. Such binding is observed before in the nitrogen and sulfur containing compounds where chlorides of AuCl<sub>4</sub><sup>-</sup> are replaced by nitrogen and sulfur (Porter *et al.* 2003, Römbke *et al.* 2001, Gmelin Handbook Au Suppl. Vol. B1). In principle, all the chlorides can be exchanged by some ligand.

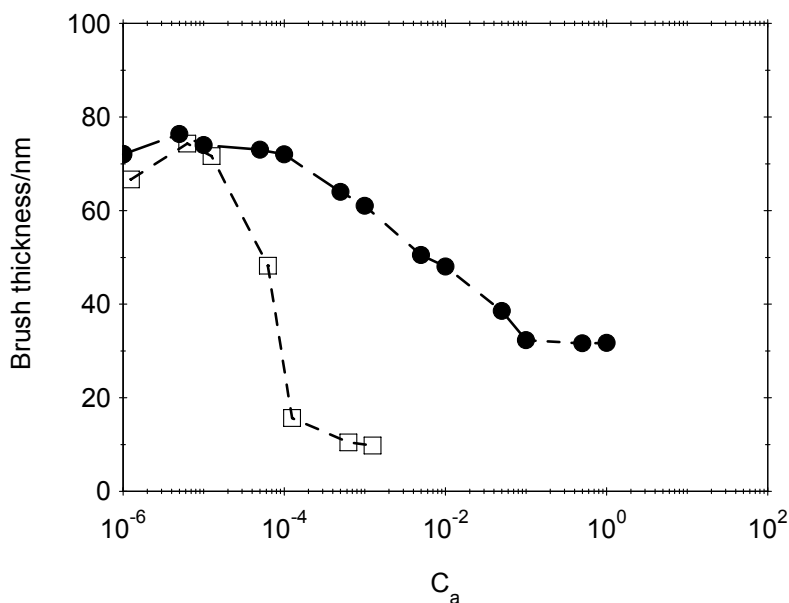


**Fig. 24** Brush thickness/nm as a function of  $C_a$ . (●) HAuCl<sub>4</sub>, (□) NaCl

An interesting study is the complexation behaviour of deprotonated brushes with the HAuCl<sub>4</sub> ions. For this study, polyelectrolyte brushes were deprotonated first by the treatment with the base. The PAEMH chains could be converted into the uncharged amino-form by treatment with strong base and subsequent purification. In this way a dense surface layer of poly(aminoethylmethacrylate) chains is generated that can be used for complexation of other metal ions as well. Fig. 22 demonstrates that the conversion of the poly(aminoethylmethacrylate hydrochloride) chains into an uncharged polymer is followed by a strong decrease of the layer thickness  $L$  as expected. The latex is still stable against coagulation, however, and may be used for uptake of ions again. Hence, the neutral amino form of the brush is titrated with HAuCl<sub>4</sub>. No salt is added in this procedure to ensure the full uptake of AuCl<sub>4</sub><sup>-</sup> ions into the brush. Since the total number of charges is known with good precision, this way offers allows to restrict the amount of the precious metal ions to the absolute minimum necessary.

Due to the high affinity of the brush particles for AuCl<sub>4</sub><sup>-</sup> ions, no ions are left in the solution. This can be shown by DLS. Titration with HAuCl<sub>4</sub> does not lead to the strong swelling as expected for a titration with HCl but to the same layer thickness  $L$  as observed previously. These shrunken brushes then complexed with the gold salt. The hydrodynamic radii were observed at each stage. Fig. 25 shows two systems studied. The shrunken brushes in case of treatment with HCl swell again due to formation of the polyelectrolyte. But with the addition of HAuCl<sub>4</sub> the brushes do not show any swelling, even when the pH was observed to be around 3.

The confinement of the counterions can be demonstrated by osmotic measurements. Osmotic coefficient describes the osmotically active counterions. This is given by ratio of real to ideal osmotic pressure. If all the counterions are free to move the measured osmotic pressure is given by the ideal term calculated from van t' Hoff's law. The counterions present in the polyelectrolyte brushes comprise three different types. The first types of counterions are those, which are condensed to the polyelectrolyte chains owing to the electrostatic interactions. Such counterions have been described in literature by 'Manning Condensation'. The second type of counterions are those, which are trapped within the brushes and contribute to the osmotic pressure of the system. The third type of counterions are able to move freely within the brush and outside into the bulk system.

The measurement of osmotic coefficient shows about 95-98% of the counterions are confined within the brush leaving only a fraction osmotically active (Das *et al.* 2002). It is also observed that the greater the contour length of the grafted polyelectrolyte chains, the lower is the number of osmotically active counterions in these spherical polyelectrolyte brushes. Hence the ions once introduced in the brush are confined within the brushes. Metal ions interact with the backbone of the brush chains and bound there after. These do not exchange with the medium.

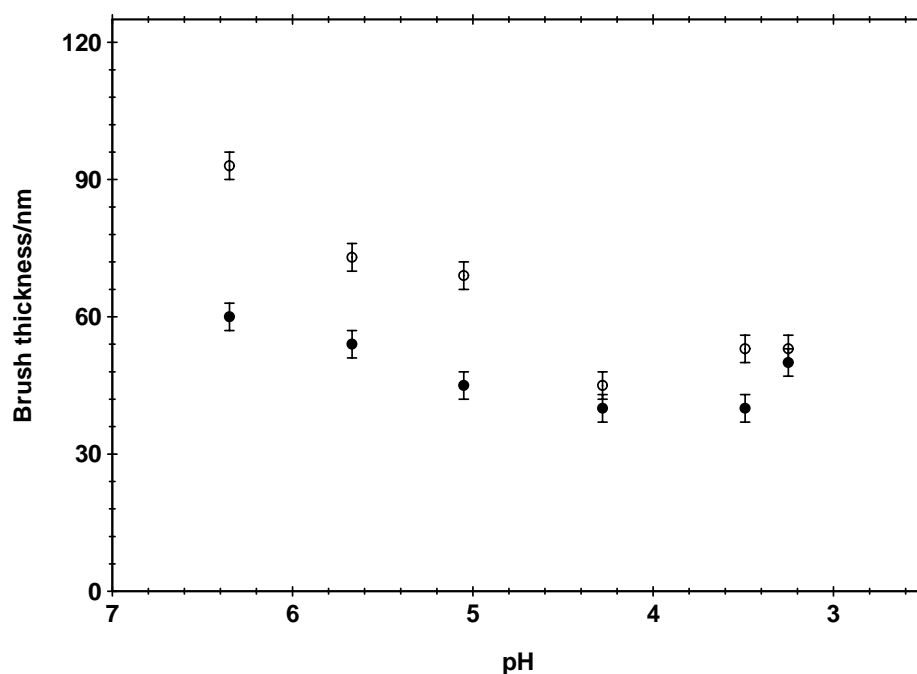


**Fig. 25** Titration of deprotonated brushes with  $H AuCl_4$ . (○) Brush thickness-160 nm, Deprotonated thickness-60 nm, (●) Brush thickness-183 nm, Deprotonated brush thickness-97 nm.

## V Generation of metal nanoparticles

**V.1 Metal Nanoparticles** in the range of 1-20 nm can be formed by a number of methods. The stability, size and properties of the particles are dependent on the synthetic methods used. The synthetic methods can be divided into physical and chemical ways. The particles find applications in catalysis, biosensors, dielectric reflectors (Fink *et al.* 1998, Urbas *et al.* 1999), quantum dots, light emitting diodes (Colvin *et al.* 1994, Dabbousi *et al.* 1995) and magnetic information storage (Joly *et al.* 2000).

**Physical Methods** include molecular beam epitaxy, sputter deposition, electron beam lithography etc. Some of the recently developed methods include metal vapor synthesis, where the metal vapor is condensed in a controlled manner to yield the nanoparticles (Ecstein *et al.* 1991, Niidome *et al.* 2000, Kamat *et al.* 1998, Kurita *et al.* 1998, Takami *et al.* 1999, Mafuné *et al.* 2001). Laser induced ablation techniques generate a broadly dispersed nanoparticles. Narrowly distributed gold nanoparticles are obtained by pulsed irradiation of gold metal plates (Mafuné *et al.* 2002).

In the solvated metal atom dispersion technique, the frozen atoms of the metal are slowly warmed up to yield the metal clusters (Klabunde *et al.* 1979). Other method to obtain narrowly dispersed particles is the digestive ripening of the metal dispersion (Stoeva *et al.* 2002).

### **Chemical Methods**

The chemical methods include the usage of ligands and polymers in the specific control of the size and in prevention of agglomeration of the particles. More advanced techniques include growth of particles in mesoscopically confined geometries such as vesicles (Watzke *et al.* 1987), zeolites (Wang *et al.* 1987), organic and inorganic gels, dendrimers, or other prestructured templates (Lianos *et al.* 1986, Steigerwald *et al.* 1988, Kortan *et al.* 1990, Pileni *et al.* 1992, Breitscheidel *et al.* 1991, Xiao *et al.* 1990, Zhao *et al.* 1991, Luong *et al.* 1988, Zhou *et al.* 1999, Rabaine *et al.* 1998, Maye *et al.* 2000, Ascendio *et al.* 2000, Hou *et al.* 1999, Antonietti *et al.* 1997).

### **Protecting agents**

The protecting agents stabilise the nanoparticles not only against aggregation, but also controls their particle size. The molecular weight and the amount of the polymer used determine the size of the nanoparticles. The wide variety of polymers has been used for protecting different metal nanoparticles such as Poly (2-hydroxyalkyl methacrylates) to protect nanoparticles of palladium, gold and silver with the radii 20 nm, 4 nm, and 8 nm

respectively (Mayer *et al.* 2000) and poly (N-Vinyl-2-pyrrolidone) for monodisperse Pt and Pd nanoparticles in the range of 17-35°A (Chadwick *et al.* 1977, Janietz *et al.* 1993). Other polymers include nafion (Quinn *et al.* 1994), polyethyleneglycol, polyvinylalcohol (Longenberger *et al.* 1995), polyphosphate (Henglein *et al.* 1995), polyacrylate (Belloni *et al.* 1994, Keita *et al.* 1996, Remita *et al.* 1994, Strelow *et al.* 1994), polyethyleneimines (Ershov *et al.* 1994, Sosebee *et al.* 1995), gelatine (Kapoor *et al.* 1994) and PMMA (Nakao *et al.* 1995) has also been used.

Linear polymers having cyano (-CN) or mercapto (-SH) functional groups which have high affinity for gold have been used to protect the gold particles of 15- 30 °A of mean diameter (Tamoto *et al.* 1997, Pei *et al.* 1995, Teranishi *et al.* 1998). Gold colloids stabilised by cationic polyelectrolytes were synthesized by Mayer *et al.* by in-situ reduction of H<sub>2</sub>AuCl<sub>4</sub> in presence of cationic polyelectrolytes having ammonium side groups (Mayer *et al.* 1997). The application of polymer protected nanoparticles is limited in catalysis as the protecting polymers have an passivating effect on the metal nanoparticles and due to dense coverage of the surface by the protecting polymers, the reachability of the reactants is limited. Moreover, separation of the nanoparticles is difficult by using simple filtration techniques due to their small particles size. The nanoparticles attached to the microsized structures are easy to separate.

### Mesoscopically confined geometries

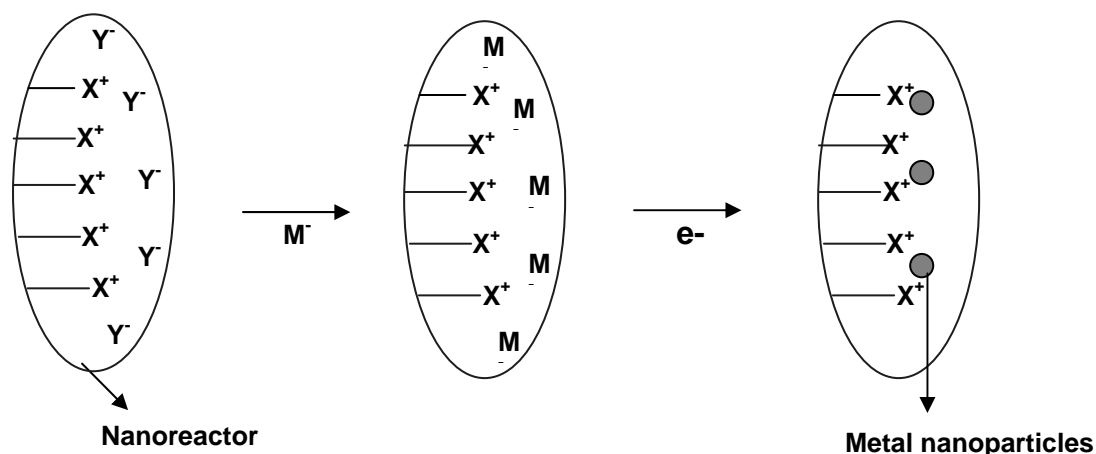


**Fig. 26** General scheme of a nanoreactor. The metal ions are confined inside the nanoreactor by physical or chemical means. The confined ions are reduced by suitable methods to generate nanoparticles. The nanoreactor can be micelles, nanostructured templates, biological vesicles etc.

**Amphibilic block copolymers** serve as building blocks to control material interfaces structurally and energetically. Thermodynamically stable hybrid materials can be made with nanoscale structure. Amphibilic block copolymers can be arranged linearly as grafts, stars or H shaped blocks. These structures have the ability to form structures such as spherical and cylindrical micelles, lyotropic phases, and mesophases. Any of these structures can be utilized to form nanoparticles (Schillen *et al.* 1994, Price *et al.* 1986, Nyrkova *et al.* 1993, Zhang *et al.* 1995, 1996, Clay *et al.* 1995).

Diblock copolymers form inverse micelles in organic solvents where the hydrophilic block is able to bind HAuCl<sub>4</sub>, LiAuCl<sub>4</sub>, H<sub>2</sub>PtCl<sub>6</sub>, CdCl<sub>2</sub>, NiCl<sub>2</sub>, TiCl<sub>3</sub>, Ti (OR)<sub>4</sub>, Si (OR)<sub>4</sub>, 3-glycidyloxypropyl trimethoxysilane (Spatz *et al.* 1998) CdCl<sub>2</sub>, CoCl<sub>2</sub>, ZnCl<sub>2</sub> to form ionic complexes of metals in the core in the micelles which are later reduced chemically to form gold nanoparticles. The particles were spherical or wire shaped according to the shape of the micelles. The particles were from 1-10 nm in size depending on the concentration of the gold salt (Spatz *et al.* 1998, 1996, 2000, Selvan *et al.* 1999, Antonietti *et al.* 1995, Lindlar *et al.* 2002, Djalali *et al.* 1999, 2002, Dziezok 1997, Youk *et al.* 2002, Antonietti *et al.* 1996). Microporous and Mesoporous materials (MCM-41) with the pore size of 2-10 nm can be efficiently used to produce stable nanoparticles. The MCM-41 is organo functionalised to produce propylamine-MCM-41 and propylthiol-MCM-41. The silanol groups present on the matrix reduces the AuCl<sub>4</sub><sup>-</sup> ions and the functional groups stabilize the gold nanoparticles. The average size of the particles was 17.5 nm. The particle size of the metal can be controlled by using the appropriate sized MCM-41 matrices (Ghosh *et al.* 2003, Mukherjee *et al.* 2001). Micellar template of the surfactant can be effectively used to produce gold nanorods (Ahmadi *et al.* 1996, Petroski *et al.* 1998, Bradley *et al.* 2000, Jana *et al.* 2001).

Amphibilic poly (organosiloxane) nanospheres for the synthesis of topologically trapped noble metal colloids has been described by Jungmann *et al.* The nanospheres with hydrophilic core and hydrophobic shell are soluble in toluene and the metal ions can be introduced in the core by solid-liquid or liquid-liquid phase transfer. The gold, palladium and silver ions can be localised into the cores of these nanospheres. The average size of the gold colloids after reduction is 1.7 + 0.7 nm (Jungmann *et al.* 2003).

Polyelectrolyte hydrogels with oppositely charged surfactants has also been used to embed noble metal nanoparticles. Complex of a cationic gel of with the anionic surfactant sodium dodecylsulfate (PADMACl/SDS and that of the anionic gel of poly (methacrylic acid) with a cationic surfactant cetylpyridinium chloride (PMA/CPC). Addition of gold salt in cationic gel distorts the structure of the gel partially. After reduction, the ordering in the gel

disappears completely and metal particles are formed. The particles size of the metal particles ranges from a few nanometres to 40 nm. The platinum particles of 2 nm sizes were also formed by the same mechanism (Svergun *et al.* 1998).

Poly- (octadecylsiloxane) has both the alkyl chains and silanol groups. The polymer forms a bilayer structure having water molecules between the layers. Intercalated water molecules between the siloxybilayers of an amphibilic polymer poly- (octadecylsiloxane) are replaced by metal ions. The metal ions were reduced by NaBH<sub>4</sub>. The 1-2 nm metal particles owing to high contrast visualizes the bilayer structure in TEM (Bronstein *et al.* 2000). Carboxylic acid fictionalized gold clusters were assembled in the scaffolds of polymers having amine functionality such as polyethyleneimines or poly-L-lysines (Maya *et al.* 2000). Liu *et al.* made pH responsive core shell by the triblock polymers. These triblock polymers were dissolved at low pH, on addition of NaOH, micellization occurred, above pH 7-8 onion like structures are formed. These structures were used as nanoreactors to produce nanoparticles of gold. The colloid produced was stable for long periods (Liu *et al.* 2002) U

Usage of dendrimers for anchoring to generate metal nanoparticles also provide a route to synthesize metal nanoparticles (Esumi *et al.* 2000, 1998, Manna *et al.* 2001, Garcia *et al.* 1999). The monomers complexed transition metal ions have been polymerized by living polymerization to form the desired polymer/block copolymer complexed transition metals (Ng *et al.* 1992).

### **Metal nanoparticles on Substrates**

Adsorbing directly preformed metal nanoparticles on the substrates provides a simple route to assemble the nanoparticles on the desired surfaces. The method has a general approach where the functional groups or the ligands having an affinity for the metal particles are supported on the substrates. The preformed metal nanoparticles are then anchored to the functionalised substrates.

In situ Au/Pt bimetallic colloids were produced on the surface of polystyrene microspheres by dispersion copolymerisation of styrene and poly (N-isopropylacrylamide) in presence of ethanol-water media in presence of HAuCl<sub>4</sub> and H<sub>2</sub>PtCl<sub>6</sub>. The ratio of Au/Pt controls the nucleation of polystyrene spheres. Hence the size of polystyrene spheres and the morphology of the particles can be controlled by the varying the Au/Pt ratio (Chen *et al.* 2002). Gold silica nanocomposites were prepared by sonochemical methods on silica microspheres in an inert atmosphere. The gold particles were of 5 nm in size (Pol *et al.* 2003).

Thin films of sequentially adsorbed interpenetrating polyelectrolyte layers can be used to produce nanoparticles of metals (Ag) and semiconductors (PbS). Silica coated gold were

synthesized by the Liz-Marzan and Philipse (Liz-Marzan *et al.* 1996, Coenen *et al.* 1988, Schärftl *et al.* 2000). Dokoutchaev *et al.* showed that microspheres of silica can anchor metal colloids of Pt, Pd and Au by electrostatic deposition onto the oppositely charged beads of polystyrene. The beads were charged by adsorption of polymers like polystyrene sulphonic acid and polyallylaminehydrochloride (PAH). The metal particles were of 12.5 nm in size in case of citrate reduction and 15-30 nm in size with the sonochemical reduction for gold particles (Dokoutchaev *et al.* 1999). A similar approach to coat the islands of gold and silver on the micro sized polystyrene latex beads was done by Siiman *et al.* The metal colloids were held on the surface by aminodextran, which were covalently bound to the aldehyde and sulfate groups on the polystyrene beads (Siiman *et al.* 2000).

Organosilanes having functional groups (-SH, -P (C<sub>6</sub>H<sub>5</sub>)<sub>2</sub>, -NH<sub>2</sub>, -CN) were coated on substrates. The functional groups on silanes bind to the gold colloids of size (2.5-120 nm) to produce macroscopic Au surfaces with a well-defined nanostructure (Katherine *et al.* 1996). Microcrystals of polydiacetylene were used as core particles to coat gold and silver layer on it (Katagi *et al.* 2000). The adhesion of polymers and inorganic materials can be done through specific interactions like dipolar interactions, hydrogen bonding, complex formation or covalent bonding such as gold nanoparticles adsorb at the surface of poly (2-vinylpyridine) and at the interface of PS and poly (2-vinylpyridine) (Kunz *et al.* 1993).

The method is easy and the complicated procedures of in situ synthesis are avoided. The particle size of the metal nanoparticles is not dependent on the support material as in the case of mesoscopically confined vesicles and controlled beforehand. But the particles below 10nm are difficult to prepare as the particles in this size range can only be generated by using protecting agents, which hinders the direct adsorption on the substrates.

Immobilization of platinum nanoparticles on polystyrene surface their activity in hydrogenation of cyclohexene in liquid phase has been reported (Mayer *et al.* 1997). The surfaces of the latexes are modified such that metal precursor complexes with the surface of the latexes which after reduction immobilizes on the latexes surface (Tamai *et al.* 1995).

**Layer by Layer assembly (LBL)** is one of the very recent techniques developed by Caruso *et al.*. In this method, gold particles can be directly adsorbed on the polystyrene surfaces by electrostatic interactions and H-bondings. Polystyrene spheres of 620nm in size were coated with poly (allylamine hydrochloride)/poly (sodium 4-styrenesulfonate) multilayers and exposed to stabilised gold nanoparticles of  $6 \pm 2$ nm in size. (Gittins *et al.* 2001, 2002, Liang *et al.* 2002, Caruso 2001) Similarly, Ji *et al.* used polyethyleneimines to adsorb onto the

polystyrene latexes which makes the latex positively charged and then adsorbing the negatively charged Au particles (Ji *et al.* 2001).

Youk prepared amphibilic spheres of 200nm with core of poly (methylmethacrylate)(PMMA) and shell of poly (allylamine)(PAA). The hydrophilic shell was treated with  $\text{HAuCl}_4$  and then reduced with  $\text{NaBH}_4$  to give gold nanoparticles. The gold particles formed were of approximately 12nm in diameter with a very low the coverage (Youk *et al.* 2003). Porous metal microspheres have been obtained by calcination of organic templates (Shchukin *et al.* 2003).

## V.2 Introduction of Gold ions in the brushes and synthesis of Gold nanoparticles

Amine functional groups and their protonated forms successfully bind to metal ions either by complexation or by ion exchange mechanism, which has already been described in the literature (Kumar *et al.* 2003, Bharathi *et al.* 1997, Myasoedov 1997, Alguacil *et al.* 2001). The discussion in the preceding sections describes the interaction of polyaminoethylmethacrylatehydrochloride brushes and  $\text{AuCl}_4^-$  ions. The experiments show that  $\text{AuCl}_4^-$  ions behave like a multivalent ion to complex with the brush such a phenomenon is not observed in the case of univalent ions of NaCl salt.

The metal ions are introduced into the polyelectrolyte brushes by the ultrafiltration method. The polyelectrolyte brushes are ultrafiltered with the of  $1 \times 10^{-4}$  M  $\text{HAuCl}_4$  solution prepared in Millipore water. The excess ions are eliminated by continuing ultrafiltration with Millipore water until the conductivity of the outgoing serum is reduced to less than  $1 \mu\text{S}$ . Washing of the chloride ions is an essential process, because the presence of chloride ions in the solution induces the aggregation of the gold particles. After extensive cleaning of the polyelectrolyte brushes, these brushes retain the yellow colour of the  $\text{HAuCl}_4$  solution. This can be attributed to the localisation of the aurate ions within the brush system.

As discussed earlier in Section IV.5, shrinkage is observed in the brush length with the addition of metal ions largely due to the formation of a complex between the polyelectrolyte chains of the brushes and the metal ions. The metal ions complexed to the polyelectrolyte chains render a higher contrast to the system. Such polyelectrolyte brushes with a higher contrast provide an interesting system to be studied by cryo TEM (V.3).

Fig. 27 is the schematic representation of the process of the introduction of metal ions into the polyelectrolyte brushes and their subsequent reduction to form nanoparticles. Stage I in Fig. 27 shows the polyelectrolyte brushes, with fully stretched chains bearing protonated amine groups. In Stage II of Fig 27, the titration of the polyelectrolyte brushes with NaOH

solution leads to the deprotonation of the functional groups to form their corresponding uncharged amine functional groups (Sec. IV.2). The aurate ions can be either be introduced at Stage I or Stage II of Fig. 27. Stage III of Fig. 27 demonstrates the polyelectrolyte brushes after the introduction of the metal ions. Having shown that aurochlorate ions are fully confined within the brush layer, we now turn to the reduction of these ions within the “nano-reactor”. This is achieved by the addition of dilute solutions of  $\text{NaBH}_4$  to the polyelectrolyte brushes complexed with the metal ions. The reduction is a spontaneous process and can be followed visually with a change in the colour from yellow to brown of the polyelectrolyte brushes. No change in colour is observed as a function of time afterwards suggesting that gold particles once formed are relatively stable and do not tend to form aggregates. Commonly used reducing agents are  $\text{LiAlH}_4$ ,  $\text{NaBH}_4$ ,  $\text{LiBEt}_3\text{H}$ , hydrazine and hydrogen. The size of the nanoparticles is largely dependant on the selection of the reducing agent. The formation of gold nanoparticles using citrate based reducing agents generally generates gold nanoparticles with particle sizes between 8-12 nm. The citrate groups are known to stabilize the gold particles after their formation. Hence, the use of citrates as reducing agents allows us to have a better control over the size of the nanoparticles formed (Okitsu *et al.* 1997).

In the case of sonochemical methods in presence of ethanol, the reactive radicals are first generated, these radicals then reduce the metal ions to zerovalent state, the reduced metal particles later aggregate to give rise to larger nanoparticles. The particles formed using sonochemical methods are generally stable for months even in the absence of protecting agents. The particle size is usually between 15-30 nm (Okitsu *et al.* 1996, 1997, Mizokushi *et al.* 1997). In principle, physical methods such as exposure to UV light can also be used. The chemical reducing agents such as  $\text{NaBH}_4$  and tetrakis (hydroxymethyl) phosphonium chloride are generally used in the formation of metal nanoparticles (Duff *et al.* 1993). The size of the nanoparticles varies depending on the chemical reducing agent used. In our case, gold nanoparticles formed by reduction with  $\text{NaBH}_4$  formed particles with the size varying between 2-3 nm, while the reduction with tetrakis(hydroxymethyl)phosphonium chloride formed particles with size less than 2 nm. During the process of reduction, the latex remains stable. The onset of a slow aggregation is only observed after several days. The factors affecting the stability of the latex covered by gold particles must still be investigated in more detail. For the present investigation, it suffices to note that the colloidal stability is not impeded by the chemical reaction-taking place in the nano-reactors.

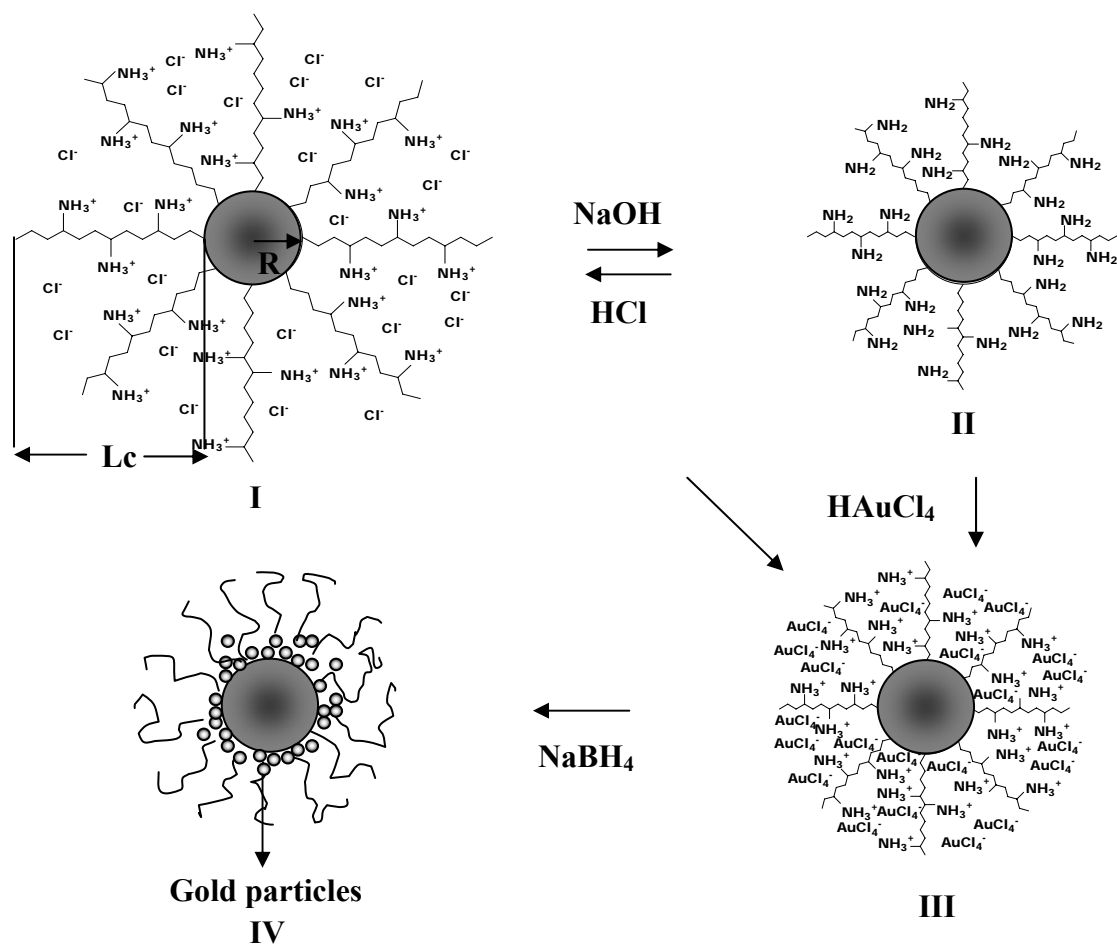


**Fig. 27** Schematic representation of formation of gold particles on the surface of the core shell system. The core shell system having shell of poly (aminoethylmethacrylate hydrochloride) [**I**] is deprotonated reversibly at high pH to give amine shell system [**II**]. **I** and **II** can be counterion exchanged/complexed with  $\text{HAuCl}_4$  to give **III**.  $\text{NaBH}_4$  reduction of **III** forms **IV** with nanosized gold particles.

It should be noted in this context that no reagents have been used for the stabilization of the Au particles. Hence the surface could be used for immobilizing further functional groups on the surface of the Au particles like sulphur or phosphorus containing reagents. The polyelectrolyte brush system after the reduction of gold nanoparticles within the polyelectrolyte brush can be used subsequently for catalysis.

### V.3 Cryogenic temperature TEM of polyelectrolyte brushes with gold ions

Although electron microscopy is a very powerful tool in the investigation of soft matter like colloids and self-assembled systems and in the field of nanotechnology, its applications in studying the samples in their native state are limited. The sample preparation for the investigation using electron microscopy requires complete drying of the solvent

medium under vacuum. Such a process may lead to the changes in the conformation of labile samples due to the surface tension, which may lead to some artifacts. Besides this, there is a strong interaction between the electron beam and the material under investigation usually leading to the damage of the system (Bellare *et al.* 1988).

These technical difficulties are eliminated by the use of Cryogenic TEM. This technique was originally developed to observe the biological samples in 3 dimensions in their native state or the hydrated state. In this technique the sample preparation is carried out by rapidly freezing the sample to be investigated. This process is called as the ice-embedding method. The irradiation induced damage is reduced in the case of cryogenic electron transmission microscope, since the instrument operates at extremely low temperatures.

In order to avoid the formation of ice crystals the samples under investigation are required to be frozen rapidly (Danino *et al.* 2000). This process is called as vitrification. Three different forms of solid ice like hexagonal, cubic and vitreous can be formed depending on the temperature and the time taken for cooling. Slow freezing results in formation of hexagonal ice crystals. The rapid freezing to temperatures below  $-100^{\circ}\text{C}$  leads to cubic ice formation (also crystalline). Extremely rapid freezing of the sample to temperatures below  $-140^{\circ}\text{C}$  results in the vitrification, which is the formation of amorphous ice. Vitrification requires the specimen to be in the form of a very thin film (50-200 nm) so as to allow sufficiently rapid heat transfer. If the temperature of the vitrified ice is raised above  $-140^{\circ}\text{C}$  an irreversible phase transition to cubic ice will occur. Liquid ethane, propane or nitrogen is used for freezing the sample.

The internal structure of the samples with low density of electrons such as biological samples and polymers are difficult to observe using TEM, as they have rather low contrast as compared to the background medium, and hence making the detailed structural studies difficult. The heavy metals ions possess higher contrast as compared to polymer or biological samples due to their high electron density. Since the electron density depends on the atomic number of the atoms constituting the system under investigation, staining the samples with the heavy metal ions enhances the contrast considerably so as to be “seen” by TEM. Conventional metal ions used for this purpose are uranyl acetate and tungsten phosphate. One of the techniques used was to coat the sample by chemical vapour of the gold. Gold, which has a high electron density, when absorbed onto the sample selectively stains the region of adsorption.

As discussed earlier, direct imaging of polyelectrolyte spherical brushes under TEM requires the drying of the sample under high vacuum. The evaporation of the solvent

leads to a collapse of the polyelectrolyte chains, which form a shell around the core particles of the polyelectrolyte brushes. Under these conditions, the visualization of the shell becomes impossible in spite of using a higher contrast. The contrast solution usually contains a protein bovine serum albumin (0.1 wt%), phosphotungstic acid (1 wt%) and sucrose sugar (2 wt%).

In Cryo-TEM, as described above, the solvent is frozen rapidly and the polyelectrolyte brushes are in their native state. At neutral pH and low ionic strength, the polyelectrolyte chains of polyelectrolyte brushes are fully stretched. This fully stretched conformation of the polyelectrolyte chains is retained as the polyelectrolyte brushes are frozen rapidly at  $-140^{\circ}\text{C}$ . It should therefore be possible to see single polyelectrolyte chains at sufficient high resolution of the electron beam. Fig. 28, demonstrates the images of polyelectrolyte brushes taken using cryo-TEM without the use of any staining agent. Although the polystyrene core particles, the individual polyelectrolyte chains are not visible, since they have a rather low contrast as compared to the spherical polystyrene core of the polyelectrolyte brushes. Although polystyrene can be seen easily, due to its compact structure with a thickness of 100 nm. The polyelectrolyte chains are very long, and the thickness of these chains is of the size of a few atoms, hence the observation of these individual chains is almost impossible without the use of any staining methods.

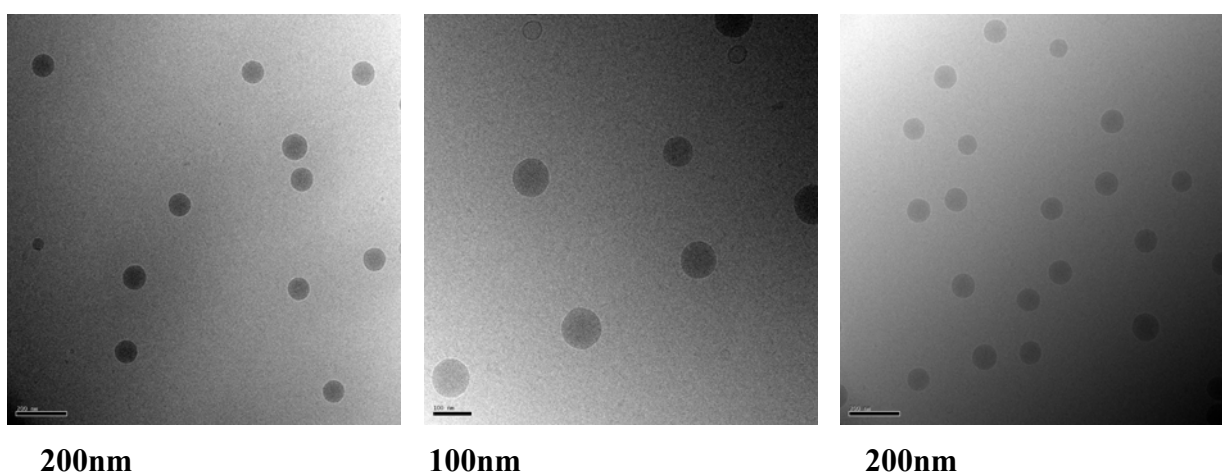
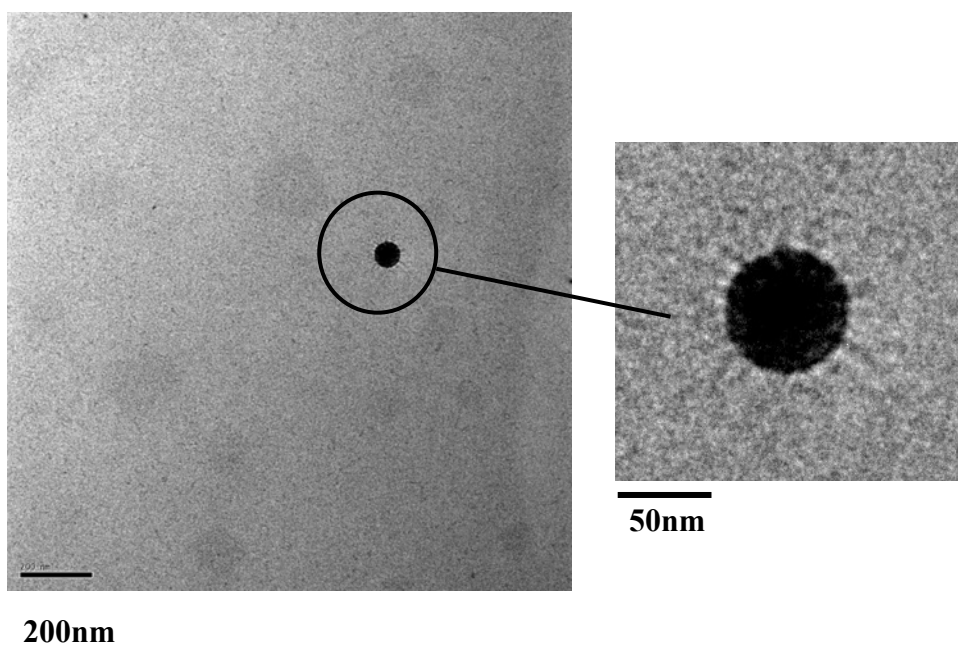


**Fig. 28** Cryogenic temperature transmission electron microscope of cationic brushes. The polystyrene core particles are clearly visible. The polymeric brush though in native state is not seen due to the low contrast. The particles were observed without any staining. The sample is 1wt %.

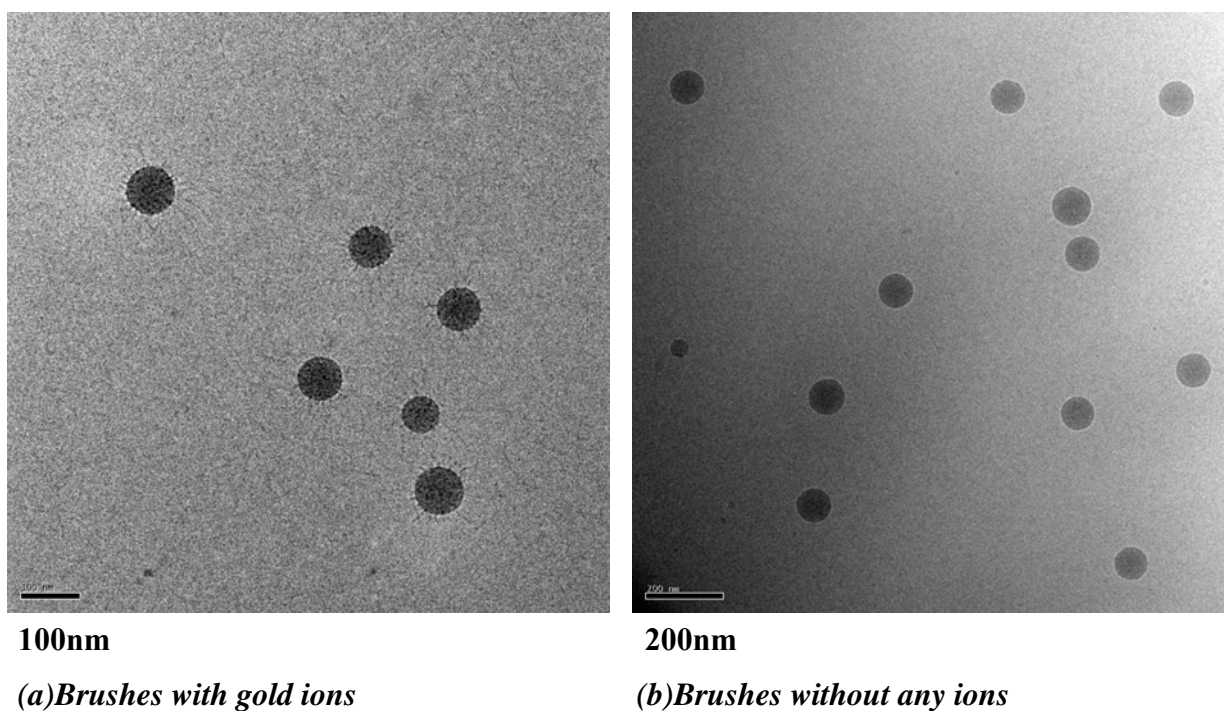
Gold has a high electron density hence when absorbed in the sample selectively stains the part where it is absorbed. For the polyelectrolyte brushes studied here, a rather unique method was employed to increase the contrast of the polyelectrolyte brushes. As discussed in earlier section, aurate ions were introduced into the polyelectrolyte brushes using ultrafiltration technique. The excess aurate ions were washed away by extensive ultrafiltration of the polyelectrolyte brushes. The gold ions present within the cationic brushes are usually in close vicinity of the polyelectrolyte chains and since they have a higher contrast, these aurate ions increase the contrast of the polyelectrolyte chains considerably, allowing us to study the structure of the polyelectrolyte brushes using cryo-TEM.

Fig. 29 demonstrates the images of polyelectrolyte brushes after the introduction of aurate ions, taken using cryo-TEM. From the Fig. 29, it is clearly evident that the aurate ions provide a very high contrast to the polyelectrolyte chains of the polyelectrolyte brushes, and hence the polyelectrolyte chains are clearly visible stretching out into the bulk solvent. A magnification of the image shown on the right side of Fig. 29 shows the structure of the polyelectrolyte chains more clearly. The polyelectrolyte chains are seen to be forming a corona around the polystyrene core.

In the magnified image, the high electron density of the gold ions is clearly visible on the polystyrene core. The hydrodynamic radii measured using dynamic light scattering is the uppermost limit to which the chains are being stretched. In cryo-TEM, as the density of the brushes decreases with the increase in the distance from the grafting surface, the weaker is the visibility of the polyelectrolyte chains. And hence in cryo-TEM only the high density areas of the brushes near the grafting surface are visible, leaving out the margins of the brushes.



**Fig. 29** Cryogenic TEM images of spherical polyelectrolyte brushes with gold ions. The brushes are visualized due to the high contrast of the staining by gold ions. The enlarged image shows the brushes more clearly.



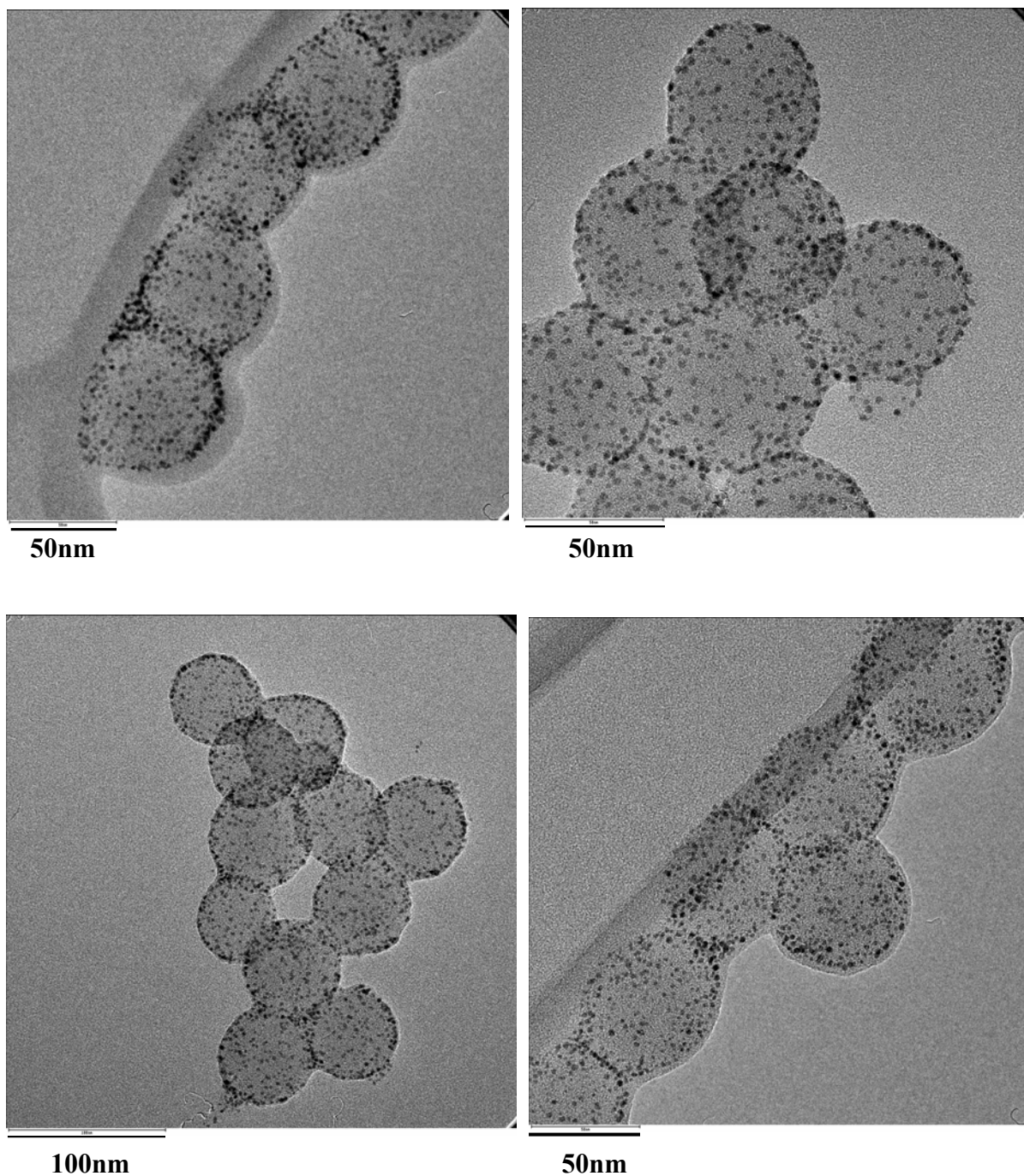
**Fig. 30** A comparison of the spherical polyelectrolyte brushes with gold ions (a) and without gold ions (b) as seen under Cryogenic TEM. The brushes are visualized due to the high contrast of the staining by gold ions.

#### V.4 HRTEM of Gold nanoparticles:

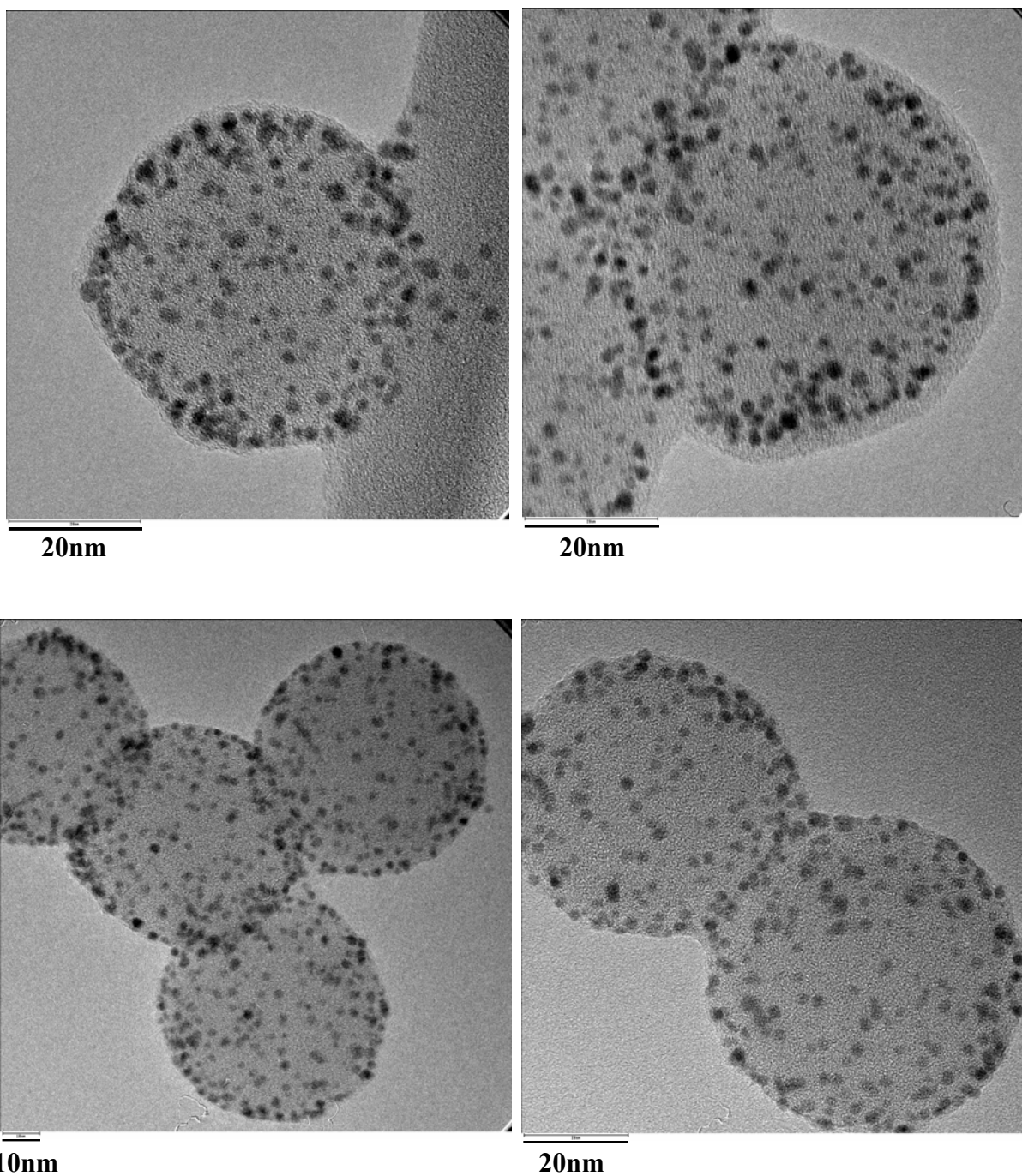
The HR-TEM measurements were carried out by Philips (FEI) CM 200 FEG equipped with an energy dispersive X-ray system. A carbon grid was used for the sample preparation. The crystallinity of the samples was evaluated from the selected area electron diffraction. EDX was used to exactly confirm the elements present. In spite of the disadvantages discussed about transmission electron microscopy in the previous section, direct imaging of the composite nanoparticles under dried state provides important information of the particles size and the nature of the nanoparticles formed. HR-TEM allows us to obtain images at much higher magnification.

Fig. 31 shows the HR-TEM images of gold nanoparticles formed by the reduction of aurate ions introduced in the polyelectrolyte brushes. From the HR-TEM images it is evident that the gold nanoparticles, which are formed by the aurate ions, present in the vicinity of the polyelectrolyte chains, are seen on the surface of the polystyrene core. All the gold nanoparticles are seen on the surface of the polystyrene core because of the collapse of the polyelectrolyte chains during the drying process of sample preparation.

Images in the Fig. 32 demonstrates the magnified image taken by HR-TEM, the gold nanoparticles seen in this image have a diameter of ca. 2.5 nm. The crystalline nature of these gold nanoparticles can be observed from the Fig. 33. The lattice fringes visible in Fig. 33 suggest that the gold nanoparticles thus formed are fully crystalline as expected. Since the aurate ions are distributed along the polyelectrolyte chains, the nucleation of gold nanoparticles takes place at multiple spots, which in turn leads to much smaller size distribution of the gold nanoparticles as compared to the gold nanoparticles formed by the reduction of a bulk solution. The Au nanoparticles formed within the polyelectrolyte brushes are relatively stable and do not form further aggregates for a considerable period of time.



**Fig. 31** HRTEM images by Philips (FEI) CM 200 FEG on carbon grid. Gold nanoparticles are formed by reduction of gold ions with  $\text{NaBH}_4$ . Gold nanoparticles are clearly visible due to high contrast as compared to polystyrene. Further confirmation can be done by energy dispersive X- ray system. Gold nanoparticles are not seen in the solvent. Clusters of polystyrene particles are seen due to the effects of surface tension during sample preparation.



**Fig. 32** HRTEM images by Philips (FEI) CM 200 FEG on carbon grid. Gold nanoparticles are clearly visible due to high contrast as compared to polystyrene. Further confirmation can be done by energy dispersive X- ray system. Gold nanoparticles are not seen in the solvent. Clusters of polystyrene particles are seen due to the effects of surface tension during sample preparation.

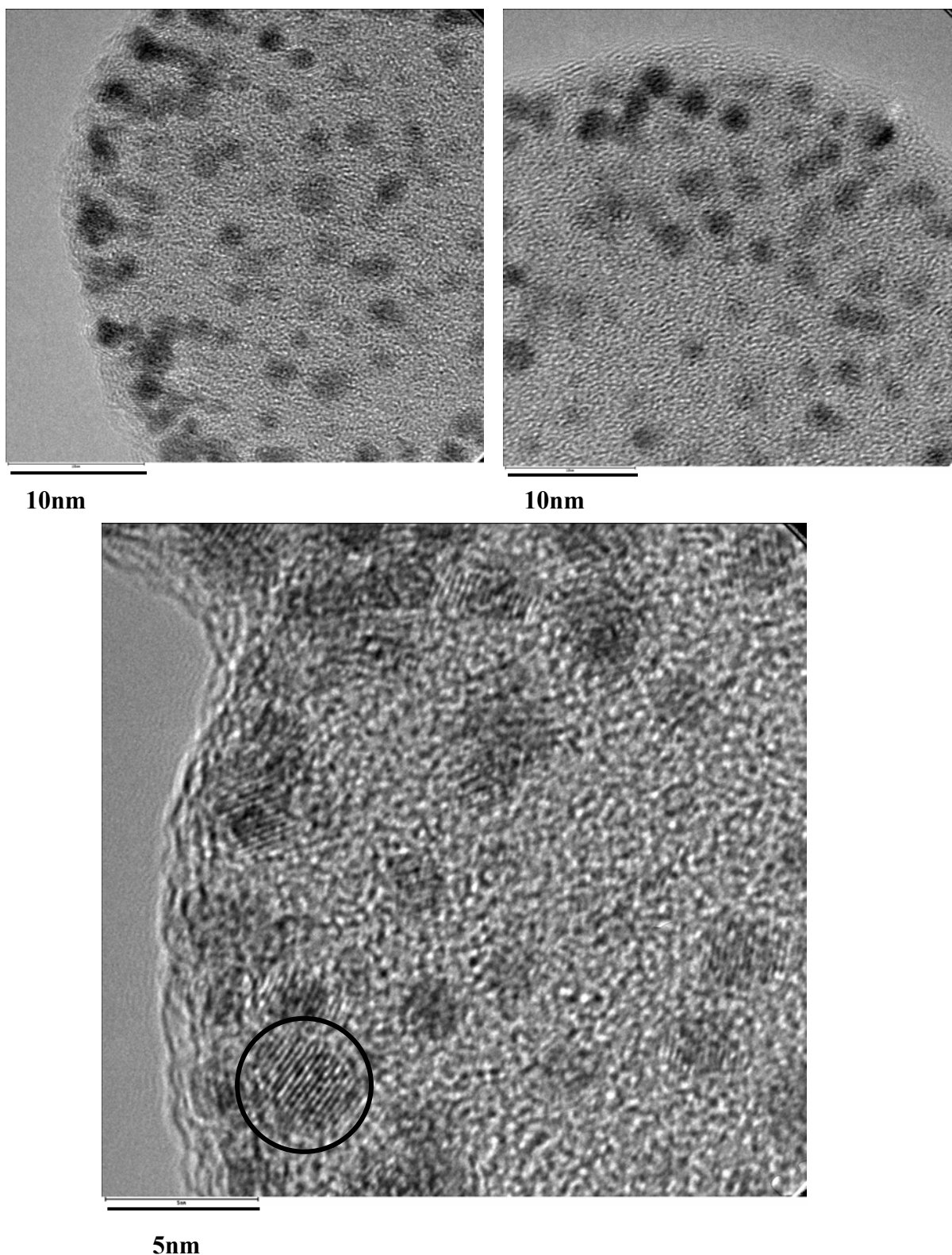


**Fig. 33** HRTEM images of gold nanoparticles formed by reduction with  $\text{NaBH}_4$  on polystyrene at higher magnification. The crystalline structure of the gold nanoparticles is clear from the crystal planes as shown in the marked region. The marked nanoparticles is approx. 3nm in size. The diffraction of the x-ray is also observed at the crystalline areas. EDX confirms the presence of the gold element at the crystalline parts.

Formation of gold nanoparticles by using tetrakis (hydroxymethyl) phosphonium chloride as a reducing agent, yields extremely small gold particles as described in literature previously. (Duff *et al.* 1993).

The use of tetrakis (hydroxymethyl) phosphonium chloride as a reducing agent, leads to the yellow coloured polyelectrolyte brush solution to colourless, while the use of sodium borohydride as a reducing agent changes the colour of the polyelectrolyte brush solution with aurate ions from yellow to brown. The polyelectrolyte brushes in which the gold nanoparticles are prepared using tetrakis (hydroxymethyl) phosphonium chloride are usually more stable as compared to the gold nanoparticles prepared by using  $\text{NaBH}_4$ , as a reducing agent. Fig. 34 demonstrates the HR-TEM images of polyelectrolyte brushes, where the gold nanoparticles are prepared by using tetrakis (hydroxymethyl) phosphonium chloride as a reducing agent. From the images it is clear that no individual gold nanoparticles are visible although the contrast around the polyelectrolyte brushes is enhanced significantly. A comparison of the polyelectrolyte brushes with gold nanoparticles (Fig 34) and polyelectrolyte brushes without any gold particles (Fig 35) shows that in the case of polyelectrolyte brushes with gold nanoparticles a gel structure is seen around the brush particles. Such a gel-like structure is absent in the case of polyelectrolyte brushes without gold nanoparticles, as is seen from Fig. 34.

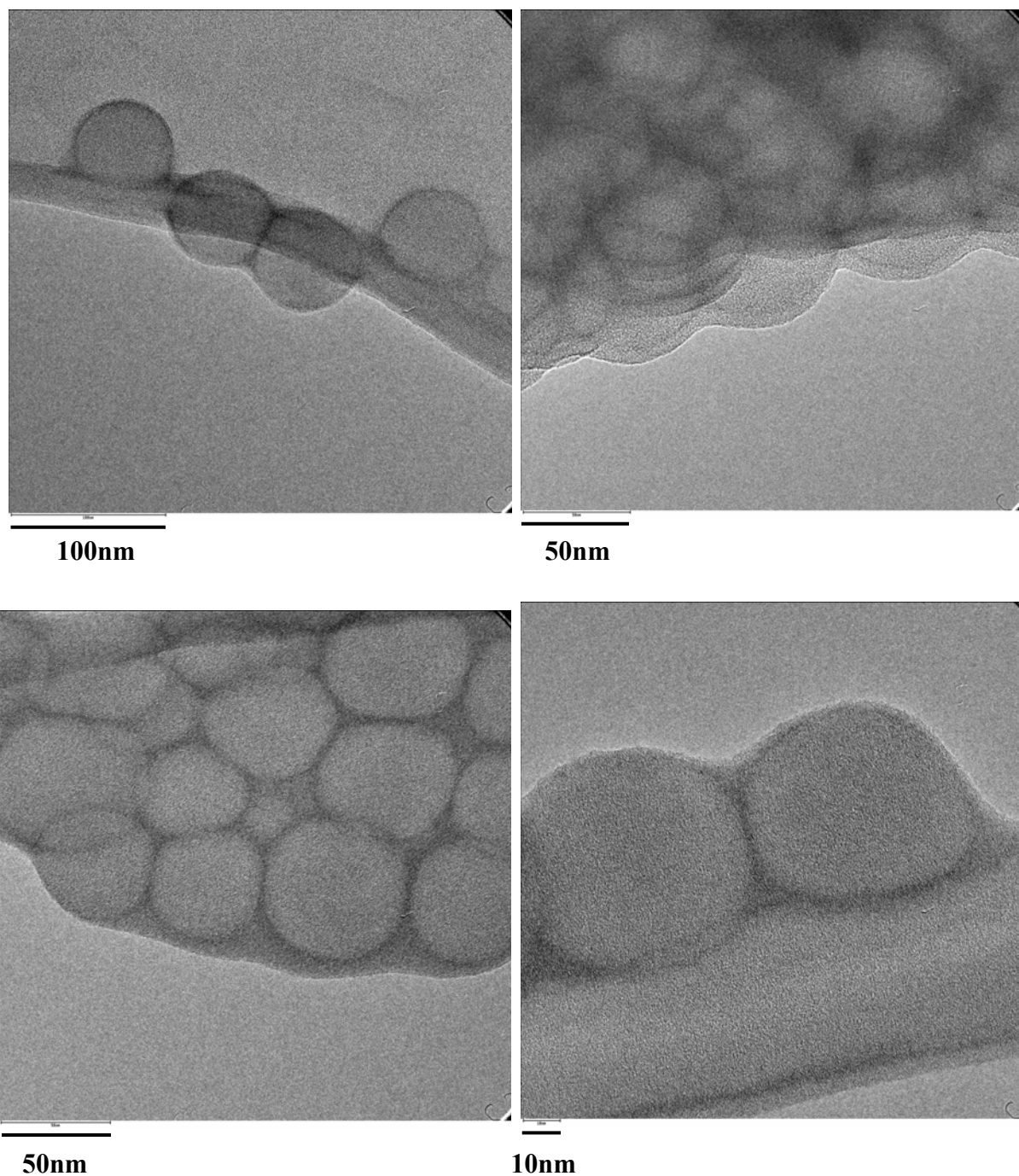


**Fig. 34** HRTEM images of gold nanoparticles formed by the reduction of ions by tetrakis(hydroxymethyl) phosphonium chloride. Though no individual gold particles are seen but the contrast of the shell is enhanced by gold particles. The amount of gold ions is same as that of the sample in Fig. 32.

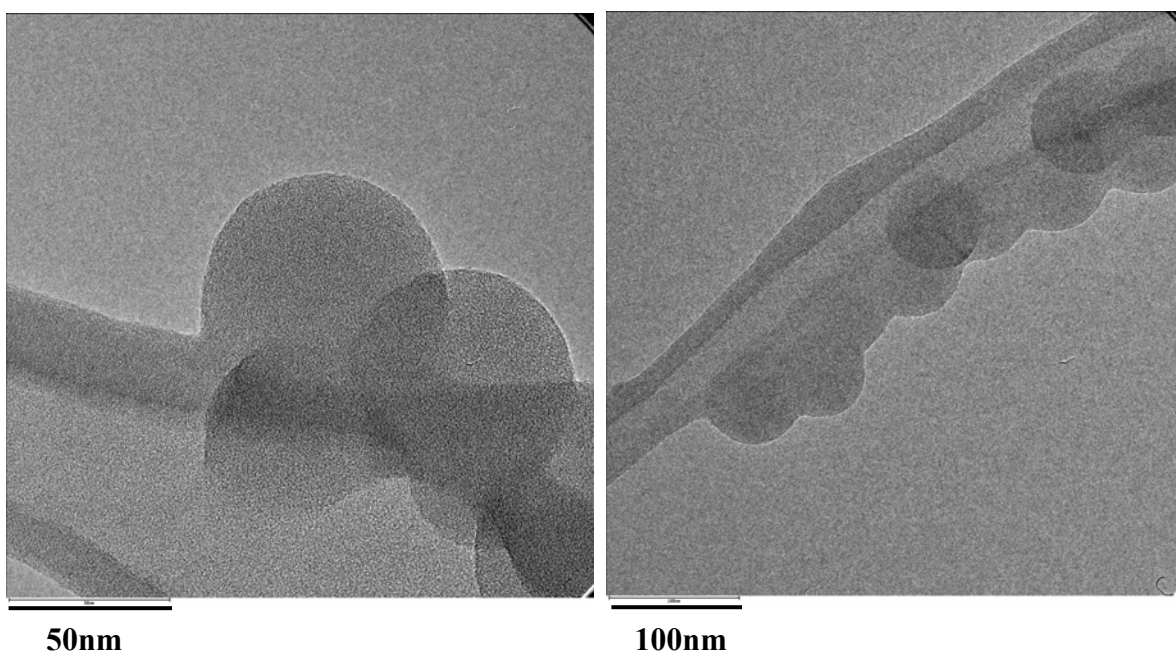


**Fig. 35** HRTEM images of carrier particles without any gold particles. The particles appear uniform without any distinction between shell and the core particles.

At higher magnification, the HR-TEM images show the presence of extremely small gold nanoparticles (Fig 36). The gold nanoparticles due to the hydrophobic interactions with the polystyrene core, attach to the polystyrene particles. The presence of elemental gold was confirmed by energy dispersive microscopy. The particle size measurement is difficult as the particles as the particles are not well separated.

The above discussion suggests that the particles size of the gold nanoparticles is dependent on the choice of the reducing agent. The smaller particles though invisible at lower magnification provides a contrast to the shell and at higher magnification are clearly visible.

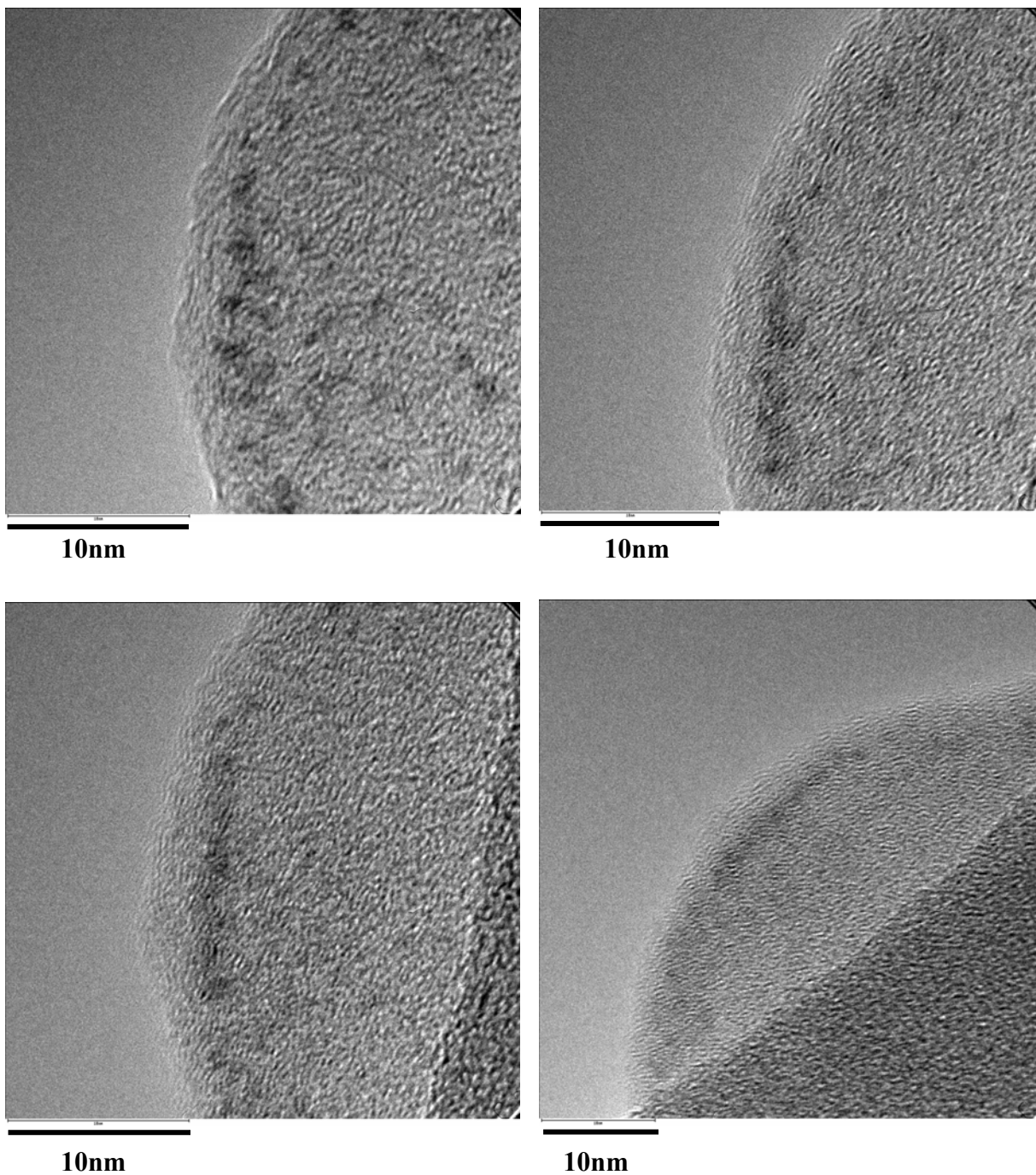


**Fig. 36.** HRTEM images of gold nanoparticles formed by the reduction of ions by tetrakis (hydroxymethyl) phosphonium chloride. Images show high magnification of the particles shown in Fig 34. Areas of high contrast can be seen easily but measurement of particles size is difficult. EDX confirms the presence of gold element in the sample.

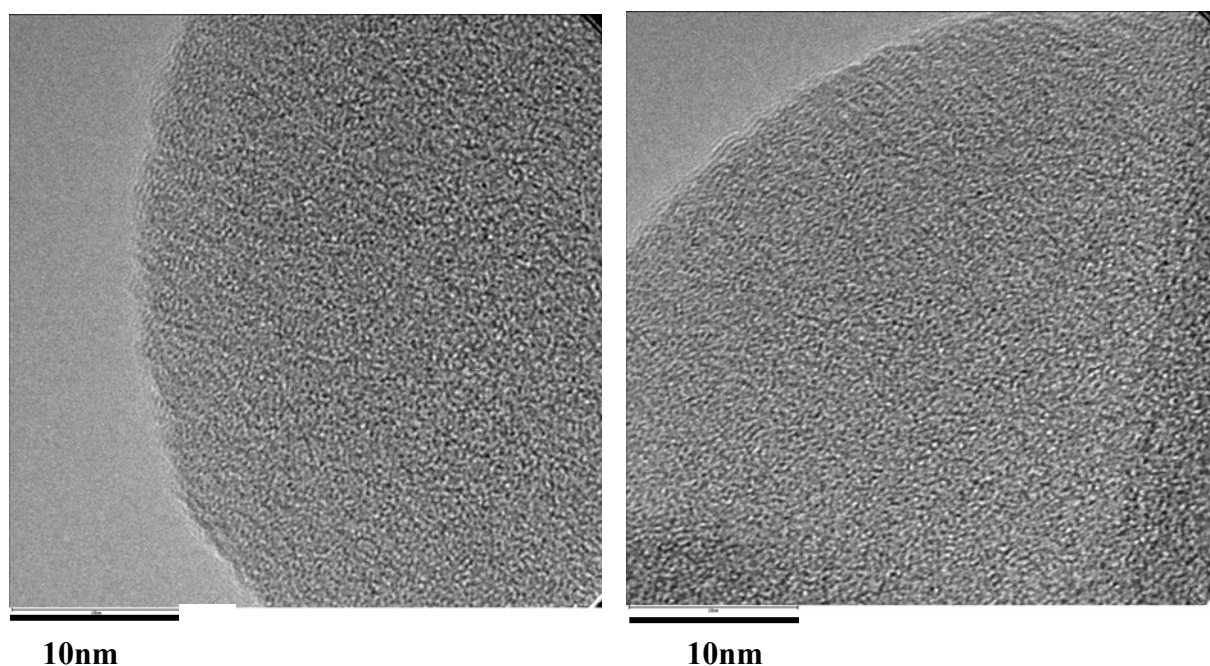


**Fig. 37.** HRTEM images of carrier particles without any gold particles. The particles appear uniform. No gold particles are seen unlike Fig. 36.

#### **V.5 UV spectroscopic studies of polyelectrolyte brushes with reduced gold nanoparticles**

An intense absorption is observed in the visible-near UV region if noble metals are exposed to ultra violet light. This absorption is caused largely if the size of the particles is below the mean free path (the distance the electrons travels between the scattering collisions with the lattice centres). This absorption results from the coherent oscillations of the free electrons and is called as ‘surface plasmon resonance’. Such strong absorption also induces a strong coupling of the nanoparticles to the electromagnetic radiation of light. This phenomenon has been reported in literature by solving the Maxwell’s equation for the absorption and scattering of electromagnetic radiation by spherical metallic particles. With the knowledge of the dielectric constants of the metal and its environment, spectra of the nanoparticles smaller than that of the wavelength of the light have already been predicted (Mulvaney 1996, Wiesner *et al.* 1989, Henglein *et al.* 1995, Creighton *et al.* 1991).

The UV-absorption spectra of gold nanoparticles largely depend on the size of the particles and the chemical environment surrounding the gold particles. Size of the gold nanoparticles also plays a vital role in determining the color of the solution of gold nanoparticles. The Gold nanoparticles less than 2 nm are usually orange or yellow colored in aqueous dispersions containing hydrolysed  $\text{AuCl}_4^-$  in poly (vinyl alcohol) or poly

(vinylpyrrolidone). The polymers in this case absorb weakly in UV region. The absorption spectrum of the gold particles shows maxima at around 680 nm for the gold particles of the sizes 8-12 nm adsorbed on the polystyrene beads (Dokoutchaev *et al.* 1999). Gold dispersions having particles larger than 3 nm in size absorb at 520 nm and are red in color.

For the current system under investigation, the gold nanoparticles, which were generated inside the polyelectrolyte brushes, are brown in color. The UV-Vis spectra shown in Fig. 38 exhibits a broad maxima at around 502-512 nm. Such a maxima is expected for gold nanoparticles, which are less than 3 nm in size. The particles having diameter more than 3 nm absorb at 520 nm and exhibit a red colour, while uncovered gold particles having an average diameter less than 1.5-2.5 nm shows absorbance between 490-500 nm and are orange-yellow colored (Hengelein *et al.* 1999, Duff *et al.* 1993). For the present system, however, the strong scattering of the latex itself precludes further analysis of the UV/VIS spectra. The resonance plasmon of gold appears only as a shoulder in UV/VIS spectrum of the latex. The subtraction of the background (polyelectrolyte brushes, in this case) leads to a broad maxima at around 502-514 nm, emanating from the absorption of light by the gold particles.

During the process of reduction, the latex remains stable. The onset of a slow aggregation is only observed after several days. The factors affecting the stability of the latex covered by gold particles must still be investigated in more detail. For the present investigation it suffices to note that the colloidal stability is not impeded by the chemical reaction taking place in the nano-reactors. It should be noted in this context that no reagents have been used for the stabilization of the Au particles. Hence the surface could be used for immobilizing further functional groups on the surface of the Au particles like sulfur or phosphorus containing reagents.

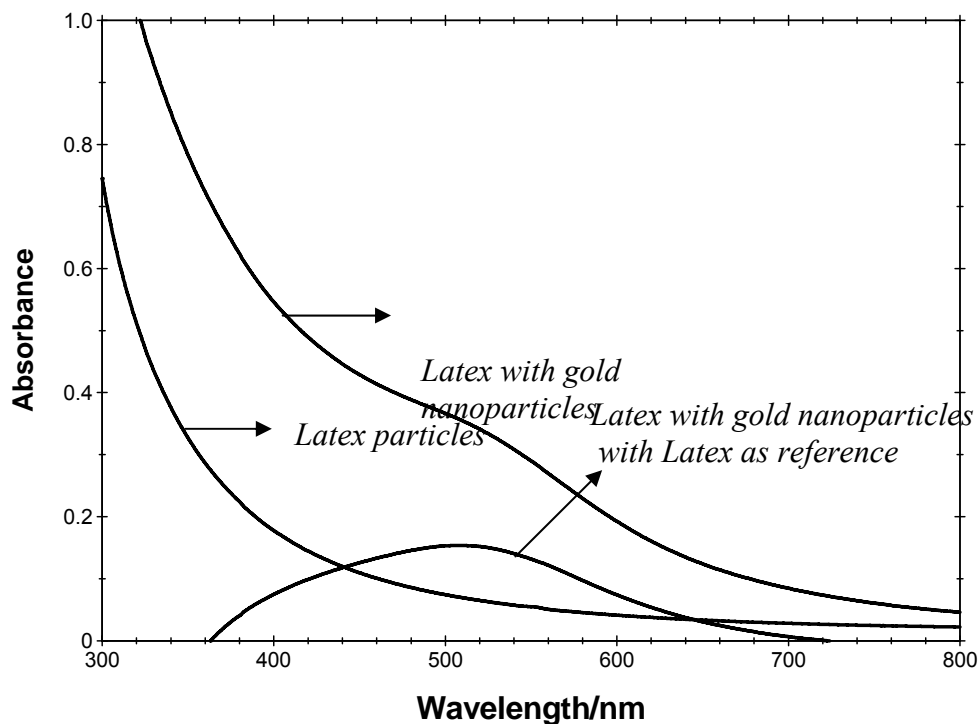


**Fig. 38** UV/VIS spectrum of the reduced gold nanoparticles in the core-shell system. Latex with gold nanoparticles show a shoulder, which is absent in the spectra of latex particles only. Subtracting the absorption of the latex by selecting it as a reference gives the absorption spectra of only gold nanoparticles.

### V.6 Synthesis of Platinum nanoparticles:

The synthesis of platinum nanoparticles was carried out exactly in the same way as that of gold nanoparticles.  $\text{H}_2\text{PtCl}_6$  solution was used as a source of platinum ions to be introduced inside the cationic brushes by using ultrafiltration method already discussed in more details previously (See Section V.2). The mechanism of formation of platinum nanoparticles is identical to that of the formation of gold nanoparticles.  $\text{H}_2\text{PtCl}_6$  solution of  $10^{-5}$  M was used for the ultrafiltration with polyelectrolyte brushes. The excess ions were removed by extensive ultrafiltration with water until the conductivity of the outgoing serum decreased very slowly or remained constant. The platinum ions were then reduced chemically by  $\text{NaBH}_4$ . The greyish black colored latex obtained was stable for months and was later used in catalysis. The characterization of the platinum nanoparticles was carried out by cryogenic temperature transmission electron microscopy.

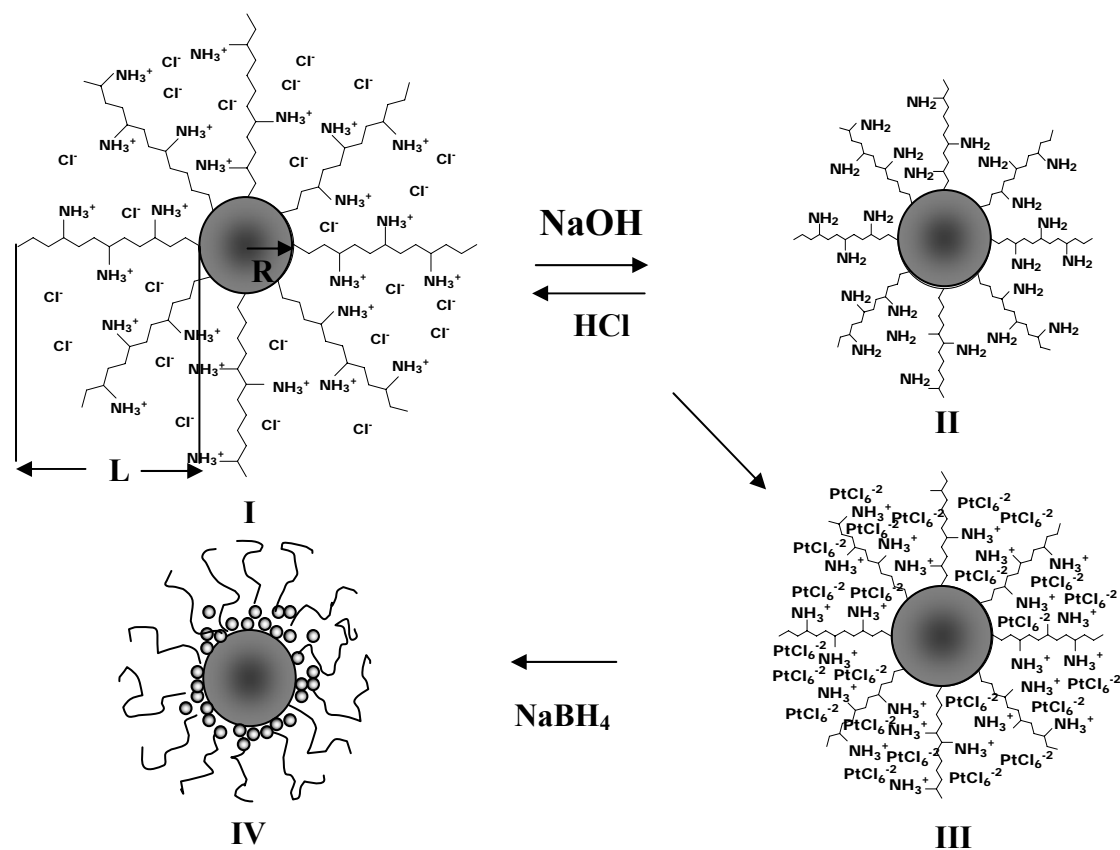


**Fig. 39** Schematic representation of formation of platinum particles on the surface of the core shell system. The core shell system having shell of poly (aminoethylmethacrylate hydrochloride) [I] is deprotonated reversibly at high pH to give amine shell system [II]. I and II can be counterion exchanged/complexed with  $\text{H}_2\text{PtCl}_6$  to give III.  $\text{NaBH}_4$  reduction of III forms IV with nanosized gold particles.

## V. 7 Cryo TEM studies of platinum nanoparticles

**Sample Preparation:** In characteristics of the latex used for the preparation of the sample of platinum nanocomposites can be seen in the Table 2 (See appendix, Sample S5). The hydrodynamic radius of the polystyrene core was 55nm and the contour length was 171nm. The nanoparticles were generated within the polyelectrolyte brushes as described in the previous section. Cryo TEM measurements of the composite particles were carried out using cryo electron microscope (CEM902a, Zeiss, D-Oberkochen, Philips CM120, NL-Eindhoven) on copper grid at 100 K.

**Pt Nanoparticles:** Images obtained by Cryo transmission electron microscopy of the platinum nanoparticles (Fig. 40) confirms the chemical reduction of Pt ions to platinum nanoparticles. Due to the high electron density of the platinum nanoparticles, the contrast of platinum nanoparticles is higher than that of the polystyrene particles so they are easily visible. The platinum particles are roughly spherical in shape.

As Cryo-TEM is done in the frozen solvent, the exact location of the platinum nanoparticles on the carrier particles can be seen in contrast to the TEM studies in the dried state where the drying of the solvent collapses the brush. As discussed in the section V.3, in the collapsed state of the brush it can not be concluded if the metal particles are on the brush or adhered to the polystyrene sphere. As seen in the images, the most of particles are seen resting on the surface of polystyrene surface. Induction of reduction by  $\text{NaBH}_4$  causes ions complexed with the chains of brushes to form nanoparticles, which later adhere to the polystyrene surface due to hydrophobic interactions between the metal nanoparticles and the polystyrene particles. The metal particles are also seen outside the carrier particles in the solution. These particles are seen on some polymeric material, which can be the brush polymer in the solution. It is not clear if these chains were present in the sample before the catalyst preparation or the chains were lost during the preparation of sample for TEM. The particles are seen well separated from each other though a few clusters are also seen. The size of the particle is between 2-5 nm. The latex particles are covered uniformly with the platinum nanoparticles. Some latex particles are seen more densely covered as compared to other latex particles.

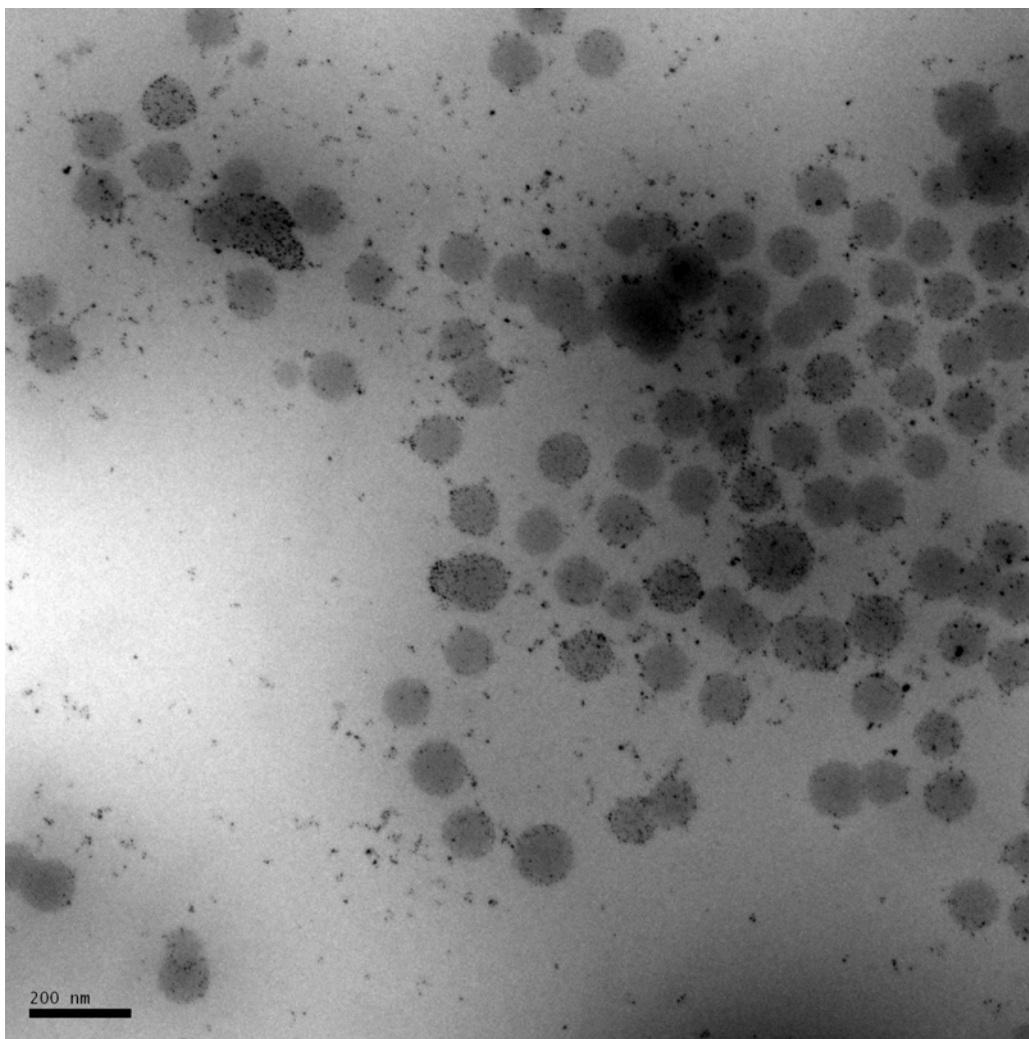
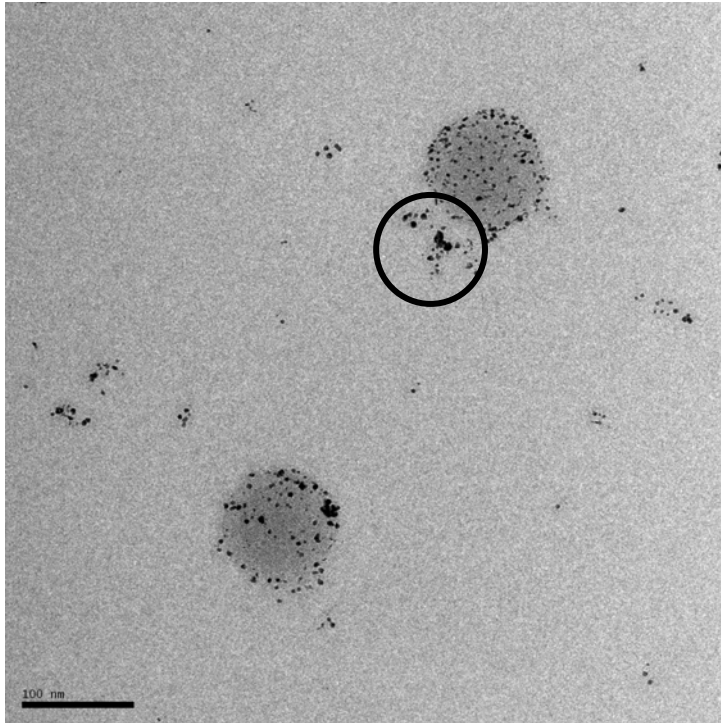
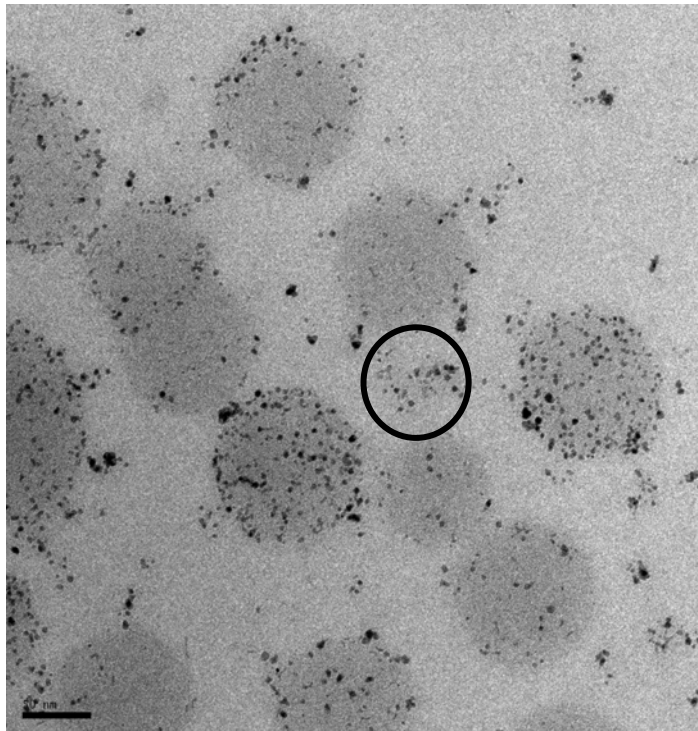


**Fig. 40** Cryogenic TEM of the platinum polystyrene nano composites. Platinum nanoparticles can be easily distinguished from the polymer particles due to its high contrast. Platinum nanoparticles are seen attached to the polystyrene surface. The metal particle seen in the solvent is attached to polymer which can be seen more easily in the high magnification.



100 nm



50 nm

*Fig. 41 Cryogenic TEM of the platinum-polystyrene nanocomposites at higher magnification. The marked regions show the platinum nanoparticles in solution attached to the polymer.*

## V. 8 Generation of silver nanoparticles

Beside gold and platinum, silver is also widely studied for the preparation of nanoparticles. The synthetic methods of silver nanoparticles is similar to the synthesis of gold and platinum nanoparticles. Polymers such as polyacrylic acid, (Boyes *et al.* 2003, Joly *et al.* 2000, Ershov *et al.* 1998) poly N-isopropylacrylamide (Wei *et al.* 1998), polymethacrylate (Quaroni *et al.* 1999) and mesoporous silica (Hornebecq *et al.* 2003, Wang *et al.* 2001) are generally used for the immobilization of silver ions.

For the present study, anionic polyelectrolyte brushes for the synthesis of the silver nanoparticles. A  $10^{-3}$  M solution of  $\text{AgNO}_3$  is stirred with latex of polyacrylic acid brushes for a period of 2 days. After the completion of ionic exchange between the polymer and  $\text{AgNO}_3$ , the latex is concentrated and ultrafiltered against double distilled water to remove excess of the Ag-ions. The entire process is carried out in dark to avoid the reduction of Ag ions by light. Turning of the latex to grey can identify reduction of the Ag ions in between the process. In case of incomplete reduction, the latex is discarded and a fresh synthesis is done. After the cleaning process, the latex is reduced chemically with  $\text{NaBH}_4$ , which turns the white coloured latex to yellow. The colour of the latex depends on the amount of the metal ions inside the latex. Incomplete cleaning of the latexes gives a range of colours from yellow to brown. The latex is stable for months.

The Ag nanoparticles can be characterized by HRTEM and cryogenic TEM. HRTEM images showed a dried sample of the silvered latex. As can be seen in the images (Fig. 42), the silver particles are polydisperse. The biggest particles of silver seen were 15nm in radii and the smallest particles seen were of 1 nm in radii. The lattice fringes of the silver nanoparticles as observed in the images and the diffraction of the X-rays at selected areas confirm the metallic nature of the silver nanoparticles. The silver particles are mostly seen spherical but some elongated spheres are also seen. Cryogenic TEM images show monodisperse nanoparticles of silver approx. 2 nm in size synthesized by the same method as described above (Fig. 43). The enlarged image of Fig 43 in Fig 44 shows the silver nanoparticles more clearly. A few clusters of silver nanoparticles are also seen in the solvent as is indicated by the marked region.

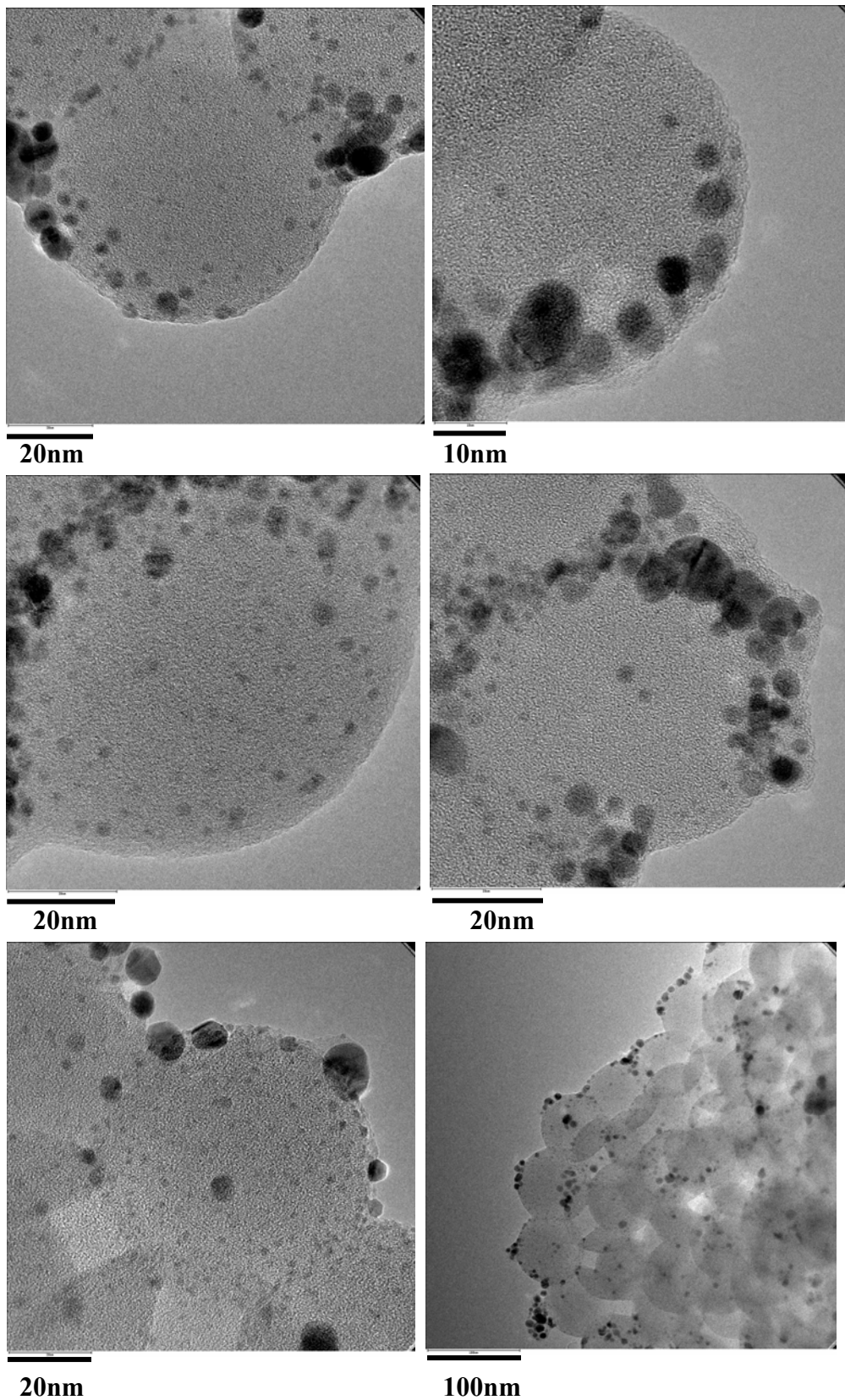
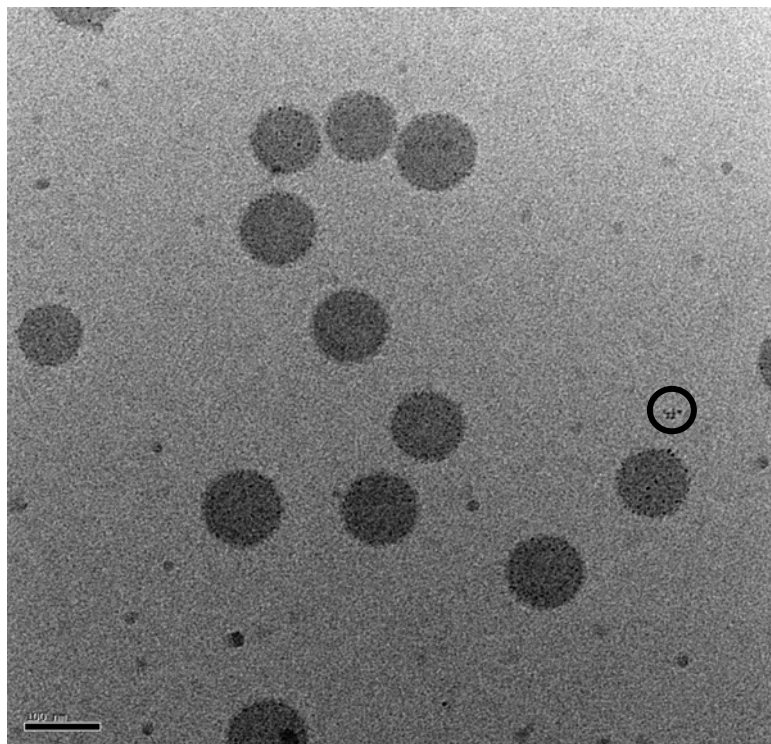


**Fig. 42** HRTEM of silver nanoparticles on polystyrene support. The particles are seen from 1nm to 15nm in radii. The lattice fringes of the silver nanoparticles show the crystalline nature of the particles. The drying of the sample during the sample preparation causes the latex particles to aggregate.



100nm

**Fig. 43** Cryogenic TEM of silver nanoparticles on polystyrene spheres. The region marked by the small circle shows the cluster of silver nanoparticles formed in the solution.

## (VI) Catalysis by metal nanoparticles

### VI.1 Catalytic activity of bulk metals

The capability of metals as catalysts depends on the optimum degree of d- band vacancy (Haruta 2003). The “coinage metals” (Cu, Ag, Au) have fully occupied d-bands. Since Cu and Ag have low ionisation potential they readily lose electrons to yield d-band vacancies and hence can be used as a catalyst more effectively than Au. For example, Cu is used in methanol synthesis and Ag for ethylene oxide synthesis. Au has a high ionization potential and has poor affinity towards molecules of other elements. There is no dissociative adsorption of  $H_2$  and  $O_2$  over the smooth surfaces of Au below temperatures 473K, as proved by surface science investigation (Sault *et al.* 1986, Saliba *et al.* 1998, Koel *et al.* 1998) and density functional theory calculations (Hammer *et al.* 1995, Haruta 2003).

Though catalytic inactivity of Au is theoretically proven, there are some early reports of the catalysis of the combustion of dihydrogen and dioxygen to give water on gold foils. The studies were done by Bone and Wheeler in the year 1906 (Bone *et al.* 1906). At higher temperatures the bulk gold is found to be active for hydrogenation of cyclohexene using gold powder and gold films (Chambers *et al.* 1966, Erkelens *et al.* 1963). Hydrogenation of acrolein has also been performed at enhanced temperatures by bulk gold (Bond *et al.* 1999).

## VI.2 Origin of catalytic activity in metal nanoparticles

Reduction in size of the metal nanoparticles to nano-range modifies the electronic and atomic structures differentiating them from the bulk metal due to quantum size effects. In metals, electrons are delocalised due to the overlap of the conduction and the valence bands in metals. The separation of the valence and the conduction band increases with reduction in size from conductor to semiconductor to insulator. During the transition from semiconductor to insulator, the continuum conduction electron band of the bulk metal splits into discrete energy levels of spacing  $\delta$ , which increases with the decreasing particles size and the line width of the conduction electron spin resonance decreases due to decreasing relaxation times. The energy level spacing  $\delta$  increases with decreasing particles volume (Aiyer *et al.* 1994, Rao *et al.* 2002).

$$\delta = (4E_F / 3N) \approx 1/d^3$$

$E_F$  is the Fermi energy of electrons,  $N$  is the number of conduction electrons, and  $d$  is the particles diameter. Quantum size effects are shown when  $d$  is small enough to fulfill the condition

$$h\nu / \delta \gg 1 \text{ and } h/\tau\delta \gg 1$$

where  $h$  is the Plank's constant,  $\nu$  is the microwave frequency and  $\tau$  is the spin relaxation time (Halperin 1986, Kawabata *et al.* 1970). The catalytic property is dependent on the electronic structure, which is directly related to the size of the metal nanoparticles. For example, for gold nanoparticles on silica, the electronic properties are modified with reduction in the size of the particles as the 5d valence band density of states of the gold particles are shifted towards higher binding energies. There is a redistribution of the valence states as compared to the bulk metal and with increasing particles size, the valence band are restored to that of the bulk metal (Guczi *et al.* 2003, Guzzi *et al.* 2000). Such studies were also carried out for Copper and silver (Paszti *et al.* 1998).

Theoretical calculations by Lopez and Norskov showed that the isolated  $Au_{10}$  clusters are expected to catalyse the CO oxidation below room temperature (Lopez *et al.* 2002). Similar calculations based on density functional theory and molecular dynamic calculations showed that the  $Au_{10}$  and  $Au_{13}$  cluster in three dimensional compact structure are sufficient to act as a catalyst without any support (Okumara *et al.* 2001, Giordano *et al.* 2001, Erkov 2000).

### VI.3 Activity of metal nanoparticles on metal oxide surfaces

The catalytic activity is found more pronounced when the support of the gold nanoparticles is metal oxide. In these cases, the alteration of the electronic properties of the metal/support interface is accounted for the catalytic properties. First experiments, which proved that Au nanoparticles on metal oxide support are active, were carried out by Bond and Sermon (Bond *et al.* 1973). They reported the hydrogenation of alkenes and alkynes at temperatures below 473 K over Au/SiO<sub>2</sub>. Oxygen and hydrogen transfer reactions over Au/MgO and Au/Al<sub>2</sub>O<sub>3</sub> were investigated by Parravano and co-workers (Cha *et al.* 1970). The first experiment to oxidise CO was done by Ozine and coworkers. The atomic Au species reacted with a solid matrix of CO and O<sub>2</sub> to form a complex, which disintegrated above 30 K to produce CO<sub>2</sub>. Haruta and coworkers reported oxidation of CO by composite oxides of Au on 3d transition metal oxides (Fe<sub>2</sub>O<sub>3</sub>, Co<sub>3</sub>O<sub>4</sub>, NiO) prepared by co-precipitation at 200 K. The activity is shown due to the moderate strength of metal-oxygen bonding (Haruta *et al.* 1983, 1987, 1989, 1993).

The changes in the electronic states of the metal nanoparticles with size reduction leading to the catalytic activities is well accepted, but in case of the metal nanoparticles supported on metal oxide support, there are many theories describing the origin of catalytic activity. The theories include the changes in the electronic properties of the metal nanoparticles, the interface, the crystalline state of the metal, and the oxygen vacancy defects in the support particles.

The quantum size effects with respect to the thickness of the gold islands (particles size) on the surface of titania is found to be the cause of catalytic activity towards oxidation of CO by Valden and Goodman (Valden *et al.* 1998, Bond *et al.* 1999). The findings suggested that unusual catalytic properties of the gold clusters originated as the one dimension of the cluster becomes smaller than three atomic spacing. The optimum gold particles size is about 4nm and the band gap is 0.4 eV, which increases in width by decreasing the particle size with further decrease giving rise to non-metallic character. The transition from metal to non-metal is seen when the number of gold atoms in the cluster becomes less than 300.

Turnover frequencies for CO oxidation for Pt and Au particles shows that Au is more active below 4 nm and the activity of Pt particles is more or less same below this size (Haruta *et al.* 1993). The effect can be described for the reaction taking on Pt surface and for Au particles taking on the interface on the edges, corners, step sites, the reaction sites being the periphery of the particles, the number of which are increased by decreasing the particles size

(Mavrikakis *et al.* 2000). The debye functional analysis of X-rays scattered by the Au particles suggested the active species to be 13-atom cluster. Amongst the two possible structures of 13 atom clusters, icosahedron and cubo-octahedron, the former is active (Cunningham *et al.* 1998). The inactive catalyst is found to be 55-atom cluster. The icosahedral cluster shows negative apparent activation energy in the temperature range of 196-273 K (Cunningham *et al.* 1999). The increase in temperature transforms icosahedron to cubo-octahedron.

The active particles of Au always exposed their densely packed (111) plane. (Akita *et al.* 2000) The (111) plane of the Au rested on the oxygen layer of the oxide support. The 2nm hemispherical particles of the Au were found to make contact angle of less than 90°. The wettability changes with the particles size which changes the electronic state of the interfaces. The particles greater than 5nm showed a contact angle greater than 90°(Akita *et al.* 2001). Similar effects of metal-support interactions with the creation of defects in the metal-oxide interface were found by Concepcion *et al.* (Concepcion *et al.* 2004). The Au hemispherical particles strongly attached to the support are found to be active at lower temperatures with better selectivity than the spherical particles loosely bound to the support (Hayashi *et al.* 1998).

Heterogeneous catalysis by a metal supported on a metal oxide support or on a mixed oxide, has been described by Frost (Frost 1998), Weng and Delmon (Weng *et al.* 1992). According to Frost, high activity of the metal/support can be attributed to the junction effect, arising from transfer of electrons from the support to the Fermi level the adjacent metal, giving rise to the oxygen vacancies that become the active sites. Weng and Delmon have explained that in case of mixed metal oxides one oxide needs to function as an activator and supplier of the oxygen while another absorb the co-reactant and receive the reactive oxygen species. In case of platinum, the metal oxide surface is found to play a less role with the reaction occurring mostly on the platinum surface (Bamwenda *et al.* 1997). 8 and 11 cluster of Au were smallest particles to be found to be catalytically active on MgO (Heiz *et al.* 2000). The activity was found to be higher on the defect rich support. Ab initio simulations showed that the partial electron transfer from the surface of the Au clusters and oxygen –vacancy defects in the support are responsible for the activity of the metal particles (Abbet *et al.* 2001, Heiz *et al.* 1999). The crystalline nature of the support is also important in determining the activity of the catalyst. For eg. only anatase TiO<sub>2</sub> and not rutile or amorphous TiO<sub>2</sub> causes Au to be selective for the epoxidation of alkenes. Modification in the structure of TiO<sub>2</sub> has been found by the embedded gold nanoparticles on it (Haruta *et al.* 1998, Mallick *et al.* 2004).

#### VI.4 Chemical reactions catalysed by metal nanoparticles

The chemical reactions catalyzed by metal nanoparticles can be categorized into two parts - Hydrogenation and Oxidation.

##### Hydrogenation reactions:

Partial hydrogenation reactions of hydrocarbons were successfully carried out by Au supported on Al<sub>2</sub>O<sub>3</sub>, SiO<sub>2</sub> and TiO<sub>2</sub> (Bond *et al.* 1973, Okumura *et al.* 2002, Jia *et al.* 2000). Selective hydrogenation of carbonyl bond of crotonaldehyde to crotyl alcohol with a conversion of 80% on Au supported on ZnO (Bailie *et al.* 2001) and by silver nanoparticles (Claus *et al.* 1997) is also reported. Allyl alcohol is produced by hydrogenation of acrolein over Au/ZrO<sub>2</sub>. Synthesis of methanol by hydrogenation of CO and CO<sub>2</sub> is achieved by Au/ZnO (Sakurai *et al.* 1995). Reduction of NO with hydrocarbons to N<sub>2</sub> in the presence of O<sub>2</sub> and H<sub>2</sub>O in engines is carried out by Au supported on Al<sub>2</sub>O<sub>3</sub> (Ueda *et al.* 1996, Salama *et al.* 1996, 1997).

Platinum has been used in hydrogenation of olefins (Grunes *et al.* 2002, Jackson *et al.* 1996, Larpent *et al.* 1991, Thybaut *et al.* 2002), acetonitrile (Arai *et al.* 1998), Heck reaction (Mandal *et al.* 2004) and hydroxylation (Laufer *et al.* 2002) on solid supports. Reactions catalysed by platinum nanoparticles stabilised by polymers and organic molecules are usually in organic phase such as hydrogenation of cyclohexene and other olefins (Mu X. -Dong *et al.* 2004, Mayer *et al.* 1998, Eklund *et al.* 2004). Dendrimer stabilised platinum particles were studied for hydrogenation of alkenes (Zhao *et al.* 1999) where the catalytic activity is found to be affected by the size of the dendrimers. Polymer stabilised Pt nanoparticles are used for electron-transfer reaction (Narayanan *et al.* 2003) and block copolymer stabilised Pt particles have been used for reduction of nitro groups to amines in aromatic compounds (Tu *et al.* 2000, Esumi *et al.* 2004) and carbonyl bonds in sugars (Maranhão *et al.* 2004). Structure, shape and size of Pt nanoparticles have been found to effect the reaction (Narayanan *et al.* 2004, Arai *et al.* 1998, Grunes *et al.* 2002). Other widely studied reactions are selective hydrogenation of  $\alpha$ - $\beta$  unsaturated aldehydes such as citral on Pt/SiO<sub>2</sub> (Singh *et al.* 2000) and hydrogenation of crotonaldehyde to crotyl alcohol on silica (Marinelli *et al.* 1995, Coloma *et al.* 2000, Margitfalvi *et al.* 2000), alumina (Santori *et al.* 2002), titania (Dandekar *et al.* 1999), CeO<sub>2</sub> (Concepción *et al.* 2004) and polymer (Michalska *et al.* 2002, Bailie *et al.* 1999). Enantioselective hydrogenation of ketones with the cinchona derivatised Pt nanoparticles is also being studied (Exner *et al.* 2003, Collier *et al.* 1999). In some cases, selectivity can be controlled by the particle size, temperature and the chemical environment of the catalyst.

## Oxidation reactions

In oxidation reactions, CO oxidation at ambient temperatures (Sakurai *et al.* 1995) has been studied most extensively. Epoxidation of propylene (Haruta 1997), complete oxidation of hydrocarbons (Walters *et al.* 1995, Aida *et al.* 1990, Takita *et al.* 1992), oxidation of nitrogen containing hydrocarbons and decomposition of ozone (Hao *et al.* 2001) are among some of other reactions studied in past.

Hutchings studied addition of HCl to ethyne to produce vinyl chloride. (Hutchings *et al.* 1996) The discovery of metal nanoparticles for hydrochlorination replaced the use of mercuric chloride supported on carbon. Besides being poisonous, the supported mercuric chloride deactivated rapidly.

### VI.5 Catalytic activity of platinum nanoparticles on spherical polyelectrolyte brushes

In this section the catalytic activity of platinum nanoparticles on the surface of the spherical colloidal brushes is discussed. The size of the metal nanoparticles is limited by the polymeric brushes, as the uptake of metal ions is dependent on the brush length. A large surface area provided by the latexes is exploited to disperse the platinum nanoparticles. As the particles are formed on the surface of the latexes, they are available for the direct contact with the reactants. The metal particles are stable against aggregation and have a larger surface area optimum for the catalytic activity. We will discuss here hydrogenation of butyraldehyde as a model reaction to test the catalytic activity of the platinum nanoparticles.

#### Model reaction

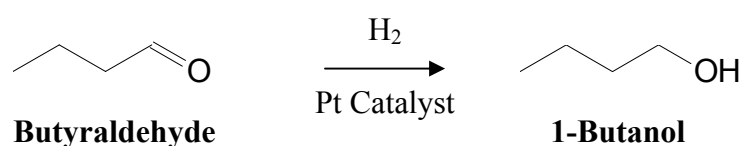


**Fig. 45** Reaction conditions: Time: 3-4 h,  $T = 40^\circ\text{C}$ , Pressure = 65 bar

The reaction is carried out with dihydrogen with the platinum nanoparticles supported on polystyrene as catalyst. The reaction is carried out in aqueous phase and in optimum conditions of  $40^\circ\text{C}$  and 70 bar pressure in an autoclave equipped with a thermostat. Solubility of substrate butyraldehyde in water is 7g/100 ml. At the concentrations used in the catalysis, the substrate is soluble in the aqueous phase. The reactant and product butyraldehyde and 1-butanol both were monitored by gas chromatography.

## Determination of active sites

The number of active sites in a catalyst is an important parameter in catalysis to determine mechanism kinetics of the reaction. In hydrogenation reactions, amount of adsorbed hydrogen per particle of the catalyst gives an exact number of active sites on the catalyst available for the reaction.

Irreversible hydrogen adsorption is determined at 40°C as the hydrogenation of butyraldehyde is carried out at this temperature. The adsorption is determined on the freeze-dried solid catalyst sample. It is assumed that the adsorption of hydrogen is same in the presence of solvent as is in the reaction conditions. The number of moles of hydrogen adsorbed per gram of the freeze dried catalyst is determined by pulse titration ChemBET3000 from Quantachrome which shows that  $1.65 \times 10^{-4} \pm 1 \times 10^{-6}$  moles of hydrogen is adsorbed per gram of the catalyst.

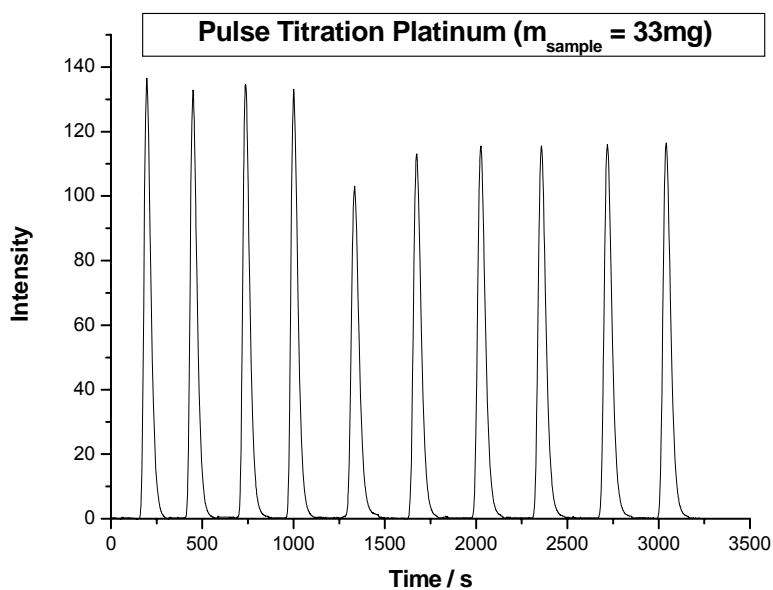


**Fig. 46** Pulse titration of Pt nanocatalyst by ChemBET3000: Moles of active centers are determined via pulse titration of hydrogen adsorption on dried catalyst (40 °C). The first four pulses show the hydrogen transmission of the instrument without any sample. The rest of the pulses are the transmission of hydrogen through the instrument with the sample. The difference of the pulse gives the hydrogen adsorbed by the sample. A value of **478 ± 46** molecules of hydrogen per platinum particle is observed.

The number of platinum particles per gram of the solid catalyst is calculated by the number of platinum particles per polystyrene spheres as observed in the TEM pictures. This value is calculated to be  $3.00 \times 10^{17}$  Pt particles / g of dried catalyst. From the above values the

number of hydrogen molecules adsorbed per platinum particle is  $478 \pm 46$ . The number of active sites in the liquid catalyst can be determined by the equivalent active sites present in the solid content of the liquid.

Alternatively, the average surface area provided by the catalyst can be determined by adsorption of nitrogen. Nitrogen adsorbs on the organic support and not on the platinum particles. Hence, by evaluation of BET isotherms of the organic support and catalyst, the difference in the active areas of can be found, which corresponds to the surface area of the catalyst. This is calculated to be  $18.1 \text{ m}^2$  per gram of the catalyst.

### **Preliminary results**

As described above hydrogenation of butyraldehyde to 1-butanol is studied in aqueous phase. The solid content of the catalyst used in all the studies is 14.4 mgs/ml. First 2 ml of the catalyst was used with 0.11mmols of the substrate i.e., butyraldehyde. A conversion of 90% to 1-butanol is observed. Further reactions were carried out to check the recyclability and kinetics of the reaction.

### **Recyclability of the catalyst**

An important aspect of the catalysis is the lifetime and reusability of the catalyst. Recyclability of the catalyst can be evaluated by carrying out a number of reactions using the same catalyst and comparing the activity for each run.

Using the same catalyst for several number of runs checked recyclability of the catalyst. 0.11mmols of substrate was used for each run. The products were extracted in ether after one run and the residues of ether were removed by sonication at  $40^\circ\text{C}$  from the catalyst. The removal of ether is important as the adsorbed ether prohibits the interaction of substrate and the catalyst resulting in failure of the reaction. Fresh substrate was introduced in the catalyst and the next run was carried out. Fig 47 shows that the catalyst is recyclable at least up to 5 runs. The efficiency of the catalyst remains unaltered during the runs. The conversion was found to be more than 95% for each run. No deactivation was observed during the reruns.

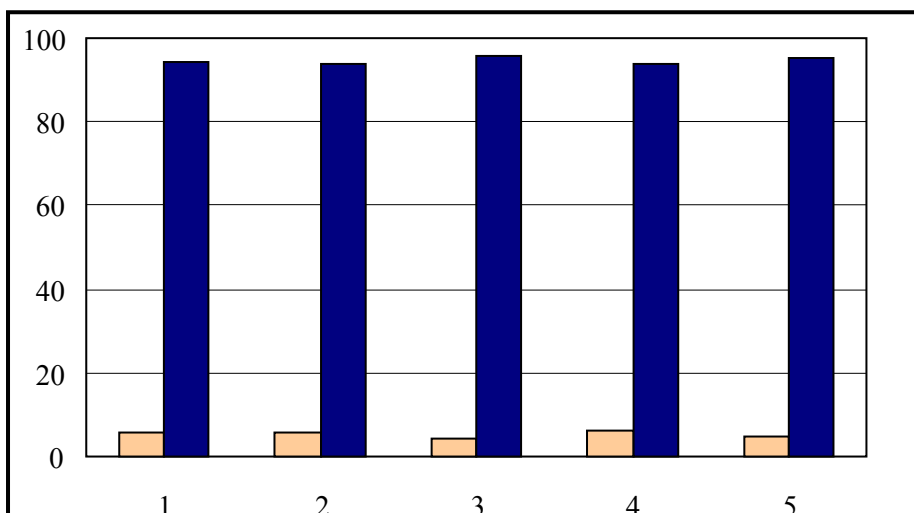


**Fig. 47** ■ Butyraldehyde, ■ 1-Butanol Recyclability of Pt catalyst in hydrogenation of Butyraldehyde for 5 runs. The number of runs on X-axis shows the number of reactions performed with a catalyst. The Y-axis shows the conversion. Reaction Conditions: Buytraldehyde: 0.1mL(0.11mmol); Catalyst Pt/Polystyrene:  $3 \times 10^{15}$  particles/ml water; Volume: 3 ml; Time: 24 h; T: 40 °C; Pressure: 70 bar

CryoTEM pictures of the catalyst before (See Section V.7) and after 5 runs are shown in Fig 48. The particle size of the platinum nanoparticles is nearly the same before and after the run. But a redistribution of the platinum nanoparticles is observed after 5 runs. The number of platinum nanoparticles is observed concentrated on some polystyrene particles and some of the polystyrene particles are found vacant (Fig 48). The higher magnification of the particles is shown in Picture 49. Though the particles are redistributed, the catalytic activity is not found to be affected. This behavior can be due to the catalysis or can also occur during the removal of products by ether. The surface area available of the catalyst affects the catalytic efficiency. With the aggregation of the nanoparticles, the surface area decreases which in turn decreases the catalytic efficiency. In above discussion, the catalytic activity is not found to be affected and also the particles size as can be seen in the Cryo TEM pictures.

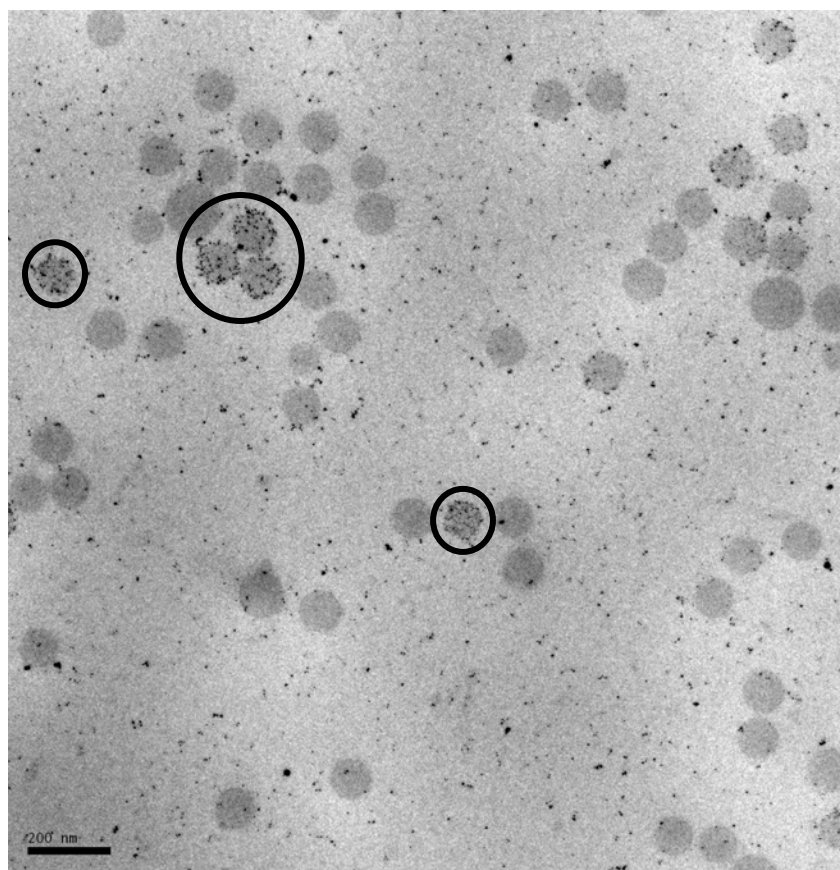


**Fig. 48** Cryogenic TEM of platinum nanocatalysts after 5 runs of butyraldehyde hydrogenation with dihydrogen. The marked particles show more number of platinum nanoparticles. The coverage of polystyrene nanoparticles is not uniform unlike the particles before catalysis (See Section V.7). More polystyrene particles are seen bare. The platinum nanoparticles bounded with polymer are also visible in the solvent.

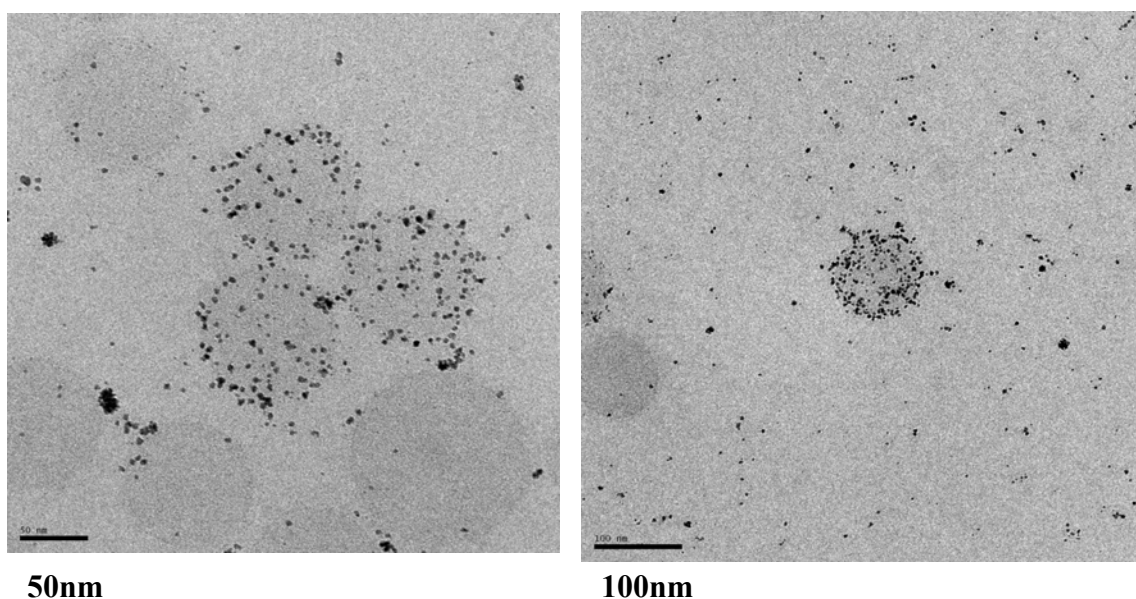


**Fig. 49.** The highlighted particles in Fig. 48 at higher magnification.

## Time dependent studies

Following the disappearance of butyraldehyde as a function of time carries out the time dependent studies of the reaction. The time dependent studies can be utilized to determine important parameters of the reaction like kinetics and reaction mechanism. For the reaction, 0.17mmols of butyraldehyde is hydrogenated with 0.047ml of catalyst diluted to 2ml of volume with water. The reaction was run for 6hrs keeping rest of the conditions constant as described before. Small samples were drawn from the reaction mixture at different times. The results are shown in Fig 50. As seen from the data, the activity is low in first 1hour. The conversion after 4.5hrs becomes nearly 95%.

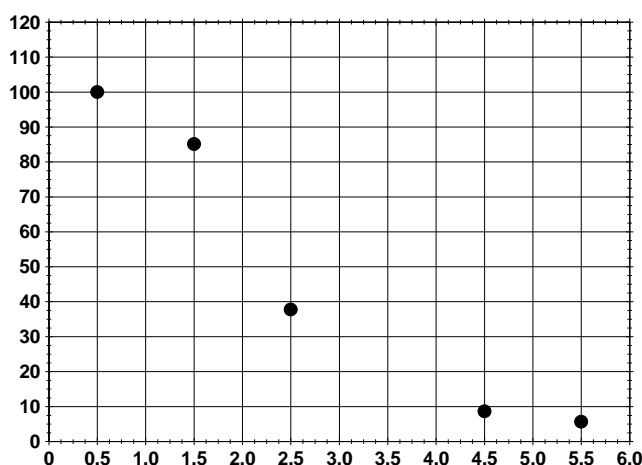


**Fig. 50** Qualitative kinetic studies. Amount of substrate: 0.15 ml (0,17 mmol) 2 ml (0.047 ml Pt-cat. + 1.953 ml water) of the same Catalyst. High conversion is observed after 5hrs. Low activity/conversion is observed initially (0-1hrs)

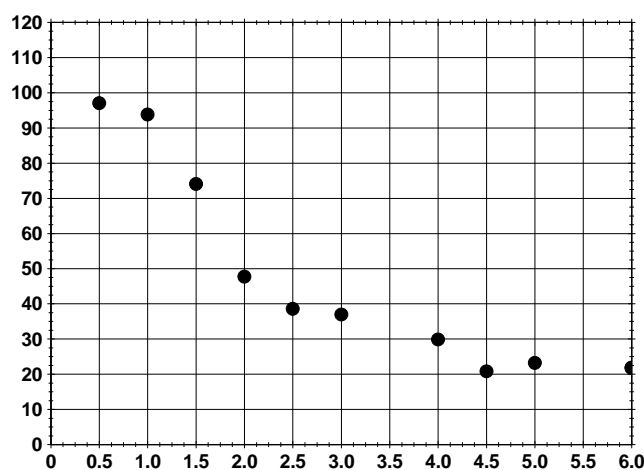


**Fig. 51** Pseudoqualitative kinetic studies. Butyraldehyde (%) as a function of time. Different catalysts with constant concentrations and constant volumes of 2 ml (0.047 ml Pt-cat. + 1.953 ml water). Amount of substrate: 0.1 ml (0,11 mmol).

An alternative way to follow kinetics is a qualitative pseudokinetics (Fig. 51). In this method, instead of drawing samples from the reaction mixture at different interval of times, fresh mixtures are reacted for each time interval. The results are similar as those of the qualitative kinetics. The reaction is complete after 6hrs.

The curve shows that the rate of the reaction is very slow initially, which increases with time and decreases at the completion of the reaction. As stated earlier, the mechanism of the reaction and rate constants of the reaction can be determined by the discussed curves.

### VI.6 Catalysis by Gold nanoparticles:

As discussed in the theory section, theoretically gold nanoparticles should be catalytically active even without an oxide support. In this section catalytic activity of the gold nanoparticles supported on cationic polyelectrolyte brushes is discussed. Polystyrene is an inert material providing no support effect as in the case of oxide support. In the current study the polystyrene latexes grafted with polyelectrolyte brushes only acts as agent to control the particle size and a defence against aggregation of the particles.

The same model reaction, hydrogenation of butyraldehyde as used for the platinum nanoparticles is chosen for the gold particles. The reactions were carried out at 40°C and in aqueous phase. The pressure was 70bar for each run. The number of gold particles per ml  $3 \times 10^{15}$  of the catalyst was determined by TEM and it was assumed that the number of gold particles is constant on all the polystyrene particles. Preliminary results of catalysis showed that gold hydrogenates the carbonyl bond but the rate and the conversion were found to be less than that of the platinum catalyst. Hence the time period of the hydrogenation was increased to 24 hrs. The solubility of butyraldehyde in water is 7gm/100ml. For the concentrations used in the reactions for catalysis, the substrate is soluble in the solvent forming a homogeneous phase. The products were extracted in ether and analysed by GC.

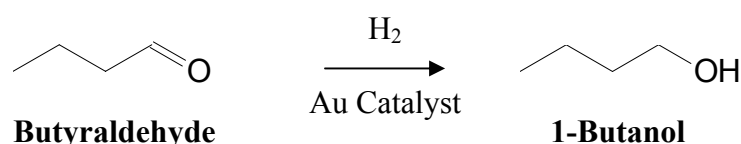


**Fig. 52** Hydrogenation of butyraldehyde by gold catalyst

The conversion after 24hrs was substantial approx. 80% as seen in the first run of the Fig. 53. The next important studies as done for the hydrogenation with platinum nanoparticles are the recyclability of the Gold nanoparticles. The studies to evaluate the recyclability were done in

exactly the same way as done for Platinum nanoparticles as discussed in previous section. The same catalyst was used for a number of runs as shown in the Fig. 53. The products after a run were extracted in ether and fresh substrate is introduced in the catalyst to check the activity further. As seen in the Fig. the conversion is not constant for all the runs.

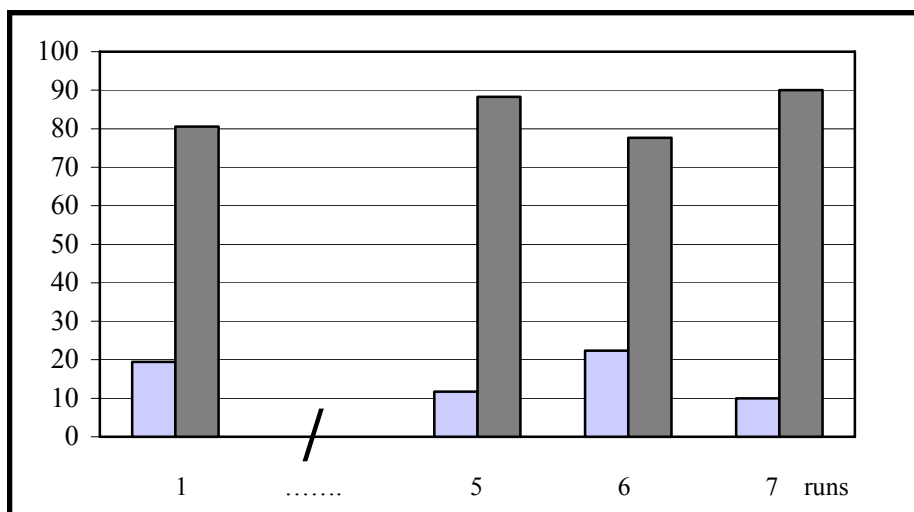


**Fig.53**    ■ Butyraldehyde,    ■ 1-Butanol    *Recyclability of Au catalyst in hydrogenation of Butyraldehyde for 7 runs. The number of runs on X-axis shows the number of reactions performed with a catalyst. The Y-axis shows the conversion. Reaction conditions: Butyraldehyde: 0.1 mL; Cat. Au/ polystyrene/H<sub>2</sub>O → 3 × 10<sup>15</sup> particles/ mL; Time: 24 h; T: 40 °C; pressure: 70 bar; Final Volume of the reaction mixture: 3 ml (2 ml Au-cat. + 1 ml water)*

Catalysis by unsupported gold for the same reaction was carried out in the same reaction conditions. The reaction showed no results and the gold nanoparticles aggregated after the 1<sup>st</sup> run. These experiments were carried out for a gold sol reduced by NaBH<sub>4</sub> and with tetrakis (hydroxymethyl phosphonium) chloride. Both the sols showed no results.

The catalysis by gold nanoparticles supported on polystyrene suggests that the activity of the gold nanoparticles can be attributed to the quantum size effects. Due to the inertness of the polystyrene, electronic interactions between the support material and the metal nanoparticles are absent. The reproducibility of the results suggests that there is no substantial increase in the particles size of the metal nanoparticles

## Summary

This thesis describes synthesis of spherical cationic polyelectrolyte brushes by “grafting from” technique. The spherical polyelectrolyte brushes have been used as “nanoreactors” for the synthesis of metal nanoparticles (Gold, Platinum and Silver). The catalytic activity of the resulting metal/polymer nanocomposites has been tested by heterogeneous hydrogenation of carbonyl groups.

The synthesis of the cationic spherical polyelectrolyte brushes is achieved by a three-step procedure. Firstly, cationic polystyrene core particles are synthesized by emulsion polymerization by using a cationic surfactant and a cationic thermal initiator. In the second step, a thin layer of photoinitiator is generated around the particles by addition of the photoinitiator under “starved conditions”. The photoinitiator is a monomer, which is added when the formation of core particles is in the last stage. The photoinitiator polymerizes with the styrene to give a covalently bound photoinitiator. The core particles are characterized by dynamic light scattering. In the third and last Step, the brushes are grafted on the core particles by photoemulsion polymerization, where the initiation is triggered by UV/VIS radiation. Dynamic Light Scattering follows the growth of the brushes. Further studies were carried out to investigate of the effect of monomer and the photoinitiator concentrations on the thickness of the brushes. At high concentrations of monomers, formation of gel is observed. The important parameters of the brushes- contour length and grafting density are determined by the cleavage of the chains from the surface by alkaline hydrolysis. The ester functionality within the photoinitiator is hydrolyzed under the harsh conditions of hydrolysis. The cleaved chains are analyzed to determine the molecular weight. The grafting of the charged polymeric chains stabilizes the colloids even under unfavorable conditions like high ionic strength and high pH.

The behavior of brushes is investigated at different ionic strength and pH. At different ionic strengths brushes show three regimes- osmotic, salted and neutral regime. At increasing ionic strength, a shrinking in brush thickness is observed due to the screening of ionic charges. The cationic brushes (polyamino ethylmethacrylate hydrochloride and poly vinylbenzylamine hydrochloride) bear protonated amine functionality. The brushes are classified as annealed brushes as they are sensitive towards pH. The brushes lose the protons at high pH, to result in the uncharged brushes, causing them to shrink, which is followed by dynamic light scattering. A sharp decrease in hydrodynamic radii is observed at high pH. The behavior of shrinking is observed at constant ionic strength to eliminate the effect of ionic

strength. The polyaminoethylmethacrylate brushes show shrinking at higher pH as compared to the polyvinylbenzylaminehydrochloride brushes.

Polyaminoethylmethacrylate brushes are used as nanoreactors to synthesize the metal nanoparticles of gold and platinum. The water-soluble metal salts are used to introduce metal ions in the brushes. The negatively charged metal ions ( $\text{AuCl}_4^-$  and  $\text{PtCl}_6^{2-}$ ) interact with the cationic chains of the brushes. Dynamic Light Scattering is used to study the influence of the metal ions on the brushes. It is observed that metal ions induce much more pronounced shrinking as compared to the monovalent ions. The shrinking can be compared with the shrinking caused by multivalent ions such as  $\text{MgSO}_4$ . The metal ions once introduced are localized within the brushes due to strong correlation of counterions with the polyelectrolyte chains. The excess ions are cleaned by ultrafiltration. The trapped counterions render high contrast to the brushes and hence visualize brushes in Cryo-TEM. The metal ions can be reduced chemically by  $\text{NaBH}_4$  to generate nanoparticles. The particles are studied by high-resolution Transmission microscopy and cryogenic TEM. The metal nanoparticles formed are well spaced and crystalline in nature. The particles formed are found to be stable against aggregation. The silver nanoparticles are formed by using the anionic brushes (polyacrylic acid) and  $\text{AgNO}_3$  as the precursor salt.

The catalytic activity of Platinum is tested by the heterogeneous hydrogenation of the carbonyl functionalities with dihydrogen under optimum conditions. The platinum nanoparticles give a 90% conversion of butyraldehyde to 1-butanol. The catalyst is found to be recyclable for a number of runs without losing the efficiency. The time dependent studies are carried out to gain insight in the mechanism and the kinetics of the reaction. The particles are found to be stable after the catalytic cycles. The gold nanoparticles supported on the polystyrene are found to be catalytically active for the same reaction. The gold particles are found to be recyclable for a number of runs without losing the efficiency. The bulk gold is completely inactive, hence the origin of catalytic activity is attributed to the quantum size effects. As the polystyrene particles are inert, the role of support particles in the origin of catalytic activity can be ruled out. The nanoparticles are found to become inactive for catalysis after 6 months of standing with a manifold increase in the particle size as revealed by microscopy.

## Zusammenfassung

Im Rahmen der vorliegenden Arbeit wurde die Synthese kationischer Polyelektrolytbürsten mittels einer „grafting from“-Technik vorgestellt. Die Polyelektrolytbürsten wurden als Nanoreaktoren zur Synthese von Metallnanopartikeln (Gold, Silber und Platin) benutzt. Die katalytische Aktivität der Metall/Polymerkomposite wurde über die heterogene Hydrierung von Carbonylbindungen getestet.

Die Synthese der Polyelektrolytbürsten wurde in drei Schritten durchgeführt. Zuerst wurde ein kationischer Kern-Latex aus Polystyrol durch eine konventionelle Emulsionpolymerisation mit einem kationischen oberflächenaktiver Tensid und einem kationischen Initiator hergestellt. Im zweiten Schritt wurde eine dünne Photoinitiatorschicht auf die Kernoberfläche aufgebracht durch die Zugabe eines Photoinitiators unter „starved conditions“. Der Photoinitiator ist ein Monomer, welches hinzugefügt wird, wenn die Bildung der Kernpartikel nahezu abgeschlossen ist. Der Photoinitiator copolymerisiert mit Styrol, wodurch kovalent gebundene Photoinitiatorgruppen erhalten werden. Die Kernpartikel wurden mittels Dynamischer Lichtstreuung charakterisiert. Im dritten und letzten Schritt wurden die Bürsten über eine sogenannte Photoemulsionspolymerisation aufpolymerisiert, welche über UV-Bestrahlung initiiert wurde. Mittels Dynamischer Lichtstreuung wurde die Ausbildung der Bürsten beobachtet. Weiter wurde der Einfluss der Monomerkonzentration und der Photoinitiatormenge auf die Bürstendicke untersucht. Bei hoher Monomerkonzentration wurde ein Gel erhalten. Die charakteristischen Parameter – Konturlänge und Pfropfungsdichte, wurden über eine Abspaltung der Ketten von der Oberfläche mittels alkalischer Hydrolyse bestimmt. Die Esterfunktionalität der Photoinitiatoreinheit wurde unter diesen Bedingungen hydrolysiert. Das Molekulargewicht der abgespaltenen Ketten wurde bestimmt. Das Aufpfropfen der Polymerketten stabilisiert die Kolloidpartikel selbst bei hohen Ionenstärken und pH-Werten.

Das Verhalten der Bürsten wurde untersucht bei verschiedenen Ionenstärken und pH-Werten. Je nach Ionenstärke werden die Bürsten als „osmotic“ oder „salted brush“ klassifiziert. Mit zunehmender Ionenstärke wird ein Schrumpfen der Bürstendicke beobachtet infolge der Ladungsabschirmung. Die kationischen Bürsten (Polyaminoethylmethacrylathydrochlorid und Polyvinylbenzylaminhydrochlorid) weisen protonierte Amingruppen auf. Die Bürsten sind als „annealed brush“ zu bezeichnen, da sie pH-sensitiv sind. Die Bürsten werden deprotoniert bei hohem pH-Wert, was zu ungeladenen

Bürsten führt. Das Schrumpfen der Bürsten wurde mittels Dynamischer Lichtstreuung verfolgt. Ein starker Rückgang im hydrodynamischen Radius wurde bei hohem pH festgestellt. Diese Untersuchungen wurden bei konstanter Ionenstärke durchgeführt, um Abschirmungseffekte auszuschließen. Die Polyaminoethylmethacrylatbürsten zeigten gegenüber Polyvinylbenylaminhydrochloridbürsten ein Schrumpfen bei hohem pH-Wert auf.

Polyaminoethylmethacrylatbürsten wurden als Nanoreaktoren zur Generierung von Metallpartikeln aus Gold und Platin herangezogen. Wasserlösliche Metallsalze wurden zur abgenutzt zur Einführung der Metallionen in die Bürsten genutzt. Die negativ geladenen Metallionen ( $\text{AuCl}_4^-$  and  $\text{PtCl}_6^{2-}$ ) wechselwirken mit den kationischen Ketten. Die Metallionen bedingen ein viel stärkeres Rückgehen der Schale als monovalente Ionen. Das Schrumpfen ist vergleichbar dem Schrumpfen in Gegenwart mehrwertiger Ionen wie  $\text{MgSO}_4$ . Die Metallionen sind räumlich fixiert aufgrund der starken Korrelation der Gegenionen mit den Polyelektrolytketten. Überschüssige Ionen werden durch Ultrafiltration abgetrennt. Die Gegenionen dekorieren die Polyelektrolytketten und erhöhen dadurch den Kontrast entlang den Ketten, was Cryo-TEM-Untersuchungen der Bürsten ermöglicht. Die Metallionen werden mit  $\text{NaBH}_4$  reduziert unter Bildung von Nanopartikeln. Die Partikel werden mittels „High resolution transmission microscopy“ und Cryo-TEM untersucht. Die Metallpartikel sind regelmäßig geformt und kristalliner Natur. Die Partikel erwiesen sich als stabil gegenüber Aggregation. Die Silbernanopartikel werden ausgehend von anionischen Bürsten (Polyacrylsäure) und  $\text{AgNO}_3$  hergestellt.

Die katalytische Aktivität von Platin wurde über die heterogene Hydrierung von Carbonylverbindungen mit Wasserstoff untersucht unter optimierten Bedingungen. Die Platinnanopartikel erlauben eine 90%ige Umsetzung von Butyraldehyd zu 1-Butanol. Der Katalysator ist mehrfach verwendbar ohne Verlust an Effizienz. Zeitabhängige Studien wurden durchgeführt, um einen Einblick in den Mechanismus und die Kinetik der Reaktion zu erhalten. Die Partikel sind über mehrere katalytische Zyklen hinweg stabil. Die Goldpartikel auf den Kolloidpartikeln sind ebenfalls katalytisch aktiv in der selben Reaktion. Die Goldnanopartikel sind auch wieder verwendbar ohne Effizienzverlust. Gewöhnliches Gold ist inaktiv. Daher ist die katalytische Aktivität auf „Quantum size effects“ zurückzuführen. Da die Polystrolpartikel inert sind, kann ein Einfluss der Trägerpartikel auf die katalytische Aktivität ausgeschlossen werden. Nach 6 Monaten werden die Goldnanopartikel inaktiv, wobei eine mehrfache Zunahme des Partikeldurchmessers einhergeht, wie mikroskopische Untersuchungen zeigten.

## VII Appendix:

### VII.1 Tables

**Table: 1** Different composition of latex system on importance of amounts of surfactant and thermal initiator. Decreasing amounts of surfactant and thermal initiator increased the particles sizes of the particles as expected from the theory of emulsion polymerisation. The first recipe showed the smallest size of the particles obtained and the 5<sup>th</sup> one showed the maximum size obtained. The polydispersity of the particles decreased with the increase in the particles size. The 1<sup>st</sup> composition was chosen for most of the synthesis work.

| Styrene (Mol Wt. 104.2) G/Mol | CTAB (Molwt. 364.5) G/mmol | V-50(Mol. wt.271.2)G/mmol | Water G/Mol | Hydrodynamic radii/nm |
|-------------------------------|----------------------------|---------------------------|-------------|-----------------------|
| 208/1.996                     | 5.31/14.56                 | 0.87/3.2                  | 845/46.95   | 40                    |
| 208/1.996                     | 2.65/7.27                  | 0.87/3.2                  | 845         | 63                    |
| 208/1.996                     | 0.20/0.548                 | 0.87/3.2                  | 845         | 100                   |
| 208/1.996                     | 1.32/3.62                  | 0.21/0.77                 | 845         | 96                    |
| 208/1.996                     | 0.20/0.548                 | 0.42/1.54                 | 845         | 135                   |

### VII.2 Experimental techniques and characterization

#### Materials:

All chemicals used for the synthesis are of analytical grade and were used as received. Styrene (BASF) was distilled under reduced pressure and stored at  $-4^{\circ}\text{C}$  until used. 2-[p-(2-hydroxy-2-methylpropiophenone)]-ethyleneglycol-methacrylate (HMEM) was used as the photoinitiator whose synthesis has been described previously. Hexadecyltrimethylammoniumbromide (CTAB), 2-2'-azodiisobutyramidinedihydrochloride (V-50)(Fluka) were used in synthesis of core particles.

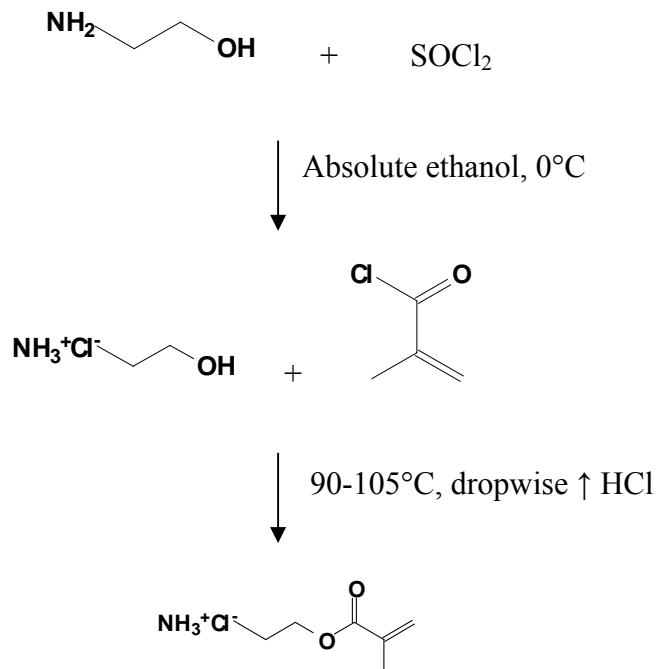
4-vinyl-pyridine (Fluka), ethanolaminehydrochloride (alfa aesar), absolute ethanol (Fluka), methacryloylchloride (Fluka), 1,2dichloroethane, 4chloromethylstyrene(Fluka), pyridine (Fluka), potassiumphthalimide (aldrich), thoinylchloride (Fluka), benzoin (Fluka), acryloylchloride (Fluka), dimethylaniline dimethylformamide (aldrich), chloroform (Fluka), diethylether (Fluka) and hydrazine hydrate (aldrich) were used as received in the synthesis of functional monomers.  $\text{MgSO}_4$  (Fluka),  $\text{NaOH}$  (Fluka),  $\text{Na}_2\text{CO}_3$ (Fluka),  $\text{KOH}$ (Fluka),  $\text{H}_2\text{SO}_4$ (Fluka) were used as received. Silica gel (Silica gel 60, Fluka) was used for chromatography. Tetrachlorogold (III) acid trihydrate (Merck), hexa chloroplatinum (IV) acid trihydrate (Merck), and  $\text{AgNO}_3$  was used to introduce metal ions in the brushes and  $\text{NaBH}_4$  and tetrakis (hydroxymethyl) phosphonium chloride (Merck) was used to reduce the

ions. The water was purified by reverse osmosis (Millipore Milli-RO) and subsequent ion exchange (Millipore Milli-Q).

### Synthesis of monomers

#### Aminoethylmethacrylate hydrochloride(AEMH)

Ethanol amine hydrochloride was heated at 50 °C with stirring, in a two neck flask equipped with a addition funnel, methacryloyl chloride was then added drop wise using the addition funnel, HCl is released as the reaction is triggered, the reaction mixture was further heated at 100 °C, until the release of HCl was totally stopped. The reaction mixture is cooled to room temperature and Aminoethylmethacrylate hydrochloride thus obtained in form of yellow oily liquid is recrystallised in 1,2 dichloroethane.



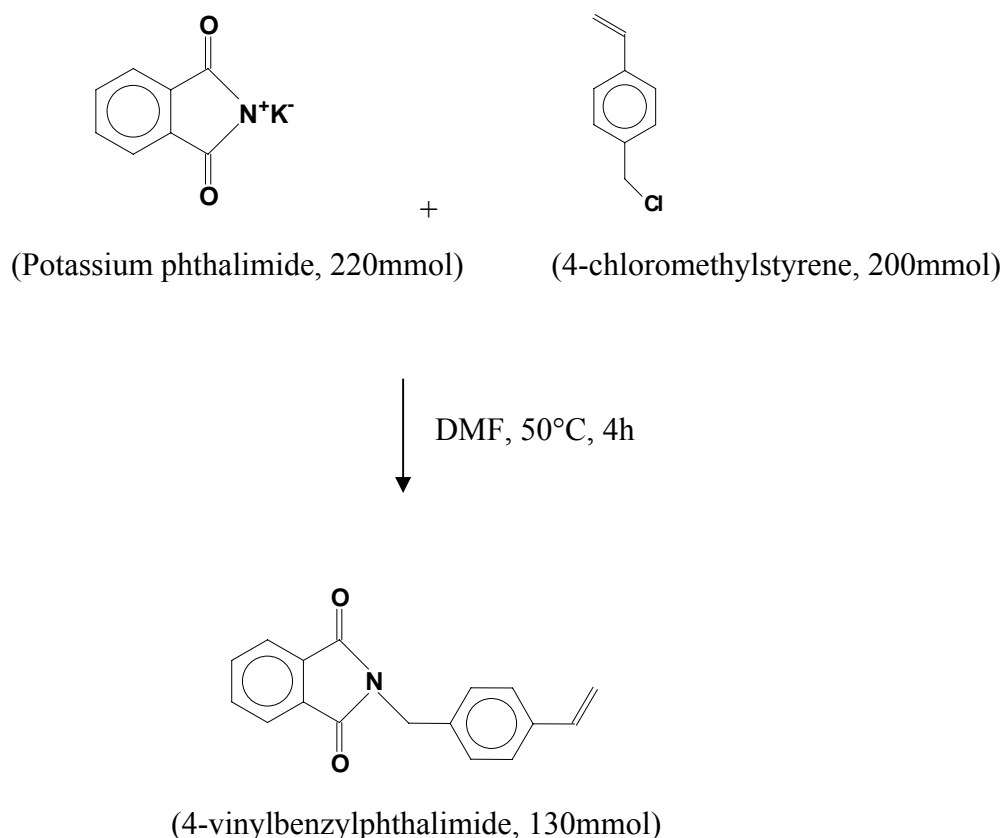
## Vinylbenzylamine hydrochloride(VBAH)

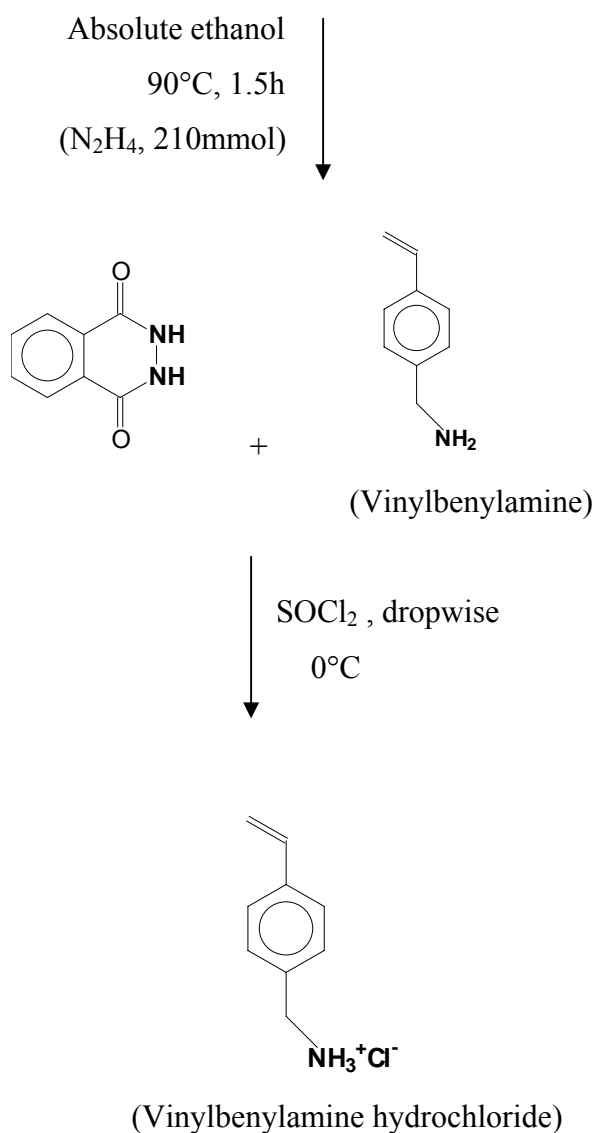
VBAH was synthesized by Gabriel synthesis. Potassium phthalimide (440mmol) was stirred in DMF (250ml) at 50°C and 4-Chloromethylstyrene (400mmol) was added to this solution. The stirring was continued for 4 hrs. The mixture was then concentrated by the evaporation of solvent under reduced pressure.

The solid 4-vinylbenzylphthalimide obtained was dissolved in  $\text{CHCl}_3$ . This organic layer was washed several times with 0.5N NaOH and further treated with water, and dried using  $\text{MgSO}_4$ . The solvent was later evaporated and the white solid obtained was recrystallized from methanol. 4-vinylbenzylphthalimide was taken in 200ml of ethanol and heated till boiling, to this solution was added 20ml of ethanolic hydrazine hydrate solution containing 210mmol of hydrazine hydrate.

A thick white mixture formed instantly was further refluxed for 3 hrs. After cooling, 3N KOH solution was added to dissolve the mixture. The organic layer was extracted with diethylether, washed several times with 5%  $\text{Na}_2\text{CO}_3$  solution and water, dried over  $\text{MgSO}_4$  and evaporated to obtain white liquid.

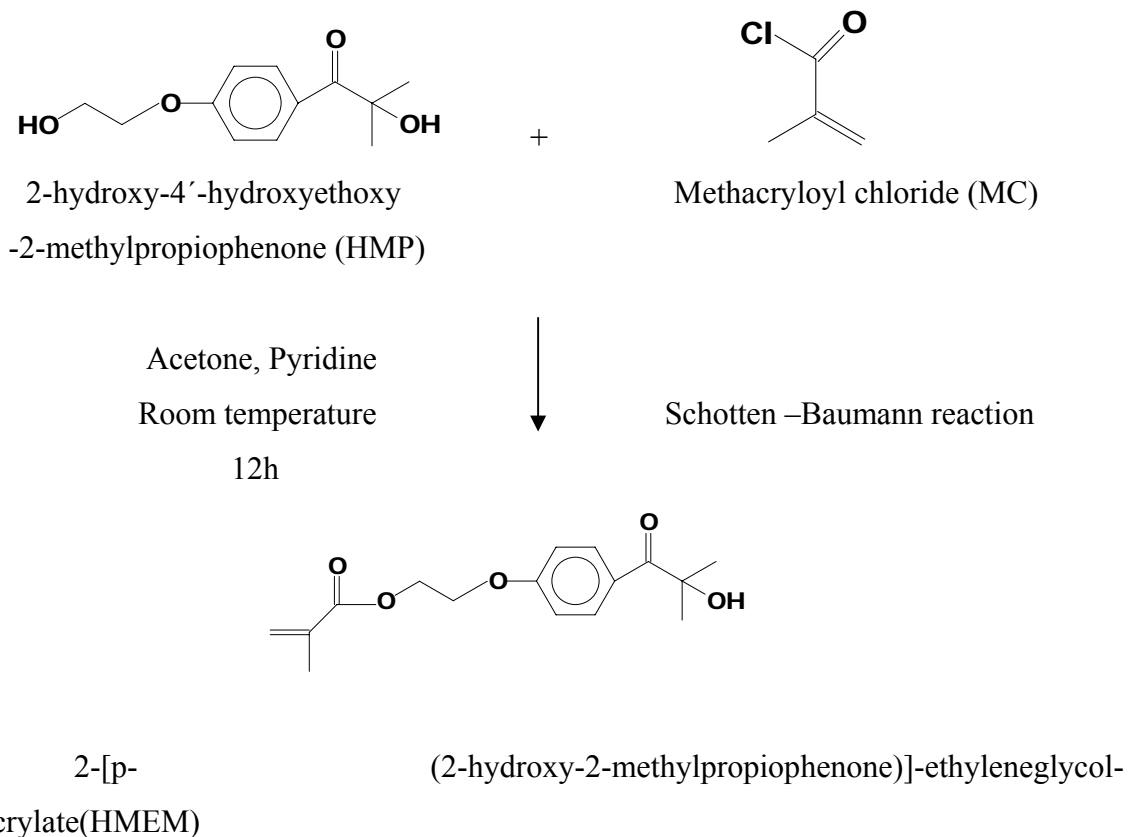
To an ethanolic solution of VBA kept at 0°C, thionylchloride was added drop wise to give a white precipitate of VBAH, which was filtered, dried under vacuum.





### Synthesis of photoinitiator (HMEM) 2-[p- (2-hydroxy-2-methylpropiophenone)]-ethyleneglycol-methacrylate

An Schotten –Baumann reaction, synthesized HMEM. 94.8g of 2-hydroxy-4'-hydroxyethoxy-2-methylpropiophenone (HMP) and 43.1 of methacryloyl chloride (MC) in 600ml of acetone using 50ml of pyridine as catalyst. At first, HMP was dissolved in the mixture of acetone and pyridine. Then MC was added dropwise into the solution, which surrounded by an ice water bath. After the addition of MC, the mixture was stirred for 12 h at room temperature. At last, the solvent was evaporated under vacuum, and the resulting product was carefully washed with water for eight times. Further purification was achieved through chromatography on silica gel (Silica gel 60, Fluka) using acetone as eluent where the thin chromatography serves as the analytical method. The overall yield was 40%



#### Synthesis of phtoinitiator HMEM

HMEM.

<sup>1</sup>H-NMR (CD<sub>3</sub>COCD<sub>3</sub>, δ in ppm): 1.53 (s, 3H, -C(CH<sub>3</sub>)<sub>2</sub>-), 1.93 (s, 3H, =C(CH<sub>3</sub>)), 2.89(s, 1H, OH), 4.45, 4.54(t, 4H, CH<sub>2</sub>CH<sub>2</sub>), 5.69, 6.10(d, 2H, CH<sub>2</sub>), 7.70, 8.28 (m, 4H, C<sub>6</sub>H<sub>4</sub>).

<sup>13</sup>C-NMR(CD<sub>3</sub>COCD<sub>3</sub>, δ in ppm): 207, 164 (CO), 134, 129, 127, 115(C<sub>6</sub>H<sub>4</sub>), 79(C<sub>ter</sub>), 68, 65(COH, OC<sub>2</sub>H<sub>4</sub>O), 28, 29(CH<sub>2</sub>, CH<sub>3</sub>).

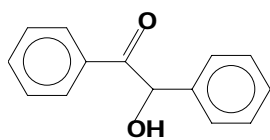
IR (film): 3440, 2978, 1719, 1667, 1601, 1508, 1456, 1375, 1307, 1257, 1166, 1044, 959, 841, 767 cm<sup>-1</sup>

UV( chloroform): λ<sub>max</sub> = 277nm

#### Synthesis of benzoin acrylate(BA)

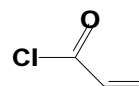
BA was prepared by Schotten –Baumann reaction as well. To a stirred solution of 22.2g (0.102mol) benzoin, 54ml of dimethylaniline and 90ml of chloroform, acryloyl chloride (AC) 57g (0.63mol) was added dropwise below 10°C. after addition of AC, they were reacted for 1 hour maintaining a gentle reflux of the solvent. The unreacted AC and solvent were removed under vacuum, and the residue was hydrolyzed with 6N aqueous H<sub>2</sub>SO<sub>4</sub>, then washed with

water ten times. The product was crystallized from ethanol two times. The overall yield was 90%.



Benzoin

+

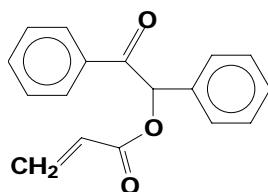


Acryloyl chloride

Chloroform  
Dimethylaniline

Schotten –Baumann reaction

70°C, 1h



Benzoin Acrylate

#### Synthesis of photoinitiator BA

$^1\text{H-NMR}$  ( $\text{CD}_3\text{COCD}_3$ ,  $\delta$  in ppm): 5.99,6.01 (d, 2H, =CH<sub>2</sub>), 6.28-6.32 (q, 2H, =CH<sub>2</sub>), 6.43,6.47(s, 1H, CH), 7.11(s, 1H, C<sub>6</sub>H<sub>5</sub>), 7.41(m, 2H, C<sub>6</sub>H<sub>5</sub>), 7.51 (t, 2H, C<sub>6</sub>H<sub>4</sub>), 7.61(m, 2H, C<sub>6</sub>H<sub>4</sub>), 8.07(d, 1H, C<sub>6</sub>H<sub>4</sub>)

IR (film): 3066, 2360, 1970, 1717, 1693, 1616, 1597, 1499, 1449, 1408, 1367, 1285, 1255, 1231, 1196, 1061, 989, 963, 936, 861, 810, 760, 696  $\text{cm}^{-1}$

UV( Chloroform):  $\lambda_{\text{max}} = 250\text{nm}$

### **Synthesis of polystyrene core particles:**

The polystyrene (PS) core latexes were synthesized in 3000ml double-wall reactor(Büchi) using a conventional emulsion polymerisation. The reactor consists of thermometer, a reflux condenser, a paddle stirrer system (IKA) and a thermostatic system (Lauda R 400). 1 mol of styrene was emulsified by CTAB (7.29 mmol) in 420 ml of water. The mixture was then heated at 80°C under nitrogen atmosphere(evacuated five times). A solution of thermal initiator V-50 (1.617mmoles) in 50ml water was introduced in the reactor. The polymerisation was continued till 20 minutes after which the photoinitiator(HMEM) was added under starved conditions (0.5ml/min) to obtain a thin shell of photoinitiator on the core particles. The temperature was reduced to 70°C. The amounts of the photoinitiator varied from 0.5mol% to 4mol % of the styrene used. After the addition of the photoinitiator the reaction was continued for 6 hrs. The latex obtained was cooled and purified by ultrafiltration till the conductivity of the serum was around 20-30 $\mu\text{S/cm}$ .

### **Synthesis of the core-shell particles by phototemulsion polymerisation:**

The amount of monomer to be added (AEMH or VBAH) was calculated by mol % of the core used in the photoemulsion polymerisation, which varied from (10-60 %). The core used was diluted to 2.5 wt% of water. The mixture of diluted core and the monomer was charged into the reactor ( heraeus TQ 150, volume: 650  $\text{cm}^3$ , range of wavelength: 200-600 nm). The mixture was evacuated and flushed with nitrogen several times. Photopolymerisation was carried out by UV-VIS irradiation with constant stirring. Samples were drawn regularly from the reaction mixture, and the increase in hydrodynamic radii was followed by dynamic light scattering (DLS). The core-shell polyelectrolyte brushes, thus obtained were cleaned by ultrafiltration, using bidistilled and deionized water (Millipore) under a pressure of 1 Bar, until the conductivity of the outgoing serum dropped under 2 $\mu\text{S/cm}$ .

### **Formation of Gold nanoparticles in the brush:**

3.22 ml of the polyelectrolyte brush system (3.10 wt%) was placed in an ultrafiltration cell, ion exchange was then carried out by serum replacement against  $5 \times 10^{-5}$  M of 2 litres  $\text{HAuCl}_4$

solution. The remaining co-ions were cleaned by ultrafiltration with pure water until the conductivity of the serum was reduced to 2  $\mu\text{s}/\text{cm}$ . The white polyelectrolyte brush system turns pale yellow after the treatment with  $\text{HAuCl}_4$  solution this brush system bearing  $\text{HAuCl}_4$  ions as counter ions was then divided into two equal parts and reduced using very dilute solution of  $\text{NaBH}_4$  and tetrakis(hydroxymethyl)phosphonium chloride. Reduction with  $\text{NaBH}_4$  changed the colour of the latex to red whereas using the latter reagent resulted in the colour change of the latex from yellow to white. Further addition of either reagent did not produce any change in the colour, suggesting that the  $\text{HAuCl}_4$  ions present in the system had been completely reduced .

### **Formation of Platinum nanoparticles**

3 ml of the polyelectrolyte brush system(core radii: 40nm, brush thickness:120nm) (2.57wt%) was placed in an ultrafiltration cell, ion exchange was then carried out by serum replacement against  $1 \times 10^{-4}$  M of 2 litres  $\text{H}_2\text{PtCl}_6$  solution. The remaining co-ions were cleaned by ultrafiltration with pure water until the conductivity of the serum was reduced to  $2\mu\text{s}/\text{cm}$ . The white polyelectrolyte brush system turns pale yellow after the treatment with  $\text{H}_2\text{PtCl}_6$  solution. This brush system bearing  $\text{H}_2\text{PtCl}_6$  ions as counter ions was reduced using very dilute solution of  $\text{NaBH}_4$ . Reduction with  $\text{NaBH}_4$  changed the colour of the latex to black. Further addition of either reagent did not produce any change in the colour,suggesting that the  $\text{H}_2\text{PtCl}_6$  ions present in the system had been completely reduced .

### **Formation of Silver nanoparticles inside the brushes**

7 ml of core shell system(core diameter: 99 nm diameter,brush length: 130 nm),solid content:1.45 %, was stirred in 0.001 M  $\text{AgNO}_3$ , in dark for 2 days for exchange of  $\text{H}^+$  ions with  $\text{Ag}^+$  ions. The core shell system was cleaned with deionised water till the conductivity was 1  $\mu\text{S}$ . The cleaned core was reduced by freshly prepared  $\text{NaBH}_4$  solution. The latex turns from white to yellow.

### **Purification of latexes**

The cleaning of both core and core shell particles is very important as the amount of surfactant on the core particles affects the thickness of the brush formed and the polyelectrolyte left on the core shell add up to the ionic strength of the solution.

## **Dialysis**

The dialysis uses membranes (cut off 12000-14000) from Visking (Medicell). The membranes were boiled for two hours before use. The latexes were filled in and the tubes are rotated to maintain a high concentration gradient of diffusible molecules across the membrane. The serum is renewed every day until its conductivity is constant.

## **Ultrafiltration**

In this process, a reservoir is connected to a cell having a membrane at its base. The latex is filled inside the cell. The pore size of the membrane is chosen such that it is permeable only to the small polyelectrolyte chains and latex particles can't pass through it. Air or nitrogen pressure is applied to the reservoir so that water flows through the connecting tubes to the cell and then through the membrane and hence separating the latex from smaller molecules. The latex particles are rotated with the help of magnetic stirrer to avoid latex from settling in the cell.

Membranes are of pore sizes 0.05 $\mu\text{m}$  to 0.1 $\mu\text{m}$ . The material of the membranes is cellulose nitrate or regenerated cellulose.

## **Contrast solution for transmission microscopy**

The contrast solution usually contains a protein bovine serum albumin (0.1 wt%), tungsten phosphonic acid (1 wt%) and sucrose sugar (2 wt%). The pH is maintained around 6-7.

## **Analytical Methods**

Photoemulsion polymerisation was done in UV-reactor (Heraeus TQ 150 Z3) the wavelength range was from 200- 600nm with the capacity of 650cm<sup>3</sup>. The pH and conductometric measurements were carried out by Q pH 70 and Q cond 2200 pH meter and conductometer, respectively. Characterization by NMR spectroscopy using a Bruker AMC 400 spectrometer. Tetramethylsilane (TMS) served as an internal standard. Gas chromatography was carried out by Agilent 6890N mit FID equipped with Agilent 19091J-413 FS- Kapillarsäule, HP-5 column.

## Instrumentation & Methods

### Dynamic Light scattering

The hydrodynamic radius was determined by dynamic light scattering using a Peters ALV 4000 goniometer. The hydrodynamic radius of the latex particles can be determined by dynamic light scattering (DLS)(sometimes termed photon correlation spectroscopy) (PCS) or quasi-elastic light scattering(QELS)).

When light shines on matter, the electric field of the light induces oscillations of the electrons in the molecules, the molecules then serve as secondary sources of light and subsequently scatter light. The intensity of scattered light is determined by the size, shape and the molecular interactions in the scattering material. Thus from the light scattering characteristics of a given system it is possible to obtain information about the structure and molecular dynamics. [Berne and Pecora 1976]

A coherent light source laser is required for the dynamic light scattering .the interference patterns are produced by the array of particles. The particles in a colloidal dispersion are in continuous Brownian Motion(particle diffusion).When the particles in a change positions, the light paths (and hence the phases) of the scattered waves are altered. As a result, the detected light fluctuates between bright (constructive interference)and dim&destructive interference).Thus the temporal fluctuations in scattered intensity provide information of the particles motions. The dynamic light exploits this fact.

In essence the moving particles shifts the scattered radiation by the Doppler effect and the Doppler shift can be obtained by a correlation analysis for a continuous time-record of the intensity scattered from the single coherence area. The correlation function represents the fluctuations in the light intensity, namely the relation between the average intensity at a time  $(t + \tau)$  and that at time  $t$ . This function in effect is a measure of the probability of a particle moving a given distance in a time  $\tau$ . [Philips 1990,Takeo 1999]

The analysis of the fluctuations in the intensity  $I$  of the light scattering yields the normalised time correlation function  $g_2(\tau)$  which is defined as [Ottewill 1997]:

$$g_2(\tau) = \frac{\langle I(0)I(\tau) \rangle}{\langle I \rangle^2}$$

Where the angular brackets denote a time-averaged result.  $\langle I \rangle$  is the conventional time average intensity which describes the average of the fluctuations taken over a long time interval.

$$\langle I(0)I(\tau) \rangle = \lim_{T \rightarrow \infty} \frac{1}{T} \int_0^T I(t)I(t+\tau)dt$$

Where  $\tau$  is the correlation time,  $T$  the averaged time.

Since the number of scattering particles is very large, the Siegert relation holds [Nicholson *et al.* 1982]

$$g_2(\tau) = 1 + C [g_1(\tau)]^2 \quad (1)$$

where  $C$  is a constant close to unity depending on the experimental conditions ( $0 < C < 1$ ) and  $g_1(\tau)$  is the temporal correlation function of the scattered light field,  $g_1(\tau)$  depends on the structure, the size polydispersity, and the inner movement of the particle.

In the case of monodisperse spherical particles the correlation function is a simple exponential function:

$$g_1(\tau) = \exp(-\Gamma \tau)$$

Where  $\Gamma$  denotes the relaxation rate:

$$\Gamma = Dq^2$$

Where  $D$  is the diffusion coefficient and  $q$  the scattering vector which is defined as

$$q = \frac{4\pi}{\lambda} \text{Sin} \frac{\theta}{2}$$

Where  $\lambda$  denotes the wavelength of the light and  $\theta$  the scattering angle. Since  $D$  is given by the Stokes-Einstein equation.

$$D = \frac{kT}{6\pi\eta R_h}$$

Where  $K$  is the Boltzmann constant,  $T$  the absolute temperature,  $\eta$  the viscosity of the medium and  $R_h$  the hydrodynamic radius of the particles.

In the case of real latex system, the distribution of the particles size must be taken into account. For polydisperse systems,  $g_1(\tau)$  consists of the sum of a great number of exponential terms. For reasonably narrow size distributions, the method of cumulants [Koppel 1972] is frequently used to obtain an average particle size [Ottewill 1997].

The size distribution assumed continual, eq 1 can be rewritten for the polydisperse system as:

$$g_1(\tau) = \int_0^{\infty} G(\Gamma) \exp(-\Gamma \tau) d\tau$$

Where  $G(\Gamma)$  is the distribution function of  $\Gamma$ . Then, according to the Siegert relation we

have;

$$g_2(\tau) - 1 = C \left[ \int_0^{\infty} G(\Gamma) \exp(-\Gamma \tau) d\tau \right]^2 \quad (2)$$

Practically,  $G(\Gamma)$  is estimated by “cumulants –fit”: fitting the experimental data by the power series of  $\Gamma$  (or  $\tau$ ) [stock and Ray 1985].

Eq 2 can be reduced to

$$\frac{1}{2} \ln \left[ \frac{g_2(\tau) - 1}{C} \right] = -K_1 \tau + \frac{1}{2!} K_2 \tau^2 - \frac{1}{3!} K_3 \tau^3 + \dots$$

Where  $K_1, K_2$  and  $K_3$  are the 1<sup>st</sup>, 2<sup>nd</sup> and 3<sup>rd</sup> moment,  $K_1, \frac{K_2}{K_1^2}$  and  $\frac{K_3}{K_1^3}$  are the cumulants of the distribution function  $G(\Gamma)$  and the characterize the average value, the width and the slope respectively. namely:

$$K_1 = \bar{\Gamma} = \bar{D}q^2$$

Then

$$\bar{D} = \frac{K_1}{q^2}$$

Where  $\bar{D}$  is the intensity weighted average diffusion coefficient:

$$\bar{D} = \frac{\sum N_i M_i^2 P_i(q) D_i}{\sum N_i M_i^2 P_i(q)}$$

Where  $P(q)$  denotes the form factor,  $N_i$  and  $M_i$  are the number and the number average molecular weight of the species  $i$  respectively.

In case of very small particles or  $q \rightarrow 0$

$\bar{D}$  represents the z-averaged value. [Wiesse 1992]:

$$\bar{D} = \frac{\sum N_i M_i^2 D_i}{\sum N_i M_i^2} = \bar{D}_z$$

Thus, the averaged hydrodynamic radius  $\bar{R}_h$  is given from [Ottewill1997]:

$$\overline{D} = \frac{kT}{6\pi\eta\overline{R}_h}$$

Where  $\overline{R}_h$  can be expressed as

$$\overline{R}_h = \frac{\sum N_i R_i^6}{\sum N_i R_i^5}$$

Moreover, the ratio  $\frac{K_2}{K_1^2}$  can provide the information about the polydispersity [Ottewill 1997]

### **UV spectroscopy:**

UV spectrophotometer (Perkin-Elmer Lambda 2S, Lambda 19) equipped with the Wolfram-halogen lamp for visible range and Deuterium lamp for UV range has been used to measure the absorption of the metal nanoparticles.

### **Transmission electron microscopy:**

Low magnification TEM microscope Hitachi H7 operated at 150V (Faculty of physics, University of Karlsruhe) has been used to investigate the core particles. The samples are prepared by mixing 1% of the latex with the contrast solution as described before. The particle size has been calculated using Carl Zeiss, TGZ3 measuring the diameter of the latex and then correcting it by the magnification value. High resolution transmission electron microscopy has been done using Philips (FEI) CM 200 FEG ( Faculty of physics, University of Karlsruhe) equipped with a energy dispersive X-ray system. The composite particles were investigated using HRTEM. The sample has been prepared on carbon grid without using the contrast solution. Crystallinity of the samples were evaluated from the selected area electron diffraction. EDX was used to exactly confirm the elements.

### **Cryogenic Transmission microscopy**

A drop of sample was put on an untreated pure copper TEM grid (600mesh, Science Services, Muenchen, Germany), where most of the liquid was removed with blotting paper leaving a thin film stretched over the grid holes. The specimens were instantly shock frozen by rapid immersion into liquid ethane and cooled to approximately 90K by liquid nitrogen in a temperature – controlled freezing unit (Zeiss cryobox, Oberkochen, Germany). The temperature was monitored and kept constant in the chamber during all the sample preparation steps. After freezing the specimens, the remaining ethane was removed using

blotting paper. The specimen was inserted into a cryotransfer holder (Gatan CT 3500, Munich, Germany) and transferred to a Zeiss 922 EFTEM (Zeiss, Oberkochen, Germany). Examinations were carried out at a specimen temperature of approximately  $-180^{\circ}\text{C}$ . The TEM was operated at 200kV acceleration voltage and a beam current of  $1\mu\text{A}$ . Images were taken with electron doses of approximately 10 to  $500\text{e}/\text{nm}^2$ . Zero loss filtered images were registered digitally by a CCD camera (Gatan ultrascan 1000, Munich, Germany) combined and processed with a digital imaging processing system (Digital micrograph 3.9, Gatan, Munich, Germany)

## VII.4 References

- Abbet, S.; Heiz, U.; Häkkinen, H.; Landman, U. *Phys. Rev. Lett.* **2001**, 86, 5950.
- Acar, N.; Tulun, T. *Euro. Polym. J.* **2001**, 37, 1599.
- Adams, H. N.; Strähle, J. Z. *Anorg. Allg. Chem.* **1982**, 485, 65.
- Ahmadi, T. S.; Wang, Z. L.; Green, T. C.; Henglein, A.; El-Sayed, M. A. *Science* **1996**, 272, 1924.
- Ahmad, A.; Senapati, S.; Khan, M. I.; Kumar, R.; Ramani, R.; Srinivas, V.; Sastry, M. *Nanotechnology* **2003**, 824.
- Ahrens, B.; Jones, P. G.; Fisher, A. K. *Eur. J. Inorg. Chem.* **1999**, 1999, 1103.
- Aida, T.; Higuchi, R.; Niiyama, H. *Chem. Lett.* **1990**, 2247.
- Aiyer, H. N.; Vijayakrishnan, V.; Subanna, G. N.; Rao, C. N. R. *Surf. Sci.* **1994**, 313, 392.
- Akin, H.; Hasirci, N. *J. App. Polym. Sci.* **1992**, 46, 1307.
- Aiken, J. D., III; Finke, R. G. *J. Mol. Catal. A: Chem.* **1999**, 145, 1.
- Aiken, J. D., III; Finke, R. G. *J. Am. Chem. Soc.* **1999**, 121, 8803.
- Aiken, J. D., III; Finke, R. G. *Chem. Mater.* **1999**, 11, 1035.
- Akita, T.; Tanaka, K.; Tsubota, S.; Haruta, M. *J. Electron Microsc.* **2000**, 49, 657.
- Akita, T.; Lu, P.; Ichikawa, S.; Tanaka, K.; Haruta, M. *Surf. Interface Anal.* **2001**, 31, 73.
- Alexander A.E.; Napper, D.H., *Chem. Ind. (London)* **1967**, 46, 1936.
- Alivisatos, A. P. *Science* **1996**, 271, 933.
- Al-Mawlawi, D.; Liu, C.Z.; Moskovits, M. *J. Mater. Res.* **1994**, 9, 1014.
- Alguacil, F. J.; Martinez, S. A.; Sastre, M. *J. Chem. Res(S)* **2001**, 384.
- Alvarez, J.; Liu, J.; Roman, E.; Kaiser, A. E. *Chem. Commun.* **2000**, 1151.
- An, S. W.; Thirtle, P. N.; Thomas, R. K.; Baines, F. L.; Billingham, N. C.; Armes, S. P.; Penfold, J. *Macromolecules* **1999**, 32, 2731.
- Anderson, R.; Griffin, K.; Johnston, P.; Alsters, P. L. *Adv. Synth. Catal.* **2003**, 345, 517.
- Antonietti, M.; Wenz, E.; Bronstein, L.; Seregina, M. *Adv. Mater.* **1995**, 174, 795.
- Antonietti, M.; Grohn, F.; Hartmann, J.; Bronstein, L. *Angew. Chem. Int. Ed.* **1997**, 36, 2080.
- Antonietti, M.; Förster, S.; Hartmann, J.; Oestreich, S. *Macromolecules* **1996**, 29, 3800.
- Antonietti, M.; Schmidt, M. *Macromolecules* **1991**, 24/25, 6636.
- Arai, M.; Takada, Y.; Nishiyama, Y. *J. Phy. Chem. B* **1998**, 102, 1968.
- Arnold, R.; Caplan, S. R. *Trans. Fara. SOC.* **1955**, 51, 857.
- Asakawa, M.; Higuchi, M.; Mattersteig, G.; Nakamura, T.; Pease, A. R.; Raymo, F. M.; Shimizu, T.; Stoddart, J. F. *Adv. Mater.* **2000**, 12, 1099.

Ascendio, J.A.; Perez, M.; Jose-Yacamán, M. *Surf. Sci.* **2000**, 447, 73.

Atik, S. S.; Thomas, J. K. *J. Am. Chem. Soc.* **1982**, 104, 5868.

Ball, P. *Nature* **1993**, 362, 123.

Ball, P. Garwin, L. *Nature* **1992**, 355, 761.

Bailie, J. E.; Abdullah, H. A.; Anderson, J. A.; Roehchester, C. H.; Richardson, N. V.; Hodge, N.; Zhang, J. G., Burrows, A.; Kiely, C. J.; Hutchings, G. J. *Phys. Chem. Chem. Phys.* **2001**, 3, 4113.

Bailie, J. E.; Hutchings, G. J. *Chem. Commun.* **1999**, 2151.

Balamurugan, S.; Mendez, S.; Balamurugan, S. S.; O'Brien II, M. J.; López, G. P. *Langmuir* **2003**, 19, 2545.

Bamwenda, G. R.; Tsubota, S.; Nakamura, T.; Haruta, M. *Catal. Lett.* **1997**, 44, 83.

Beccat, P.; Bertolini, J. C.; Gauthier, Y.; Massadier, J.; Ruiz, P. *J. Catal.* **1990**, 126, 451.

Bellare, J. R.; Davis H. T.; Scriven L. E.; Talmon, Y. *J. Electron Micro. Techn.* **1988**, 10, 87.

Belloni J., Amblard, J.; Marignier, J. L.; Mostafavi, M. *Springer Ser. Chem. Phys.* **1994**, 56, 290.

Bharathi, S.; Lev, O. *Chem. Commun.*, **1997**, 2303.

Biesalski, M.; Rühle, J. *Macromolecules* **2002**, 35, 499.

Biesalski, M.; Rühle, J. *Macromolecules* **1999**, 32, 2309.

Biesalski, M.; Rühle, J. *Langmuir* **2000**, 16, 1943.

Biesalski, M.; Rühle, J. *Macromolecules* **2003**, 36, 1222.

Biffis, A.; Orlandi, N.; Corain, B. *Adv. Mater.* **2003**, 15, 1551.

Biver, C.; Hariharan, R.; Mays, J.; Russel, W. B. *Macromolecules* **1997**, 30, 1787.

Blaul J., Wittemann, M., Ballauff, M., Rehahn, M. *J. Phys. Chem. B.*, **2000**, 104, 7077.

Borsla, A.; Wilhelm, A. M.; Delmas, H. *Catal. Today* **2001**, 66, 389.

Börner, H. G.; Duran, D.; Matyjaszewski, K.; Silva, M. D.; Sheiko, S. S. *Macromolecules* **2002**, 35, 3387.

Bond, G. C.; Sermon, P. A. *Gold Bull* **1973**, 6, 102.

Bond, G. C.; Sermon, P. A. *J. Chem. Soc., Chem. Commun.* **1973**, 444.

Bond, G.C.; Thompson, D.T. *Catal. Rev. -Sci. Eng.* **1999**, 41, 319.

Bone, W. A., Wheeler R.V. *Trans. Royal Chem. Soc.* **1906**, 206, 1.

Bönnemann, H.; Richards, R. M., *Eur. J. Inorg. Chem.* **2001**, 2455.

Boudart, M. *Nature* **1994**, 372, 320.

Boyes, S. G., Akgun, B.; Brittain, W. J.; Foster, M. D. *Macromolecules* **2003**, 36, 9539.

Bradley, J. S.; Tesche, B.; Busser, W.; Masse, M.; Reetz, M. T. *J. Am. Chem. Soc.* **2000**, 122, 4631.

Brandup, J. and Emmergut, E. H., Eds., *Polymer handbook*, 3<sup>rd</sup> ed. Wiley, New York, **1989**.

Breitscheidel, B.; Zieder, J.; Schubert, U. *Chem. Mater.* **1991**, 3, 559.

Bronstein, L. M.; Chernyshov, D. M.; Valetsky, P. M.; Wilder, E. A.; Spontak, R. J. *Langmuir* **2000**, 16, 8221.

Bronstein, L. M.; Mirzoeva, E. Sh.; Seregina, M. V.; Valetsky, P. M.; Solodovnikov, S. P.; Register, R. A. *Nanotechnology* **1996**, 622, 102

Brouwer, W. M. *Eur. Polym. J.* **1990**, 26, 1, 35.

Bruchez, M. Jr. ; Moronne, M.; Gin, P. ; Weiss, S., Alivisatos, A. P. *Science* **1998**, 281, 2013

Brus, L. *Curr. Opin. Colloid Interface Sci.* **1996**, 1, 197.

Brust, M.; Bethall, D.; Schiffrin, D. J.; Kiely, C. J. *Adv. Mater.* **1995**, 7, 795.

Brust, M.; Walker, M.; Bethell, D.; Schiffrin, D. J.; Whyman, R. *J. Chem. Soc. Chem. Commun.* **1994**, 801.

Brust, M.; Fink, J.; Bethell, D.; Schiffrin, D. J.; Kiely, C. J. *J. Chem. Soc. Chem. Commun.* **1995**, 1655.

Buchmeiser, M. R.; Sinner, F.; Mupa, M.; Wurst, K. *Macromolecules* **2000**, 33, 32.

Capek, I. *Adv. Colloid Interface Sci.* **2001**, 92, 195.

Carlini, C.; Angiolini, L. *Adv. Polym. Sci.* **1995**, 123, 127.

Carlini, C. *British Polymer J.* **1986**, 18, 236.

Carlini, C.; Ciardelli, F.; Donati, D.; Gurzoni, F. *Polymer* **1983**, 24, 599.

Carlini, C.; Gurzoni, F. *Polymer* **1983**, 24, 101.

Caruso, F.; Spasova, M.; Salgueirino-Maceira, V.; Liz-marzan, L. M. *Adv. Mater.* **2001**, 13, 1090.

Cattalini, L.; Tobe, M. L. *Inorg. Chem.* **1966**, 5, 1145.

Cha, D. Y.; Parravano, G. *J. Catal.* **1970**, 18, 200.

Chadwick D. J.; Will be, C. *J. Chem. Soc. , Perkin Trans. I* **1977**, 887.

Chambers, R. P.; Boudart, M. *J. Catal.* **1966**, 5, 517.

Chan, W. C. W.; Nie, S. *Science* **1998**, 281, 2016.

Chen, C.; Serizawa, T.; Akashi, M. *Chem. Mater.* **2002**, 14, 2232.

Chen. C–W. *Langmuir* **1997**, 13, 6465.

Chen. C. W. ; Chen. M. Q.; Serizawa T.; Akashi, M. *Chem. Commun.* **1998**, 831.

Cheng, G.; Böker, A.; Zhang, M.; Krausch, G.; Müller, A. H. E. *Macromolecules* **2001**, 34, 6883.

Claus, P.; Kraak, P.; Schödel, R. *Stud. Surf. Sci. Catal.* **1997**, 108, 281.

Clay, R.T.; Cohen, R. E. *Supramol. Sci.* **1995**, 2, 183.

Cobbe, S.; Connolly, S.; Ryan, D.; Nagle, L.; Eritja, R.; Fitzmaurice, D. *J. Phys. Chem. B* **2003**, 107, 470.

Cochin, D.; Lashewsky, A. *Macromolecules* **1997**, 30, 2278.

Coenen, S.; de Kruif, C. G. *J. Colloid Interface Sci.* **1988**, 124, 104.

Coloma, F.; Llorca, J.; Homs, N.; de la Piscina, P. R.; Rodríguez-Reinoso, F.; Sepúlveda-Escribano, A. *Phys. Chem. Chem. Phys.* **2000**, 2, 3063.

Collier, P. L.; Iggo, J.A.; Whymann, R. *J. Mol. Catal. A.* **1999**, 146, 149.

Collier, C. P.; Saykally, R. J., Shaing, J. J., Henrichs, S.E. Heath, J. *Science*, **1997**, 277, 1978.

Colvin, V. L.; Schlamp, M. C.; Alivisatos, A. P. *Nature* **1994**, 370, 354.

Concepcion, P.; Corma, A.; Silvestre-Albero, J.; Franco, V.; Chane-Ching, J.Y. *J. Am. Chem. Soc.* **2004** 126, 5523.

Creighton, J. A.; Eadon, D. G. *J. Chem. Soc., Faraday Trans.* **1991**, 87, 3881.

Crooks, R. M.; Zhao, M. Q.; Sun, L.; Chechik, V.; Yeung, L. K. *Acc. Chem. Res.* **2001**, 34, 181.

Currie, E. P. K.; Sieval, A. B.; Avena, M.; Zuilhof, H.; Sudhölter, E. J. R.; Cohen Stuart, M. A. *Langmuir* **1999**, 15, 7116.

Currie, E. P. K.; Wagemaker, M.; Cohen Stuart, M. A.; Van Well, A. A. *Macromolecules* **1999**, 32, 9041.

Cunningham, D. A. H.; Vogel, W.; Kageyama, H.; Tsubota, S.; Haruta, M. *J Catal* **1998**, 177, 1.

Cunningham, D. A. H.; Vogel, W.; Haruta, M. *Catal. Lett.* **1999**, 63, 43.

Dabbousi B. O.; Bawendi, M. G.; Onitsuka, O.; Rubner, M. F. *Appl. Phys. Lett.* **1995**, 66, 1316.

Dandekar, A.; Vannice, M. A. *J. Catal.* **1999**, 183, 344.

Danino, D.; Talmon, Y. *Phy. Chem. Bio. Inter.* **2000**, 799.

Daoud, M.; Cotton J. P. ; *J. Physique(Paris)* **1982**, 43, 531.

Das, B.; Guo, X.; Ballauff, M. *Progr. Colloid Polym. Sci.*, 2002, **121**, 34.

DeBoer, B.; Simon, H. K. ; Werts, M. P. L., Van der Vegte, E. W.; Hadziioannou, G. *Macromolecules*, **2000**, 33, 349.

De Hann, V. O.; Bijstervosch, H. D.; de Graff, A. W.; Leermakers, F. A. M.; Stuart, M. A. C.; Van Well, A. A., *Langmuir*, **1995**, 11, 4467.

Delair T. *Colloid. Polym. Sci.* **1994**, 72, 962.

Delbecq, F.; Sautet, P. *J. Catal.* **1995**, 152, 21.

Djalali R, S-You. Li, M. Schmidt, *Macromolecules* **2002**, 35, 4282.

Djalali, R.; Hugenberg, N.; Fischer, K.; Schmidt, M. *Macromol. Rapid Commun.* **1999**, 20, 444.

Dokoutchaev, A.; James, J. T.; Koene, S. C.; Pathak, S.; Prakash, G. K. S.; Thompson, M. E. *Chem. Mater.* **1999**, 11, 2389.

Duff, D.G.; Baiker, A.; Edwards, P. P. *Langmuir* **1993**, 9, 2301.

Duff, D. G.; Baiker, A. *Langmuir* **1993**, 9, 2310.

Duff, D. G.; Baiker, A.; Edwards, P. P. *J. Chem. Soc., Chem. Commun.* **1993**, 96.

Duff, D. G.; Baiker, A.; Edwards, P. P. *Langmuir* **1993**, 9, 2301.

Duff, D. G.; Baiker, A.; Gameson, I.; Edwards, P. P. *Langmuir* **1993**, 9, 2310.

Dziedzok, P.; Sheiko, S. S.; Fisher, K.; Schmidt, M.; Möller, M. *Angew. Chem.* **1997**, 109, 2894.

Ecstein, H.; Kreibig, U. *Z. Phys. D: At., Mol. Clusters* **1991**, 26, 239.

Eklund, S.E.; Clifffel, D.E. *Langmuir* **2004**, 20, 6012.

Ejaz, M.; Yamamoto, S.; Ohno, K.; Tsujii, Y.; Fukuda, T. *Macromolecules* **1998**, 31, 5934.

Emory, S. R., Nie, S. *J. Phy. Chem. B* **1998**, 102, 493.

Erkov, S. *Physica E* **2000**, 8, 210.

Ershov, B.G.; Henglein, A. *J. Phys. Chem. B* **1998**, 102, 10663.

Ershov, B. G. *Russ. Chem. Bull.* **1994**, 43, 16.

Erkelens, J.; Kemball, C.; Galwey, A. K. *Trans. Faraday Soc.* **1963**, 59, 1181.

Esumi, K.; Isono, R.; Yoshimura, T. *Langmuir* **2004**, 20, 237.

Esumi, K.; Suzuki, A.; Yamahira, A.; Torigoe, K. *Langmuir* **2000**, 16, 2604.

Esumi, K.; Suzuki, A.; Aihara, N.; Usui, K.; Torigoe, K. *Langmuir* **1998**, 14, 3157.

Exner, C.; Pfaltz, A.; Studer, M.; Blaser, Ulrich. H. *Adv. Synth. Catal.* **2003**, 345, 1253.

Feldstien, M. J., Keating, C. D.; Liao, Y.-H.; Natan, M. J.; Scherer, N. F. *J. Am. Chem. Soc.* **1997**, 119, 6638.

Fendlar, J. H.; Meldrum, F. *Adv. Mater.* **1995**, 7, 607.

Ferrick, M. R.; Murtagh, J.; Thomas, J. K. *Macromolecules* **1989**, 22, 4, 1515.

Fink, Y.; Winn, J. N.; Fan, S.; Chen, C.; Michel, J.; Joannopoulos, J. D.; Thomas, E. L. *Science* **1998**, 27 1679.

Fleer, G. J., *Ber. Bunsenges, Phys. Chem.*, **1996**, 100, 936.

Frost, J. C. *Nature* **1998**, 334, 577.

Foussier, J.P., *Photoinitiation, Photopolymerization, Photocuring, Fundamentals and Applications Fundamentals and applications*, Hanser Publishers, Munich, **1995**.

Foussier, J. P.; Loughnot, D. J. *J. Appl. Polym. Sci.* **1986**, 32, 6209.

Fukumi, K.; Chayahara, A.; Kadono, K.; Sakaguchi, T.; Horino, Y.; Miya, M.; Fujii, K.; Hayakawa, J.; Satou, M. *J. Appl. Phys.* **1994**, 75, 3075.

Galvagno, S.; Poltarzewski, Z.; Donato, A.; Neri, G.; Pietropaolo, O. R.; *J. Chem. Soc., Chem. Commun.* **1986**, 1729.

Galvagno, S.; Donato, A.; Neri, G.; Pietropaolo, R. *Catal. Lett.* **1991**, 8, 9.

Galvano, S.; Parravano, G. *J. Catal.* **1978**, 55, 178.

Garcia M. E., Baker, L. A., Crooks, R. M. *Anal. Chem.* **1999**, 71, 256.

Gardea-Torresdey, J. L.; Parsons, J. G.; Gomez, E.; Peralta-Videa, J.; Troiani, H. E.; Santiago, P.; Yacaman, M. J.; *Nano Lett.* **2002**; 2(4); 397.

Ganachaud, F.; Mouterde, G.; Delair, Th.; Elaissari, A.; Pichot, C. *Polym. Adv. Technol.* **1995**, 6, 480.

Ghosh, A.; Patra, C. R.; Mukherjee, P.; Sastry, M.; Kumar, R. *Microporous Mesoporous Mater.* **2003**, 58, 201.

Giordano, L.; Pacchioni, G.; Bredow, T.; Sanz, J. F. *Surf. Sci.* **2001**, 471, 21.

Gittins, D. I.; Susha, A. S.; Schoeler, B.; Caruso, F. *Adv. Mater.* **2002**, 14, 508.

Gittins, D. I.; Caruso, F. *Angew. Chem. Int. Ed.* **2001**, 40, 3001.

Gmelin handbook Au Suppl. Vol. B1.

Gomez – Cisneros, M.; Lopez, R. G.; Peralta, R. D.; Cesteros, L. C.; Katime, I.; Mendizabal, E.; Puig, J. E. *Polymer* **2002**, 43, 2993.

Goodman, D.; Kizhakkedathu, J. N.; Brooks, D.E. *Langmuir* **2004**, 20, 2333.

Goodwin, J. H.; Ottewill, R. H. *Brit Polymer J.* **1978**, 10, 173.

Goodwin, J. W.; Ottewill, R. H. *Colloid. Polym. Sci.* **1979**, 257, 61.

Grabar, K. C.; Allison, K. J.; Baker, B. E.; Bright, R. M.; Brown, K. R.; Freeman, R. G.; Fox, A. P.; Keating, C. D.; Musick, M. D.; Natan, M. J. *Langmuir* **1996**, 12, 2353.

Graf, C.; Blaaderen, A. V. *Langmuir* **2002**, 18, 524.

Grunes, J.; Zhu, J.; Anderson, E. A.; Somorjai, G. A. *J. Phys. Chem. B* **2002**, 106, 11463.

Grunwaldt, J.-D.; Kiener, C.; Wögerbauer, C.; Baiker, A. *J. Catal.* **1999**, 181, 223.

Guenoun, P.; Schalchli, A.; Sentenac, D.; Mays, J. W.; Benattar, J. J. *Phys. Rev. Lett.* **1995**, 74, 3628.

Guenoun, P.; Muller, F.; Delsanti, M.; Auvray, L.; Chen, Y. J.; Mays, J. W.; Tirrell, M. *Phys. Rev. Lett.* **1998**, 81, 3872.

Guczi, L.; Peto, G.; Beck, A.; Frey, K.; Geszti, O.; Molnar, G.; Daroczi, C. *J. Am. Chem. Soc.* **2003**, 125, 4332.

Guczi, L.; Horvarth, D.; Pászti, Z.; Tóth, L.; Horváth, Z. E.; Karacs, A.; Pető, G. *J. Phys. Chem. B* **2000**, 104, 3183.

Guo, X.; Ballauff, M. *Langmuir* **2000**, 16, 8719.

Guo, X.; Weiss, A.; Ballauff, M. *Macromolecules* **1999**, 32, 6043.

Guo, X.; Ballauff, M. *Phys. Rev. E*, **2001**, 64, 051406.

Guo, X. *Dissertation, Synthesis and study of the colloidal polyelectrolyte brushes prepared by photo-emulsion polymerisation*, 2001, Universität Karlsruhe, Germany.

Habicht, J.; Schmidt, M.; Rühle, J.; Johannsman, J. *Langmuir* **1999**, 15, 2460.

Halperin, W. P. *Rev. Mod. Phys.* **1986**, 58, 533.

Halpern, A.; Tirrell, M.; Lodge, T.P. *Adv. Polym. Sci.* **1992**, 100, 31.

Hammer, B.; Nørskov, J. K. *Nature* **1995**, 376, 238.

Hao, Z.; Cheng, D.; Guo, Y.; Liang, Y. *Applied Catal. B* **2001**, 33, 217.

Hariharan, R.; Biver, C.; Mays, J.; Russel, W.B. *Macromolecules* **1998**, 31, 7506.

Hariharan, R.; Biver, C.; Russel, W. B. *Macromolecules* **1998**, 31, 7514.

Hariharan, R.; Russel, W. B. *Langmuir* **1998**, 14, 7104.

Haruta, M. *Catal. Today* **1997**, 36, 153.

Haruta, M. *Chemical Record* **2003**, 3, 75.

Haruta, M.; Kobayashi, T.; Sano, H.; Yamada, N. *Chem. Lett.* **1987**, 405.

Haruta, M.; Sano, H. *Stud. Surf. Sci. Catal.* **1983**, 16, 225.

Haruta, M.; Yamada, N.; Kobayashi, T.; Iijima, S. *J. Catal.* **1989**, 115, 301.

Haruta, M.; Tsubota, S.; Kobayashi, T.; Kageyama, H.; Genet, M. J.; Delmon, B. *J. Catal.* **1993**, 144, 175.

Haruta, M.; Uphade, B. S.; Tsubota, S. A. Miyamoto, *Res. Chem. Intermed.* **1998**, 24, 329.

Hansen, P. L.; Cohen, J. A.; Podgornik, R.; Parsegia, V. A. *Biophys. J.* **2003**, 84, 350.

Hayashi, T.; Tanaka, K.; Haruta, M. *J. Catal.* **1998**, 178, 566.

Hayashi, S.; Abe, T.; Higashi, N.; Niwa, M.; Kurihara, K. *Langmuir* **2002**, 18, 3932.

Hedrick, J. L.; Mansky, P.; Huang, E.; Russell, T. P.; Hawker, C. J. *Macromolecules* **1999**, 32, 1424.

Heiz, U.; Schneider, W.-D. *J. Phys. D: Appl. Phys.* **2000**, 33, R85.

Heiz, U.; Sanchez, A.; Abbet, S.; Schneider, W.-D. *J. Am. Chem. Soc.* **1999**, 121, 3214.

Hengelein, A. *Langmuir* **1999**, 15, 6738.

Henglein, A. *J. Phys. Chem.* **1993**, 97, 5457.

Henglein, A.; Ershov, B. G.; Malow, M. *J. Phys. Chem.* **1995**, 99, 14 129.

Hennion, M.; Picart, C.; Caude, M.; Roseet, R. *Analysis* **1978**, 6, 369.

Hermnason, K. D.; Lumsdon, S. O.; Williams, J. P.; Kaler, E. W.; Velev, O. D. *Science* **2001**, 294, 1082.

Hertler, W. R.; Sogah, D. Y.; Boettcher F. P. *Macromolecules* **1990**, 23, 1264.

Hornebecq, V.; Antonietti, M.; Cardinal, T.; Treguer-Delapierre, M. *Chem. Mater.* **2003**, 15, 1993.

Huang, X.; Wirth, M. J. *Macromolecules* **1999**, 32, 1694.

Huang, W. X.; Kim, J. B.; Bruening, M. L.; Baker, G. L. *Macromolecules* **2002**, 35,1175.

Hughes, A. R.; St. Pierre, T. *Macromol. Synth.* **1977**, 6.

Huijs, F.; Lang, J. *Colloid Polym. Sci.* **2000**, 278, 746.

Husseman, M.; Malmström, E. A.; Mcnamara, M.; Mate, M.; Mecerreyes, D.; Benoit, D. G.; Hutchings, G.J. *Gold Bull.* **1996**, 29, 123.

Hwang, S.; Lee, M. C.; Choi, W. *Appl. Catal. B* **2003**, 46, 49.

Ingall, M. D. K.; Honeyman, C. H.; Mercure, J. V.; Bianconi, P. A.; Kunz, R. R. *J. Am. Chem. Soc.* **1999**, 121, 3607.

Ista, L. K., Mendez, S.; Perez-Luna, V. H.; Lopez, G. P. *Langmuir* **2001**, 17, 2552.

Ito, Y., Inaba, M., Chung, D. J., Imanishi, Y. *Macromolecules* **1992**, 25, 7313.

Jackson, S. D.; McLellan, G. D.; Webb, G.; Conyers, L.; Keegan, M. B. T.; Mather, S.; Simpson, S.; Wells, P. B.; Whan, D. A.; Whyman, R. *J. Catal.* **1996**, 162, 10.

Jana, N. R.; Gearheart, L.; Murphy, C. J. *Adv. Mater.* **2001**, 13, 1389.

Janietz, S.; Shulz, B.; Torronen, M.; Sundholm, G. *Eur. Polm. J.* **1993**, 29, 545.

Jayachandran. K. N.; Takacs-Cox. A.; Brooks. D.E. *Macromolecules* **2002**, 35, 4247.

Ji, T.; Lirtsman V. G.; Avny, Y.; Davidov, D. *Adv. Mater.* **2001**, 13,1253.

Jia, J.; Haraki, K.; Kondo, J. N.; Domen, K.; Tamaru, K. *J. Phys. Chem.* **2000**, B104, 11153.

Joly, S.; Kane, R.; Radzilowski, L.; Wang, T.; Wu, A.; Cohen, R. E.; Thomas, E. L.; Rubner, M. F. *Langmuir* **2000**, 16, 1354.

Johnson, S. R.; Evans, S. D.; Mahon, S. W.; Ulman, A. *Langmuir* **1997**, 13, 51.

Jones, D. M.; Smith, J. R.; Huck, W. T. S.; Alexander, C. *Adv. Mater.* **2002**, 14, 166, 1130.

Jordan, R.; Ulman, A. *J. Am. Chem. Soc.* **1998**, 120, 243.

Jordan, R.; West, N.; Ulman, A.; Y-Ming, C.; Nuyken, O. *Macromolecules* **2001**, 34, 1606.

Jordan R., Ulman, A.; Kang, J. F.; Rafailovich, M. H. *J. Am. Chem. Soc.* **1999**, 121, 1016.

Jordan, R.; Graf, K.; Riegler, H.; Unger, K. K. *Chem. Commun.* **1996**, 9, 1025.

Joynes, D.; Sherrington, D.C. *Polymer* **1997**, 38, 1427.

Jungmann, N.; Schmidt, M.; Maskos, M. *Macromolecules* **2003**, 36, 3974.

Juang, A.; Scherman, O. A.; Grubbs, R. H.; Lewis, N. S. *Langmuir* **2000**, 17, 1321, 2001.

Kamat, P.V.; Flumiani, M.; Hartland, G. W.; *J. Phys. Chem. B* **1998**, 102, 3123.

Kang E. T., Zhang, Y. *Adv. Mater.* **2000**, 12, 1481.

Kapoor, S.; Lawless, D.; Kennepohl, P.; Meisel, D.; Serpone, N. *Langmuir* **1994**, 10, 3018.

Katagi, H.; Kasai, H.; Okada, S.; Oikawa, H.; Matsuda, H.; Nakanishi, H. *Polym. Adv. Technol.* **2000**, 11, 778.

Kawaguchi, D.; Satoh, M. *Macromolecules*, **1999**, 32, 7828.

Kawabata, A. *J. Phys. Soc. Jpn.* **1970**, 29, 902.

Kawaguchi, D.; Kawauchi, S.; Satoh, M.; Komiyama, J. *Polymer* **1998**, 39, 6.

Kawai, T.; Sugita, K.; Saito, K.; Sugo, T. *Macromolecules* **2000**, 33, 1306.

Keita B., L. Nadjjo, C. De Cointet, J. Amblard, J. Belloni, *Chem. Phys. Lett.* **1996**, 249, 297.

Kelley, T. W.; Schorr, P. A.; Johnson, K. D.; Tirrell, M.; Frisbie, C. D. *Macromolecules*, **1998**, 31, 4297.

Kent , M. S.; Lee, L.T.; Farnoux, B.; Rondelez, F. *Macromolecules*, **1992**, 25, 6240.

Kent , M. S.; Lee, L.T.; Farnoux, B.; Rondelez, F.; Smith, G. H. *J. Phys. Chem.* **1995**, 103, 2320.

Khan M. A.; Perruchot, C.; Armes, S. P.; Randall, D. P. *J. Mater. Chem.*, **2001**,11, 2363.

Kim, J.; Brtuening, M. L.; Baker G.L. *J. Am. Chem. Soc.* **2000**, 122, 7616.

Klabunde, K. J.; Timms, P. L.; Skell, P. S.; Ittel, S. *Inorg. Synth.* **1979**, 19, 59.

Klein, J.; Kamiyama, Y.; Yoshizawa, H.; Israelachvili, J.N.; Fredrickson, G.H.; Pincus, P.; Fetters, L.J. *Macromolecules* **1993**, 26, 5552.

Koel, J.; Wang, B. E. *J. Phys. Chem.* **1998**, A 102, 8573.

Koper, G. J. M.; Van Duijvenbode, R. C.; Danny D. P.; Stam, W.; Steuerle, U.; Borkovec, M. *Macromolecules* **2003**, 36, 2500.

Kortan, A. R.; Hull, R.; Onila, R. J.; Bawendi, M. B.; Steigerwald, M. J.; Carroll, R. J.; Brus, L. E. *J. Am. Chem. Soc.* **1990**, 112, 1328.

Kong. X.; Kawai, T.; Abe, J.; Iyoda, T. *Macromolecules*, **2001**, 34, 1837.

Kukula, H.; Schlaad, H. *Macromolecules* **2002**, 35, 7157.

Kukushkin, Yu. N.; Danilina, L. I.; Fedyanin, Np.; Iretskii, A. V. *Russ. J. Inorg. Chem.* **1981**, 268 ,1766.

Kumar, A.; Mandal, S.; Selvakannan, P. R.; Pasricha, R.; Mandale, A. B.; Sastry, M. *Langmuir* **2003**, 19, 6277.

Kumar, A.; Pattarkine, M.; Bhadbhade, M.; Mandale, A. B.; Ganesh, K. N.; Datr, S. S.; Dharmadhikari, C. V. Sastry, M. *Adv. Mater.* **2001**, 13, 341.

Kurita, H.; Takami, H.; Koda, S. *Appl. Phys. Lett.* **1998**, 72, 789.

Kunz, M. S.; Shull, K. R.; Kellock, A. J. *Colloid Interface Sci.* **1993**, 156, 240.

Larpent, C.; Menn, B. F.; Patin, H. *J. Mol. Catal.* **1991**, 65, L35.

Laufer, W.; Niederer, J. P. M.; Hoelderich, W. F. *Adv. Synth. Catal.* **2002**, 344, 1084.

Leff, D. V.; Brandt, L.; Heath, J. R. *Langmuir* **1996**, 12, 4723.

Lewis, L. N. *Chem. Rev.* **1993**, 93, 2693.

Lewis, E. A.; Barkley, T. J.; Reams, R. R.; Hansen, L. D.; Pierre, T. S. *Macromolecules* **1984**, 17, 2874.

Liang, Z.; Susha, A. S.; Caruso, F. *Adv. Mater.* **2002**, 14, 1160.

Lianos, P.; Thomas, J. K. *Chem. Phys. Lett.* **1986**, 125, 299.

Lim, Y. T.; Park, O. O.; Jung, H. T. *J. Colloid Interface Sci.* **2003**, 263, 449.

Lindlar, B.; Boldt, M.; Eiden-Assmann, S.; Maret, G. *Adv. Mater.* **2002**, 14, 1656.

Liu, S.; Weaver, J. V. M.; Save, M.; Arms, S. P. *Langmuir* **2002**, 18, 8350.

Li, Y.; El-Sayed, M. A. *J. Phys. Chem. B* **2001**, 105, 8938.

Li, Z.-Y.; Younan, Xia. *Phys. Rev. B* **2001**, 64, 1531081.

Li, P.; Zhu, J.; Sunintaboon, P.; Harris, F. W. *J. Dispersion Sci. Technol.* **2003**, 24, 607.

Liu, Z. M.; Vannice, M. A. *Catal. Lett.* **1997**, 43, 51.

Liz-Marzan L. M.; Giersig, M.; Mulvaney, P. *Langmuir* **1996**, 12, 4329.

Longenberger, L.; Mills, G. J. *J. Phys. Chem.* **1995**, 99, 475.

Lopez, N.; Norskov, J. K. *J. Am. Chem. Soc.* **2002**, 124, 11262.

Luong J. C. *Superlattices Microstruct.* **1988**, 4, 385.

Luo, N., Hutchison, J. B.; Anseth, K. S.; Bowmann, N. C. *Macromolecules* **2002**, 35, 2487.

Luo, N., Hutchison, J. B., Anseth, K. S.; Bowmann, N. C. *J. Polym. Sci. A* **2002**, 40, 1885.

Luzinov, I.; Minko, S.; Senkovsky, V.; Voronov, A.; Hild, S.; Marti, O.; Wilke, W. *Macromolecules* **1998**, 31, 3945.

Luzinov, I.; Julthongpiput, D.; Malz, H.; Pionteck, J.; Tsukruk V. V. *Macromolecules* **2000**, 33, 1043.

Lyatskaya, Y. V.; Leermakers, F. A. M.; Fleer, G. J.; Zhulina, E. B.; Birshstein, T. M. *Macromolecules*, **1995**, 28, 3562.

Madaeni, S. S.; Ghanbarian, M. *Polym. Int.* **2000**, 49, 1356.

Mafuné, F.; Kohno, J.; Takeda, Y.; Kondow, T. *J. Phys. Chem.* **2001**, 105, 9050.

Mafuné, F.; Kohno, J.; Takeda, Y.; Kondow, T. *J. Phys. Chem.* **2002**, 106, 7575.

Mandal, S.; Selvakannan, P. R.; Roy, D.; Choudhary, R. V.; Sastry, M. *Chem. Comm.* **2002**, 3002.

Mandal, S.; Roy, D.; Chaudhari, R.V.; Sastry, M. *Chem. Mater.* **2004**, 16, 3714.

Manna A., Toyoko I., Keigo A., Masahiko O., Toshinobu Y. *Chem. Mater.* **2001**, 13, 1674.

Mallick, K.; Witcomb, M. J.; Scurrrell, M. S. *App. Catal. A.* **2004**, 259 163.

Maranhão L.C. A.; Sales, F. G.; Pereira, J. A. F. R.; Abreu, C. A. M. *React. Kinet. Catal. Lett.* **2004**, 81, 169.

Margitfalvi, J. I.; Tompes, A.; Kolosova, I.; Valyon, J. *J. Catal.* **1998**, 174, 246.

Marinelli, T. B. L.; Ponec, W.; V. *J. Catal.* **1998**, 156 51.

Marinelli, T. B. L. W.; Nabuurs, S.; Ponec, V. *J. Catal.* **1995**, 151, 431.

Maroto, J. A.; De Las Nieves, F. J. *Colloid Polym. Sci.* **1997**, 275, 1148.

Maroto, J. A.; De Las Nieves, F. J. *Colloid Polym. Sci.* **1998**, 276, 453.

Martin C. R., *Chem Mater.* **1996**, 8, 1739.

Masatake H. *The Chemical Record*, **2003**, Vol. 3, 75.

Matyjaszewski, K.; Miller, P. J.; Shukla, N.; Immaraporn, B.; Gelman, A.; Luokala, B. B.; Siclovan, T. M.; Kickelbick, G.; Vallant, T.; Hoffmann, H.; Pakula, T. *Macromolecules* **1999**, 32, 8719.

Mavrikakis, M.; Stoltze, P. Nørskov, J. K. *Catal. Lett.* **2000**, 64,101.

Maya L., Muralidharan, G.; Thundat, T. G.; Kenik, E. A. *Langmuir* **2000**, 16, 9151.

Mayya, K. S.; Patil, V.; Sastry, M. *Langmuir* **1997**, 13, 2575.

Mayya, K. S.; Patil, V.; Sastry, M. *Langmuir* **1997**, 13, 3944.

Maye M. M., Zheng, W. X.; Leibowitz, F. L. Ly, N. K. Zhong, C. J. *Langmuir* **2000**,16, 490.

Maye, M. M.; Luo, J.; Han, Li; Kariuki, N. N., Zhong, C-Jian. *Gold Bulletin* **2003**, 36, 75.

Mayer A. B. R., Mark, J. E. Hausner, S. H. *Angew. Makromol. Chem.* **1998**, 259, 45.

Mayer A. B. R., J. E. Mark, *J. Polym. Sci., Part B: Polym. Phys.* **1997**, 35, 1207.

Mayer, A. B. R.; Mark, J. E. *J. Macromol. Sci., Pure Appl. Chem.* **1997**, A34, 2151.

Mayer, A. B. R., Mark, J. F. *Polymer* **2000**, 41, 1627.

Mbindyo, J. K. N.; Reiss, B. D.; Martin, B. R.; Keating, C. D.; Ntan, M. J.; Mallouk, T. E. *Adv. Mater.* **2001**, 13, 249.

Meier, L. P.; Shelden, R. A.; Caseri, W. R.; Suter, U. W. *Macromolecules* **1994**, 27,1637.

Mei Y., A. Wittemann, G. Sharma, M. Ballauff , Th. Koch, H. Gliemann, J. Horbach, Schimmel, Th. *Macromolecules* **2003**, 36, 3452.

Michalska, Z. M.; Ostaszewski, B.; Zientarska, J.; Rynkowski, J. M. *J. Mol. Catal. A: Chem.* **2002**, 185, 279.

Milner, S.T. *Science* **1991**, 251, 905.

Minko, S.; Patil, S.; Datsyuk, V.; Simon, F.; Eichhorn, K.-J.; Motornov, M.; Usov, D.; Tokarev, I.; Stamm, M. *Langmuir* **2002**, 18, 289.

Minqi, Z.; Crooks, R. M. *Angew. Chem.. Int. Ed.* **1999**, 38, 364.

Miraballes-Martinez, I.; Forcada, J. *J. Poly. Sci., A* **2000**, 38, 4230.

Miraballes-Martínez, I., Martín-Molina, A., Galisteo-González, F., Forcada, J. *J. Poly. Sci., A* **2001**, 39, 2929.

Mizukoshi, Y.; Okitsu, K.; Maeda, Y.; Yamamoto, T. A.; Oshima, R.; Nagata, Y. *J. Phy. Chem. B* **1997**, 101, 7033.

Murata, H.; Ruhe, J., *Polym. Prepr. (Am. Chem. Soc., Div. Polym. Chem.)* **2003**, 44, 560.

Mu X.-Dong, Evans, D. G.; Kou, Y. *Catal. Lett.* **2004**, 3, 97.

Mukherjee, P.; Patra, C. R.; Kumar, R.; Sastry, M. *Phys. Chem. Comm.* **2001**, 5, 1.

Mulvaney, P. *Langmuir* **1996**, 12, 788.

Myasoedova, G. V.; Shcherbinina, N. I.; Zakhartchenko, E. A.; Kolobov, S. S.; Lileeva, L. V. Komozin, P. N.; Marrov, I. N.; Belyaeva, V. K. *Solvent Extr. Ion Exch.* **1997**, 15, 1107.

Nakao, Y. *Colloid Interface Sci.* **1995**, 171, 386.

Narayanan, R.; El-Sayed, M. A. *J. Am. Chem. Soc.* **2004**, 126, 7194.

Narayanan, R.; El-Sayed, M. A. *J. Phys. Chem., B* **2003**, 107, 12416.

Netti, M. C.; Coyle, S.; Baumberg, J. J.; Ghanem, M. A.; Birkin, P. R.; Bartlett, P. N.; Whittaker, D. M.; *Adv. Mater.* **2001**, 13, 1368 .

Ng, Y.; Chan, C.; Craig, G. S. W.; Schrock, R. R.; Cohen, R. E. *Chem. Mater.* **1992**, 4, 885.

Niidome, Y.; Hori, A.; Sato, T.; Yamada, S. *Chem. Lett.* **2000**, 310.

Ning, L.; Hutchison, J. B.; Anseth, K. S.; Bowmann, N. C. *Macromolecules* **2002**, 35, 2487.

Ning, L.; Hutchison, J. B.; Anseth, K. S.; Bowmann, N. C. *J. Polym. Sci., A* **2002**, 40, 1885.

Nyrkova, I. A.; Khokhlov, A. R.; Doi, M. *Macromolecules* **1993**, 26, 26.

Okitsu, K.; Mizukoshi, Y.; Bandow, H.; Yamamoto, T. A.; Nagata, Y.; Maeda Y. *J. Phys. Chem., B* **1997**, 101, 5470.

Okitsu, K.; Bandow, H.; Maeda, Y.; Nagata, Y.; *Chem. Mater.* **1996**, 8, 315.

Okumura, M.; Akita, T.; Haruta, M. *Catal. Today* **2002**, 74, 265.

Okumara, M.; Kitagawa, Y.; Haruta, M.; Yanaguchi, K. *Chem. Phys. Lett.* **2001**, 346, 163.

Okumura, K.; Tanaka, M.; Ueda, A.; Haruta, M. *Solid State Ionics* **1997**, 95, 143.

Okumura, M.; Tsubota, S.; Iwamoto, M.; Haruta, M. *Chem. Lett.* **1998**, 315.

Okumura, M.; Haruta, M. *Chem. Lett.* **2000**, 396.

Oldenburg, S.J.; Averitt, R.D.; Halas, N. J. *Chem. Phy. Lett.* **1998**, 288, 243.

Ottewill, R. H.; Shaw, J. H. *Kolloid Z and Z for polymere*, **1966**, 218, 1, 34.

Ottewill, R. H.; Rastogi, M. C. *J. Chem. Soc., Faraday Trans.* **1959**, 56, 854.

Otsu, T. *J. Poly. Sci. Part A: Polym. Chem.* **2000**, 38, 2121.

Ozin, G. A.; Yang, S. M. *Adv. Funct. Mater.* **2001**, 11, 95.

Pawlowski, D.; Tieke, B. *Langmuir* **2003**, 19, 6498.

Paszti, Z.; Peto, G.; Horvarth, Z. E.; Karacs, A.; Gucci, L. *Solid State Commun.* **1998**, 107, 323.

Pei, Q.; Yang, Y. *Chem. Mater.* **1995**, 7, 1568.

Perruchot, C.; Khan, M. A.; Kamitsi, A.; Armes, S. P.; Von Werne, T.; Patten, T. E. *Langmuir* **2001**, 17, 4479.

Petroski, J. M.; Wang, Z. L.; Green, T. C.; El-Sayed, M. A. *J. Phy. Chem. B* **1998**, 102, 3316.

Piehler, J.; Brecht, A.; Valiokas, R.; Liedberg, B.; Gauglitz, G. *Biosens. Bioelectron.* **2000**, 15, 473.

Pileni, M. P.; Motte, L.; Petit, C. *Chem. Mater.* **1992**, 4, 338.

Pincus, P. *Macromolecules* **1991**, 24, 2912.

Pol, V. G. L.; Gedanken, A.; Calderon-Moreno, J. *Chem. Mater.* **2003**, 15, 1111.

Ponec, V. *Appl. Catal., A* **1997**, 149, 27.

Porter, L. A.; Ji, D.; Westcott, S. L.; Graupe, M.; Czernuszewicz, R. S.; Halas, N. J.; Lee, T. R. *Langmuir* **1998**, 14, 7378.

Porter, K. A.; Schier, A.; Schmidbaur, H. *Organometallics* **2003**, 22, 4922.

Price, C.; Chan, E. K. M.; Hudd, A. L.; Stubbersfield, R. B. *Polym. Commun.* **1986**, 27, 196.

Prinz, C.; Muller, P.; Maaloum, M. *Langmuir* **2000**, 16, 6636.

Prinz, C.; Muller, P.; Maaloum, M. *Macromolecules* **2000**, 33, 4896.

Prucker, O.; Rühle, J. *Macromolecules* **1998**, 31, 592.

Prucker, O.; Rühle, J. *Macromolecules* **1998**, 31, 602.

Quinn, M.; Mills, G. *J. Phys. Chem.* **1994**, 98, 9840.

Quaroni, L.; Chumanov, G. *J. Am. Chem. Soc.* **1999**, 121, 10642.

Rabaine, S.; Fanucci, G. E.; Seip, C. T.; Adair, J. H.; Talham, D. R. *Langmuir*, **1998**, 14, 708.

Rao, C. N. R.; Kulkarni, G. U.; Thomas, P. J.; Edwards, P. P. *Chem. Eur. J.* **2002**, 8, 28.

Reiter, G.; Khanna, R. *Phys. Rev. Lett.* **2000**, 85, 2753.

Reiter, G.; Khanna, R. *Langmuir* **2000**, 16, 6351.

Reiter, G.; Auroy, P.; Auray, L. *Macromolecules* **1996**, 29, 2150.

Remita S.; Mostafavi, M.; Delcourt, M. O. *New J. Chem.* **1994**, 18, 581.

Römbke, P.; Schier, A.; Schmidbaur, H. *J. Chem. Soc., Dalton Trans.* **2001**, 2482.

Romanov, S. G.; Maka, T.; Sotomayer Torres, C. M.; Müller, M.; Zentel, R. *Appl. Phys. Lett.* **1999**, 75, 1057.

Roucoux, A.; Jürgen, S.; Patin, H. *Chem. Rev.* **2002**, 102, 3757.

Rubio-Hernandez, F. J.; de las Nieves, F. J.; Hidalgo-Alvarez, R.; Bijsterbosch, B. H. J. *Dispersion Sci. Technol.* **1994**, 15, 1.

Sakota, K. *J. Appl. Polym. Sci.* **1976**, 20, 1725.

Salama, T.M.; Ohnishi, R.; Iejikawa, M. *J. Chem. Soc., Faraday Trans.* **1996**, 92, 301.

Salama, T. M.; Ohnishi, R.; Shido, T.; Iejikawa, M. *J. Catal.* **1996**, 162, 169.

Salama, T.M.; Ohnishi, R.; Iejikawa, M. *Stud. Surf. Sci. Catal.* **1997**, 105, 1571.

Salamon, J.C. ed. *Polymeric Materials encyclopedia, Volume 7, CRC press*, **1996**.

Saliba, N.; Parker, D. H.; Koel, B. E. *Surf. Sci.* **1998**, 410, 270.

Sakurai, H.; Haruta, M. *Appl. Catal., A* **1995**, 127, 93.

Sanchez, A.; Abbet, S.; Heiz, U.; Schneider, W.-D.; Häkkinen, H.; Barnett, R. N.; Landmann, U. *J. Phy. Chem. A* **1999**, 103, 9573.

Santori, G. F.; Casella, M. L.; Siri, G. J.; Aduriz, H. R.; Ferretti, O. A. *Appl. Catal., A* **2000**, 197, 141.

Santori, G. F.; Casella, M. L.; Siri, G. J.; Adúriz, H. R.; Ferreti, O. A. *React. Kinet. Catal. Lett.* **2002**, 75, 225.

Sault, A.G.; Madix, R. J.; Campbell, C. T. *Surf. Sci.* **1986**, 169, 347.

Schärftl, W. *Adv. Mater.* **2000**, 12, 1899.

Schillen, K.; Brown, W.; Johnsen, R. M. *Macromolecules* **1994**, 27, 4825.

Schlaepfer, C. W.; Zelewsky, A.V. *Comments Inorg. Chem.* **1990**, 9, 181.

Schmid, G.; Corain, B. *Eur. J. Inorg. Chem.* **2003**, 3081.

Schmid, G. *Chem. Rev.* **1992**, 92, 1709.

Schmidt, T. J.; Noeske, M.; Gasteiger, H. A.; Behm, R. J. *J. Electrochem. Soc.* **1998**, 145, 925.

Selvan, S. T.; Hayakawa, T.; Nogami, M.; Möller, M. *J. Phy. Chem. B* **1999**, 103, 7441.

Sharma, G.; Ballauff, M. *Macromol. Chem. Rapid Comm.* **2004**, 25, 547.

Shchukin, D.G.; Caruso, R. A. *Chem. Comm.*, **2003**, 1478.

Shibata, M.; Kuwata, N.; Matsumoto, T.; Kimura, H. *Chem. Lett.* **1985**, 1605.

Shipway, A. N.; Willner, I. *Chem. Commun.*, **2001**, 2035.

Shipway, A. N.; Willner, I. *Acc. Chem. Res.*, **2001**, 34, 421.

Shipway, A. N.; Katz, E.; Willner, I., *Struct. Bonding(Berlin)*, **2001**, 99, 237.

Sidorenko, A.; Minko, S.; Schenk- Meuser, K.; Duschner, H.; Stamm, M. *Langmuir* **1999**, *15*, 8349.

Siiman, O.; Burshteyn, A. *J. Phys. Chem. B* **2000**, *104*, 9795.

Silva da, A. B.; Jordao, E.; Mendes, M. J.; Fouilloux, P. *Appl. Catal., A* **1997**, *148*, 253.

Singh, U.K.; Vannice, M.A. *J. Catal.* **2000**, *191*, 165.

Singh, N.; Karim, A.; Bates, F. S.; Tirrell, M.; Furusawa, K. *Macromolecules* **1994**, *27*, 2586.

Sosebee, T., Giersig, M. Holzwarth, A. Mulvaney, P. *Ber. Bunsen-Ges. Phys. Chem.* **1995**, *99*, 40.

Spatz, J. P.; Mößmer, S.; Möller, M.; Kocher, M.; Neher, D.; Wegner, G. *Adv. Mater.* **1998**, *10*, 6473.

Spatz, J. P.; Eibeck, P.; Mößmer, S.; Möller, M.; Herzog, T.; Ziemann P.; *Adv. Mater.* **1998**, *10*, 849.

Spatz, J. P.; Sheiko, P. S.; Möller, M. *Macromolecules* **1996**, *29*, 3220.

Spatz, J. P.; Mößmer, S.; Möller, M. *Chem. Eur. J.* **1996**, *2*, 1552.

Spatz, J. P.; Roescher, A.; Möller, M. *Adv. Mater.* **1996**, *8*, 337.

Spatz, J. P.; Mößmer, S.; Hartmann, C.; Möller, M.; Herzog, T.; Krieger, M.; Boyen, Hans-Gerd; Ziemann, P.; Kabius, B. *Langmuir* **2000**, *16*, 407.

Steigerwald, M. L.; Alivisatos, A. P.; Gibson, J. M.; Harris, T. D.; Kortan, R.; Muller, A. J.; Thayer, A. M.; Duncan, T. M.; Douglass, D. C.; Brus, L. E. *J. Am. Chem. Soc.* **1988**, *110*, 3046.

Stoeva, S.; Klabunde, K. J.; Sorensen, Ch. M.; Dragieva, I. *J. Am. Chem. Soc.* **2002**, *124*, 2305.

Strelow, F.; Fojtik, A.; A. Henglein, *J. Phys. Chem.* **1994**, *98*, 3032.

Sukhishvili, S.A.; Granick, S. *Langmuir* **1997**, *13*, 4935-38.

Sun, T.; Seff, K. *Chem. Rev.* **1994**, *94*, 857.

Sun, S.; Murray, C. B.; Weller, D.; Folks, L. Maser, *Science* **2000**, *287*, 1989.

Sumerlin Brent S., Lowe, A. B.; Stroud, P. A.; Zhang, P.; Urban, M. W.; McCormick, C. L. *Langmuir* **2003**, *19*, 5559.

Svergun, D. I.; Shtykova, E. V.; Dembo, A. T.; Bronstein, L. M.; Platonova, O. A.; Yakunin, A. N.; Valetsky, P. M.; Khokhlov, A. R. *J. Chem. Phy.* **1998**, *109*, 11109.

Svoboda, K. ; Block, S. M. *Opt. Lett.* **1994**, *19*, 930.

Takai, Y. G.; Aoki, T.; Sanui, K. M.; Ogata, N.; Sakurai, Y.; Okano, T. *Macromolecules* **1994**, *27*, 6163.

Takami, A.; Kurita, H.; Koda, S. *J. Phys. Chem. B* **1999**, *103*, 1226.

Takita, Y.; Imamura, T.; Mizuhara, Y.; Abe, Y.; Ishihara, T. *Appl. Catal., B* **1992**, 1, 79.

Tamai, H.; Sakurai, H.; Hirota, Y.; Nishiyama, F.; Yasuda, H. *J. Appl. Polym. Sci.* **1995**, 56, 441.

Tamoto, N.; Adachi, C.; Nagai, K. *Chem. Mater.* **1997**, 9, 1077.

Templeton, A. C.; Hostetler, M. J.; Kraft, C. T.; Murray, R. W. *J. Am. Chem. Soc.* **1998**, 120, 1906.

Templeton, A.C.; Hostetler, M. J.; Warmouth, E. K.; Chen, S.; Hartshorn, C. M.; Krishnamurthy, V. M.; Forbes, M. D. E.; Murray, R. W. *J. Am. Chem. Soc.* **1998**, 120, 1959.

Teranishi, T.; Kiyakawa, I.; Miyake, M. *Adv. Mater.* **1998**, 10, 596.

Teranishi, T., Miyake, M. *Chem. Mater.* **1998**, 10, 594.

Thomas, J. M. *Pure Appl. Chem.* **1988**, 60, 1517.

Thybaut, J. W.; Saeys, M.; Marin, G.B. *Chem. Eng. J.* **2002**, 90, 117.

Toshima, N.; Nakata, K.; Kitoh, H. *Inorg. Chim. Acta* **1997**, 265, 149.

Tran, Y.; Auroy, P. *J. Am. Chem. Soc.* **2001**, 123, 3644.

Tran, Y.; Auroy, P.; Lee, L-T. *Macromolecules* **1999**, 32(26), 8952.

Tsubota, S.; Haruta, M.; Kobayashi, T.; Ueda, A.; Nakahara, Y. *Stud. Surf. Sci. Catal.* **1991**, 63, 695.

Tu, W.; Liu, H.; Liew, K. Y. *J. Colloid Interface Sci.* **2000**, 229, 453.

Uchida, E.; Ikada, Y. *Macromolecules* **1997**, 30, 5464.

Ueda, A.; Haruta, M. *Appl. Catal. B.*, **1996**, 285, 81.

Urbas, A.; Fink, Y.; Thomas, E. L. *Macromolecules* **1999**, 32, 4748

Van der Hul, *Brit Polymer Journal* **1970**, 2,121.

Valden, M.; Lai, X.; Goodman, D.W. *Science* **1998**, 281, 1647.

Van Zanten, J. H. *Macromolecules* **1994**, 27, 6797.

Von Werne, T.; Patten, T. E. *J. Am. Chem. Soc.* **2001**, 123, 7497.

Walter, H.; Harrats, C.; Müller Buschbaum, P.; Jerome, R.; Stamm, M. *Langmuir* **1999**, 15, 1260.

Walters, R. D.; Weimer, J. J.; Smith, J. E. *Catal. Lett.* **1995**, 30, 181.

Ward, R. S.; *IEEE Eng. Med. Biol. Mag.* **1989**, 6, 22.

Wang, W.; Asher, S. A. *J. Am. Chem. Soc.* **2001**, 123, 12528.

Wang, Y.; Herron, N. *J. Phys. Chem.* **1987**, 91, 257.

Watzke, H. J., Fendler, J. H. *J. Phys. Chem.* **1987**, 91, 854.

Wie, C. C.; Chen, M-Qing.; Serizawa, T.; Akashi, M. *Adv. Mater.* **1998**, 10, 1122.

Weisbecker, C. S.; Merritt, M. V.; Whitesides, G. M. *Langmuir* **1996**, 12, 3763.

Weller, H. *Angew. Chem.* **1993**, 105, 43, *Angew. Chem. Int. Ed.* **1993**, 32, 41.

Weller, H.; Eychmüller, A. *Adv. Photochem.* **1995**, 20, 165.

Weng, L.-T.; Delmon, B. *Appl. Catal., A* **1992**, 81, 141.

Wesley, R. D.; Cosgrove, T. *Langmuir* **2000**, 16, 4467.

Westcott, S. L.; Oldenburg, S. J.; Lee, T. R.; Halas, N. J. *Langmuir* **1998**, 5396.

Wiebolt, J., Zimehl, R. *Prog. Colloid Polym. Sci.* **1998**, 109, 260.

Wiesner, J.; Wokaun, A. *Chem. Phys. Lett.* **1989**, 157, 569.

Wu, T.; Efimenko, K.; Genzer, J. *Macromolecules* **2001**, 34, 684.

Xia, X.; Hu, Z. *Langmuir* **2004**, 20, 2094.

Xiao, K. Z.; Baral, S.; Fendler, J. H. *J. Phys. Chem.* **1990**, 94, 2043.

Xu, Z.; Xiao, F.-S.; Purnell, S. K.; Alexeev, O.; Kawi, S.; Deutsch, S. E.; Gates, B. C. *Nature* **1994**, 372, 346.

Yamamoto, S.; Ejaz, M.; Tsujii, Y.; Matsumoto, M.; Fukuda, T. *Macromolecules* **2000**, 33, 5608.

Yang Ya Jiang, Engberts, J. B. F. N. *Euro. Polym. J.* **1992**, 28/8, 881.

Youk, J. H.; Park, M.; Locklin, J.; Advincula, R.; Yang, J.; Mays, J. *Langmuir* **2002**, 18, 2455.

Youk, J. H. *Polymer* **2003**, 44, 5053.

Yuan, Y.; Kozlova, A. P.; Asakura, K.; Wan, H.; Tsai, K.; Iwasawa, Y. *J. Catal.* **1997**, 170, 191.

Zelewsky, A. V., Barbosa, L.; Schläpfer, C. W. *Coord. Chem. Rev.* **1993**, 123, 229.

Zhang, L. F.; Eisenberg, A. *Science* **1995**, 268, 1728.

Zhang, L. F.; Yu, K.; Eisenberg, A. *Science* **1996**, 272, 1777.

Zhao, B.; Brittain, W. J. *J. Am. Chem. Soc.* **1999**, 121, 3557.

Zhao, M.; Crooks, R. M. *Angew. Chem. Int. Ed.* **1999**, 38, 364.

Zhao, B.; Brittain, W. J. *Macromolecules* **2000**, 33, 8813.

Zhao, B.; Brittain, W. J.; Zhou, W.; Cheng, S. Z. D. *J. Am. Chem. Soc.* **2000**, 122, 2407.

Zhao, X. K.; Fendler, J. H. *Chem. Mater.* **1991**, 3, 168.

Zhao, X. K.; McCormick, L.; Fendler, J. H. *Chem. Mater.* **1991**, 3, 922.

Zhou, Y.; Wang, C.Y.; Zhu, Y.R.; Chen, Z. Y. *Chem. Mater.* **1999**, 11, 2310.

Zhou, Y.; Yu, S. H.; Wang, C.Y.; Li, X. G.; Zhu, Y. R.; Chen, Z.Y. *Adv. Mater.* **1999**, 11, 850.

Zhulina, E. B.; Borisov, O. V.; Birshtein, T. M. *J. Phys.: Condens. Matter.* **1994**, 6, A317.

Zhulina, E. B.; Israels, R.; Fleer, G. J. *Colloids Surf. A: Physicochem, Eng. Asp.*, **1994**, 86, 11.

Zhulina, E. B.; Birshtein, T. M.; Borisov, O. V. *Macromolecules*, **1995**, 28, 1491.

Zhulina, E. B.; Wolterink, J. K.; Borisov, O. V. *Macromolecules* **2000**, 33, 4945.

Zhulina, E. B.; Borisov, O. V.; Birshtein, T. M. *Macromolecules* **1999**, 32, 8189.

## Glossary

|             |  |
|-------------|--|
| ABA.2HCl    | Azo bis isobutyramidine hydrochloride                      |
| ABP         | 4-acryloxybenzophenone                                     |
| ADMBA.2HCl  | Azo N, N' dimethyleneisobutyramidine hydrochloride         |
| AEMH        | Aminoethylmethacrylatehydrochloride                        |
| AFM         | Atomic force microscopy                                    |
| Ag          | Argentum(Silver)   |
| AIBN        | 2, 2'-azobis (2-methylpropionitrile)                       |
| ARTP        | Atomic radical transfer polymerization                     |
| Au          | Aurum (gold)   |
| BA          | Benzoin acrylate   |
| BSA         | Bovine Serum Albumin                                       |
| $C_a$       | Added ionic strength                                       |
| Cd          | Cadmium  |
| CMC         | Critical micelle concentration                             |
| CPC         | Cetylpyridinium chloride                                   |
| Cryo TEM    | Cryogenic temperature transmission electron microscope     |
| $C_s$       | Local ionic strength inside the brush                      |
| CTAB        | Hexadecyltrimethylammonium bromide                         |
| Cu          | Cuprum(copper)   |
| $\bar{D}$   | Intensity weighted average diffusion coefficient           |
| D           | Diffusion coefficient                                      |
| DLS         | Dynamic Light Scattering                                   |
| DMF         | Dimethyl formamide   |
| EDX         | Energy dispersive x-rays                                   |
| $E_F$       | Fermi energy of electrons                                  |
| F           | Free energy of the chains                                  |
| $F_{el}$    | Elastic free energy  |
| $F_{int}$   | Interaction energy between the statistical segments        |
| $g_1(\tau)$ | Temporal correlation function of the scattered light field |
| $g_2(\tau)$ | Normalised time correlation function                       |
| $G(\Gamma)$ | Distribution function of $\Gamma$                          |
| GC          | Gas Chromatography   |

|                     |   |
|---------------------|---|
| GPC                 | Gel permeation chromatography                                       |
| h                   | Brush height  |
| HMEM                | 2-[p-(2-hydroxy-2-methylpropiophenone)]-ethyleneglycol-methacrylate |
| HRTEM               | High resolution transmission electron microscopy                    |
| $\langle I \rangle$ | Conventional time average intensity                                 |
| $l_k$               | Kuhn length of the brush polymer                                    |
| K                   | Mark- Houwink constant  |
| KPS                 | Potassium persulfate  |
| $L_c$               | Contour length of the grafted polymeric chains                      |
| $M_\eta$            | Viscosity average molecular weight                                  |
| nm                  | Nanometer   |
| $N_\xi$             | Number of segments in the blob                                      |
| P(q)                | Form factor   |
| PAA                 | Polyallylamine  |
| PCS                 | Photon correlation spectroscopy                                     |
| PDMAEMA             | Poly(2-dimethylamino)ethylmethacrylate)                             |
| PEI                 | Polyethyleneimine   |
| PMMA                | Poly(methyl methacrylate)   |
| PS                  | Polystyrene   |
| Pt                  | Platinum  |
| PVP                 | Polyvinylpyridine   |
| q                   | Scattering vector   |
| QELS                | Quasi-elastic light scattering                                      |
| R                   | Core radius   |
| $R_h$               | Hydrodynamic radius of the particles                                |
| SDS                 | Sodium dodecyl sulfate  |
| T                   | Averaged time   |
| TEM                 | Transmission electron microscopy                                    |
| THMP                | Tetrakis(hydroxymethyl)phosphonium chloride                         |
| UV/VIS              | Ultraviolet/visible   |
| V-50                | 2-2`azodiisobutyramidine dihydrochloride                            |
| VBAH                | Vinylbenzylamine hydrochloride                                      |

|           |  |
|-----------|--|
| $\Phi(Z)$ | Segment density profile of the surface attached chains |
| $\sigma$  | Grafting density of the surface attached chains        |
| $\theta$  | Scattering angle                                       |
| $\lambda$ | Wavelength of the light                                |
| $\Gamma$  | Relaxation rate  |
| $\tau$    | Correlation time                                       |
| $\Pi$     | Osmotic pressure                                       |
| $\eta$    | Viscosity of the polymers                              |
| $[\eta]$  | Intrinsic viscosity of the polymers                    |
| $\zeta$   | Neutralization length                                  |
| $\xi(r)$  | Size of the blob                                       |
| $\rho(r)$ | Segment density inside a blob                          |
| $\nu$     | Excluded volume parameter                              |
| $\alpha$  | Degree of dissociation of the chargeable groups        |



## **Publications**

1) Engineering the interaction of latex spheres with charged surfaces: AFM investigation of spherical polyelectrolyte brushes on mica.

Mei Y., A. Wittemann, G. Sharma, M. Ballauff , Th. Koch, H. Gliemann, J. Horbach , Th. Schimmel, *Macromolecules* **2003**, 36, 3452

2) Cationic Spherical Polyelectrolyte Brushes as Nanoreactors for the Generation of Gold Particles.

Sharma, G.; Ballauff, M. *Macromol. Chem. Rapid Comm.* **2004**, **25**, 547



## Curriculum Vitae

### Personal details:

Name : Geeta Sharma  
Date of Birth : 21.03.1976  
Nationality : Indian

### Education:

June 1981- June1991 Kendriya Vidyalaya Nasik Road Camp, Nasik, India  
June 1991- June1993 Kendriya Vidyalaya Nasik Road Camp, Nasik, India

### Graduation:

June 1993- June1996 R.Y.K. College, Nasik, India

### Post Graduation:

June 1997- June1999 Department of Chemistry, Pune University, Pune, India

**Title for Master work:** “Synthesis of ( $\pm$ )2-O-benzoyl-4-o-(p-bromobenzoyl)-myo-inositol 1,3,5-orthoformate”.

**Project Advisor:** Dr. Shashidhar, National Chemical Laboratories, Pune, India

### Work Experience:

June 1999-Nov 2000 Research officer in “Unilever Research”.

### Ph.D. Thesis:

**Thesis advisor:** Prof. Matthias Ballauff

Jan 2001- Nov 2004 Polymer Institute, Karlsruhe University, Germany

Nov 2004 Onwards- Physical Chemistry I, Bayreuth University, Germany

Title: “Generation of metal nanoparticles in spherical polyelectrolyte brushes and their application in heterogeneous catalysis”.



## **Erklärung**

Hiermit erkläre ich, dass ich die Arbeit selbständig verfasst und keine anderen als die angegebenen Quellen und Hilfsmittel benutzt habe.

Ferner erkläre ich, dass ich nicht anderweitig mit oder ohne Erfolg versucht habe, eine Dissertation einzureichen oder mich einer Doktorprüfung zu unterziehen.

Bayreuth, den 03. 08. 05

Geeta Sharma